

LAWRENCE TECHNOLOGICAL UNIVERSITY



**USE OF UNBONDED CFCC FOR TRANSVERSE
POST-TENSIONING OF SIDE-BY-SIDE BOX-BEAM BRIDGES**

Submitted to

MICHIGAN DEPARTMENT OF TRANSPORTATION

Testing and Research Section
Construction and Technology Division
Contract No. 2004-0105

by

**Dr. Nabil F. Grace, Project Investigator
and Dr. Elin Jensen, Co-Project Investigator**

Department of Civil Engineering
Lawrence Technological University
Southfield, MI 48075-1058, USA.

February, 2008

Technical Report Documentation Page

1. Report No. Research Report RC-1509	2. Government Accession No.	3. MDOT Project Manager Roger Till	
4. Title and Subtitle Use of Unbonded CFCC for Transverse Post-Tensioning of Side-by-Side Box-Beam Bridges		5. Report Date February 2008	
7. Author(s) Dr. Nabil Grace, Dr. Elin Jensen, Dr. Vasant Matsagar, Mena Bebawy, Elsam Soliman, and Joseph Hanson		6. Performing Organization Code	
9. Performing Organization Name and Address Center for Innovative Material Research (CIMR), Department of Civil Engineering, Lawrence Technological University, 21000 West Ten Mile Road, Southfield, MI-48075		8. Performing Org. Report No.	
12. Sponsoring Agency Name and Address Michigan Department of Transportation (MDOT) Construction and Technology Division P.O. Box 30049 Lansing, MI-48909		10. Work Unit No. (TRAIS)	
		11. Contract Number: 2004-0105	
		11(a). Authorization Number:	
15. Supplementary Notes		13. Type of Report & Period Covered Final Report, Sept. 2006-Feb. 2008	
		14. Sponsoring Agency Code	
16. Abstract <p>An experimental and numerical research project was developed to address the effect of the level of transverse post-tensioning (TPT) and the number of the transverse diaphragms on the performance of side-by-side box-beam bridges using unbonded carbon fiber composite cables (CFCC). The experimental program included the construction, instrumentation, and testing of one half-scaled 30° skew bridge model. The numerical program investigated the sensitivity to longitudinal cracking for a wide range of side-by-side box-beam bridges with different spans and different widths. The experimental program consisted of load distribution tests conducted during three different deck slab conditions; uncracked, cracked, and repaired stage. The transverse strain distribution tests were conducted when the bridge deck was uncracked. The cracked stage involved the initiation of longitudinal cracks above the shear-key locations while the repaired stage involved the replacement of an assumed damaged exterior beam with a new one. The distribution of the transverse strain developed at the top surface of the deck slab and the deflection across the width of the bridge were examined by varying the number of transverse diaphragms (five, four, and three) and the levels of TPT forces (20, 40, and 80 kip) at each transverse diaphragm. An ultimate load test was performed to evaluate the performance of the unbonded CFCC used for TPT during failure.</p> <p>Analysis of the experimental results shows that the application of TPT significantly improved load distribution among the side-by-side box-beams. Increasing the level of TPT forces generally improved the deflection response of the bridge model in all the three cases studied. Different arrangements of the TPT forces had insignificant influence on the transverse strains developed in the region between the diaphragms. From the ultimate load test results, it was noted that the TPT system coupled with the deck slab distributed the eccentric load in the transverse direction until the complete failure of the bridge model. The numerical study revealed that the influence of the live load alone is not the major cause of the longitudinal cracks. Combining the temperature gradient with the live load can lead to the development of longitudinal cracks between the adjacent beams. The adequate number of diaphragms is a function of the bridge span while the adequate TPT force level is a function of the bridge width. The developed recommendations are presented in design charts relating the number of diaphragms to the bridge span and the level of the TPT force to the bridge width. The onset of longitudinal cracks can be delayed using adequate TPT arrangements.</p>			
17. Key Words Box-beam bridges, transverse post-tensioning, longitudinal cracks, transverse diaphragms		18. Distribution Statement No Restrictions. This document is available to the public through the Michigan Department of Transportation (MDOT).	
19. Security Classification (Report) Unclassified	20. Security Classification (Page) Unclassified	21. No. of Pages	19. Price

Keywords:

Carbon Fiber Composite Cable (CFCC)
Composite Materials
Finite Element Analysis
Flexure Strength
Load Distribution
Differential Camber
Prestressed Concrete
Shear-Key
Side-by-Side Box-Beam Bridge
Skew Alignment
Strain Distribution
Transfer Length
Transverse Post-Tensioning
Load Fraction

Center for Innovative Materials Research (CIMR)
Structural Testing Center
Department of Civil Engineering
Lawrence Technological University
21000 West Ten Mile Road
Southfield, MI 48075-1058, USA.
Tel: 1-248-204-2556
Fax: 1-248-204-2568
E-mails: Nabil@LTU.edu, Jensen@LTU.edu
Web pages: <http://www.NabilGrace.com>, <http://qbx6.LTU.edu/Jensen>

The publication of this report does not necessarily indicate approval or endorsement of the findings, opinions, conclusions, or recommendations of either inferred or specially expressed herein, by the Regents of the Lawrence Technological University or the Michigan Department of Transportation.

TABLE OF CONTENTS

TABLE OF CONTENTS	iii
LIST OF FIGURES	viii
LIST OF TABLES	xvii
EXECUTIVE SUMMARY	xix
ACKNOWLEDGEMENTS	xxi
CHAPTER 1: INTRODUCTION	1
1.1 Introduction.....	1
1.2 Project Objectives.....	7
1.3 Report Organization	8
CHAPTER 2: LITERATURE REVIEW	9
2.1 Introduction.....	9
2.2 Transverse Post-Tensioning	11
2.3 Finite Element Modeling of Transverse Post-Tensioning Arrangements	12
2.4 Shear-Key Performance	12
2.4.1 Location of Shear-Key and Grout Material.....	13
2.4.2 Thermal Stresses	14
2.4.3 Construction Practices.....	14
2.5 Transverse Diaphragms.....	15
2.6 Load Distribution.....	18
2.7 Level of Prestressing	20
2.8 CFRP Bonded and Unbonded Transverse Prestressing	21
2.9 Effect of Skew Angle on Load Distribution	22
2.10 Summary.....	24
CHAPTER 3: NUMERICAL METHODOLOGY	25
3.1 Introduction.....	25
3.2 Components of the Bridge Model.....	25
3.2.1 Box-Beams	26
3.2.2 Box-Beam Reinforcement	33
3.2.3 Transverse Post-Tensioning Strands (TPT Strands)	35

3.2.4	Deck Slab.....	36
3.2.5	Deck Slab Reinforcement	41
3.2.6	Elastomeric Bearing Pads	42
3.2.7	Shear-Keys	44
3.3	Construction Loads.....	46
3.4	Load Combinations	47
3.5	Analysis Calibration	51
3.5.1	Half-Scale Bridge Model	53
3.5.1.1	Bridge Model Components and Material Properties	55
3.5.1.2	Loading Scheme	57
3.5.1.3	Comparison Between Numerical and Experimental Results	59
CHAPTER 4: NUMERICAL INVESTIGATION OF TRANSVERSE POST-TENSIONING ARRANGEMENT		66
4.1	Introduction.....	66
4.2	Adequate Number of Diaphragms	66
4.2.1	Analysis Progression.....	66
4.2.2	MDOT Specifications	67
4.2.3	Loading Steps.....	67
4.2.4	Bridge Models Generated Using 48 in. Wide Box-Beams.....	70
4.2.4.1	50 ft Span Bridge Model	70
4.2.4.2	62 ft Span Bridge Model	89
4.2.4.3	100 ft Span Bridge Model	96
4.2.4.4	124 ft Span Bridge Model	103
4.2.4.5	Effect of Deck Slab Concrete Strength on the TPT Arrangement	110
4.2.5	Bridge Models Constructed Using 36 in. Wide Box-Beams.....	112
4.2.5.1	50 ft Span Bridge Model	112
4.2.5.2	62 ft Span Bridge Model	115
4.2.5.3	100 ft Span Bridge Model	117
4.2.6	Discussion of the Results	121
4.3	Appropriate Transverse Post-Tensioning Force.....	123
4.3.1	Models Geometry.....	124

4.3.2	Bridge Models Generated Using 48 in. Wide Box-Beams	124
4.3.3	Bridge Models Generated Using 36 in. Wide Box-Beams	125
4.3.4	Bridge Models Generated Using 48 in. Wide Box-Beams	130
4.3.4.1	Two-Lane Bridge Model (Span = 50 ft, Width = 45 ft)	130
4.3.4.2	Three-Lane Bridge Model (Span = 50 ft, Width = 58 ft)	135
4.3.4.3	Four-Lane Bridge Model (Span = 50 ft, Width = 70 ft)	136
4.3.4.4	Five-Lane Bridge Model (Span = 50 ft, Width = 78 ft)	137
4.3.4.5	Two-Lane Bridge Model (Span = 100 ft, Width = 45 ft)	138
4.3.4.6	Three-Lane Bridge Model (Span = 100 ft, Width = 58 ft)	140
4.3.4.7	Four-Lane Bridge Model (Span = 100 ft, Width = 70 ft)	141
4.3.4.8	Five-Lane Bridge Model (Span = 100 ft, Width = 78 ft)	142
4.3.5	Bridge Models Generated Using 36 in. Wide Box-Beams	145
4.3.6	Discussion of the Results	149
CHAPTER 5: EXPERIMENTAL INVESTIGATION		151
5.1	Introduction	151
5.2	Bridge Model Construction Phase	152
5.2.1	Materials	152
5.2.1.1	Concrete	153
5.2.1.2	Steel Reinforcement	155
5.2.1.3	Carbon Fiber Reinforced Polymers (CFRP) Reinforcement	156
5.2.2	Formwork	160
5.2.3	Reinforcement Cages	166
5.2.4	End-Blocks	169
5.2.5	Transverse Diaphragms	171
5.2.6	Prestressing of Steel Strands	173
5.2.7	Concrete Placement	176
5.2.8	Release of Pre-Tensioning Forces	178
5.2.9	Transporting Precast Beams from Casting Yard to Test Frame	180
5.2.10	Addition of Superimposed Dead Load	180
5.2.11	Deck Slab Construction	184
5.2.11.1	Formwork Construction	184

5.2.11.2	Shear-Key Casting.....	184
5.2.11.3	Deck Slab Reinforcement.....	185
5.2.11.4	Placing of Concrete.....	186
5.2.12	Construction of Additional Exterior Box-Beam	186
5.3	Test Program Phase	190
5.3.1	Data Acquisition System.....	190
5.3.2	Instrumentation of the Bridge Model	190
5.3.3	Tests Conducted on the Bridge Model	191
5.3.3.1	Strain Distribution Test.....	192
5.3.4	Load Distribution Test	198
5.3.5	Stages of Test Program	203
5.3.5.1	Uncracked Deck Slab	203
5.3.5.2	Cracked Deck Slab.....	203
5.3.5.3	Damaged Beam Replacement	205
5.3.5.4	Ultimate Load Test	210
	CHAPTER 6: EXPERIMENTAL RESULTS AND DISCUSSIONS	212
6.1	Introduction.....	212
6.2	Transverse Strain Distribution	212
6.2.1	Introduction	212
6.2.2	Longitudinal Variation of Transverse Strains	213
6.2.3	Effect of Number of Diaphragms	216
6.2.4	Effect of Levels of TPT Forces.....	232
6.3	Load Distribution.....	243
6.3.1	Introduction	243
6.3.2	Derivation of Load Fraction and Percentage Improvement.....	243
6.3.3	Cracking of Deck Slab	245
6.3.4	Effect of Number of Diaphragms	248
6.3.4.1	Introduction.....	248
6.3.4.2	Deflection and Load Fraction of the Bridge Model.....	248
6.3.4.3	Improvement in the Behavior of the Bridge Model.....	255
6.3.5	Effect of Levels of TPT Forces.....	258

6.3.5.1	Introduction	258
6.3.5.2	Deflection and Load Fraction of the Bridge Model.....	258
6.3.5.3	Improvement in the Behavior of the Bridge Model.....	265
6.4	Ultimate Load Test	268
6.4.1	Introduction	268
6.4.2	Load-Deflection Response.....	269
6.4.3	Failure Mode	269
6.4.4	Concrete Compressive Strains	276
6.4.5	Variation of TPT Forces	277
6.4.6	Theoretical and Experimental Load-Carrying Capacities.....	278
6.4.7	Ductility	278
6.4.8	Evaluation of TPT System	279
CHAPTER 7: CONCLUSIONS AND RECOMMENDATIONS		285
7.1	Findings and Conclusions from the Experimental Study.....	285
7.1.1	Introduction	285
7.1.2	Conclusions	286
7.1.2.1	General	286
7.1.2.2	Strain Distribution Test.....	286
7.1.2.3	Load Distribution Test.....	287
7.1.2.4	Ultimate Load Test	287
7.1.3	Recommendations for Field Implementations and Future Research.....	288
7.2	Findings and Conclusions from the Numerical Study.....	289
7.2.1	Introduction	289
7.2.2	Adequate Number of Diaphragms	290
7.2.3	Appropriate TPT Force	291
REFERENCES.....		293
APPENDIX A: TRANSFER LENGTHS, PRE-TENSIONING FORCES, AND		
DIFFERENTIAL CAMBER MONITORING		299
APPENDIX B: CRACKING OF DECK SLAB.....		311
APPENDIX C: FLEXURAL DESIGN OF THE BRIDGE MODEL		320

LIST OF FIGURES

Figure 1.1-1	Deterioration of concrete due to leakage and corrosion.....	2
Figure 1.1-2	Deterioration due to lack of adequate post-tensioning in transverse direction.....	3
Figure 1.1-3	Damaged exterior prestressed concrete box-beam due to impact.....	4
Figure 1.1-4	Longitudinal cracks in deck slab along shear-keys between box-beams.....	5
Figure 1.1-5	Close-up view of field application of transverse diaphragm for unbonded CFRP strand.....	5
Figure 1.1-6	Details of seven transverse diaphragms for unbonded CFRP post-tensioning strands.....	6
Figure 1.1-7	Corrosion of longitudinal prestressing strands.....	6
Figure 2.5-1	Effect of number of internal transverse diaphragms on the load distribution factor when skew angle is 60° (Khaloo and Mirzabozorg, 2003).....	17
Figure 2.5-2	Design chart for effective post-tensioning force (El-Remaily et al., 1996).....	18
Figure 2.6-1	Reported experimental program by Klaiber et al. (2001).	19
Figure 2.7-1	Diaphragm effects on load distribution factors (Cai and Sahawy, 2004).....	21
Figure 2.9-1	Effect of bridge skew angle on load distribution factor (Barr et al., 2001).	23
Figure 3.2-1	Cross-sectional details for box-beams.	27
Figure 3.2-2	Cross-sectional details for box-beams (continued).	28
Figure 3.2-3	Cross-sectional details for box-beams (continued).	29
Figure 3.2-4	Brick element used in modeling box-beams (ABAQUS Manual, 2006).	30
Figure 3.2-5	Three dimensional view for box-beam sides.	31
Figure 3.2-6	Compressive behavior for the concrete material in the box-beams (Nawy, 2003).	32
Figure 3.2-7	Tensile behavior for the concrete material in the box-beams (Nawy, 2003).....	33
Figure 3.2-8	Stress-strain curve for prestressing steel strands (Nawy, 2003).....	35
Figure 3.2-9	CFCC with end bearing plates.	36
Figure 3.2-10	Deck slab FE mesh.	37
Figure 3.2-11	Deck slab connection with box-beams.	39
Figure 3.2-12	Deck slab reinforcement.....	41
Figure 3.2-13	Idealized stress-strain curve for reinforcement bars.....	42

Figure 3.2-14 Elastomeric bearing pad for one beam.....	43
Figure 3.2-15 Meshing of the bearing pad.....	44
Figure 3.4-1 AASHTO LRFD HL-93 load (longitudinal direction).....	49
Figure 3.4-2 Truck in AASHTO load HL-93.....	50
Figure 3.4-3 Typical positive temperature gradient over the bridge depth in Michigan.....	51
Figure 3.5-1 Half-scale experimental bridge model.....	54
Figure 3.5-2 FE bridge model components.....	56
Figure 3.5-3 FE model meshing.....	57
Figure 3.5-4 Load setup (experimental model).....	58
Figure 3.5-5 Load setup (numerical model).....	58
Figure 3.5-6 Deflection of the bridge model under vertical load of 20,000 lb.....	60
Figure 3.5-7 Deflection of the bridge model under vertical load of 30,000 lb.....	60
Figure 3.5-8 Deflection of the bridge model under vertical load of 40,000 lb.....	61
Figure 3.5-9 Deflection of the bridge model under vertical load of 50,000 lb.....	61
Figure 3.5-10 Deflection of the bridge model under vertical load of 60,000 lb.....	62
Figure 3.5-11 Deflection of the bridge model under vertical load of 70,000 lb.....	62
Figure 3.5-12 Crack development in the slab under vertical load up to 40,000 lb.....	63
Figure 3.5-13 Crack development in the slab under vertical load of 50,000 lb.....	63
Figure 3.5-14 Crack development in the slab under vertical load of 60,000 lb.....	64
Figure 3.5-15 Crack development in the slab under vertical load of 70,000 lb.....	64
Figure 3.5-16 Crack development in the slab under vertical load of 80,000 lb.....	65
Figure 3.5-17 Crack development in the experimental bridge model under load of 80,000 lb.....	65
Figure 4.2-1 Assembly of 50 ft span bridge model.....	76
Figure 4.2-2 Exaggerated deformed shape of the slab before and after applying positive temperature gradient (Scale 1:500).....	77
Figure 4.2-3 Crack development in the slab bottom surface after applying AASHTO HS-25 truck.....	78
Figure 4.2-4 Crack development in the slab after applying AASHTO HL-93 load.....	79
Figure 4.2-5 Crack development in the slab after applying AASHTO HS-25 truck.....	80
Figure 4.2-6 Crack development in the slab after applying AASHTO HS-93 truck.....	81

Figure 4.2-7 Crack development in the slab bottom surface due to TPT force.	82
Figure 4.2-8 Crack development in box-beam sides due to TPT force.	82
Figure 4.2-9 Modified assembly for 50 ft span bridge model.	83
Figure 4.2-10 Crack development in the slab after applying AASHTO HS-25 truck.	84
Figure 4.2-11 Crack development in the slab after applying AASHTO HL-93 load.	85
Figure 4.2-12 Crack development in slab after applying AASHTO HS-25 truck.	86
Figure 4.2-13 Crack development in slab after applying AASHTO HL-93 load.	87
Figure 4.2-14 Service loads contribution in deck slab principal stresses.	88
Figure 4.2-15 Assembly for 62 ft span bridge model.	91
Figure 4.2-16 Crack development in slab after applying AASHTO-HS 25 truck.	92
Figure 4.2-17 Crack development in slab after applying AASHTO HL-93 truck.	93
Figure 4.2-18 Assembly for modified 62 ft span bridge model.	94
Figure 4.2-19 Service loads contribution in deck slab principal stresses.	95
Figure 4.2-20 Assembly for 100 ft span bridge model.	98
Figure 4.2-21 Crack development in the slab after applying equivalent AASHTO HS-25 truck.	99
Figure 4.2-22 Crack development in the slab after applying equivalent AASHTO HL-93 load.	100
Figure 4.2-23 Assembly for modified 100 ft span bridge model.	101
Figure 4.2-24 Service loads contribution in deck slab principal stresses.	102
Figure 4.2-25 Assembly of 124 ft span bridge model.	105
Figure 4.2-26 Crack development in the slab after applying equivalent AASHTO HS-25 truck.	106
Figure 4.2-27 Crack development in the slab after applying equivalent AASHTO HL-93 load.	107
Figure 4.2-28 Modified assembly of 124 ft span bridge model.	108
Figure 4.2-29 Service loads contribution in deck slab principal stresses.	109
Figure 4.2-30 50 ft span bridge model constructed using 36 in. wide box-beams.	113
Figure 4.2-31 Crack development in the slab bottom surface after applying AASHTO HL- 93 load.	114

Figure 4.2-32 Crack development in the slab bottom surface after applying 120% of AASHTO HL-93 load.	114
Figure 4.2-33 Assembly of 62 ft span bridge model constructed using 36 in. wide box-beams.	115
Figure 4.2-34 Crack development in the slab bottom surface after applying AASHTO HL-93 load.	116
Figure 4.2-35 Crack development in the slab bottom surface after applying 120% of AASHTO HL-93 load.	116
Figure 4.2-36 Assembly of 100 ft span bridge model constructed using 36 in. wide box-beams.	118
Figure 4.2-37 Crack development in the slab bottom surface after applying AASHTO HL-93 load.	118
Figure 4.2-38 Modified assembly of 100 ft span bridge model constructed using 36 in. wide box-beams.	119
Figure 4.2-39 Crack development in the slab bottom surface after applying equivalent AASHTO HL-93 load.	120
Figure 4.2-40 Crack development in the slab bottom surface after applying 120% of equivalent AASHTO HL-93 load.	120
Figure 4.2-41 Adequate number of diaphragms for bridges constructed using 48 in. wide beams.	122
Figure 4.2-42 Adequate number of diaphragms for bridges constructed using 36 in. wide beams.	122
Figure 4.3-1 FE models to establish the appropriate TPT force.	126
Figure 4.3-2 Bridge widths examined under different loading cases.	127
Figure 4.3-3 Load locations for live loads (3-lane model, isometric view).	128
Figure 4.3-4 Load locations for live loads (3-lane model, front view).	129
Figure 4.3-5 Crack development in the slab bottom surface after applying AASHTO HS-25 truck (Location I, TPT = 125,000 lb/diaphragm).	132
Figure 4.3-6 Crack development in the slab bottom surface after applying 120% of AASHTO HS-25 truck (Location I, TPT = 125,000 lb/diaphragm).	132

Figure 4.3-7	Crack development in the slab bottom surface after applying AASHTO HS-25 truck (Location II, TPT = 125,000 lb/diaphragm).....	133
Figure 4.3-8	Crack development in the slab bottom surface after applying 120% of AASHTO HS-25 truck (Location II, TPT = 125,000 lb/diaphragm).	133
Figure 4.3-9	Crack development in the slab bottom surface after applying AASHTO HS-25 truck (Location III, TPT = 125,000 lb/diaphragm).	134
Figure 4.3-10	Crack development in the slab bottom surface after applying AASHTO HS-25 truck (Location III, TPT = 150,000 lb/diaphragm).	134
Figure 4.3-11	Bridge models generated using 36 in. wide box-beams (spans).	147
Figure 4.3-12	Bridge models generated using 36 in. wide box-beams (widths).	148
Figure 4.3-13	Appropriate TPT force vs. bridge width (valid for bridges constructed using 36 or 48 in wide box-beams).....	150
Figure 5.1-1	General view of precast prestressed box-beam bridge model.....	151
Figure 5.2-1	Compressive strength of concrete with time.	154
Figure 5.2-2	Typical uniaxial compression test setup for concrete cylinders.....	155
Figure 5.2-3	Dimensions of 1×7, 0.67 in. diameter CFCC for TPT.	159
Figure 5.2-4	Cross-section of formwork.....	160
Figure 5.2-5	Details of the steel notches.	161
Figure 5.2-6	Formwork prepared for box-beams.	161
Figure 5.2-7	Cross-section of the formwork for the interior box-beams.	162
Figure 5.2-8	Cross-section of the formwork for the exterior box-beams.	162
Figure 5.2-9	Longitudinal section of the formwork.	163
Figure 5.2-10	Plan view of the formwork for box-beams.	164
Figure 5.2-11	Plan view of the formwork for box-beams with projected side plates.	165
Figure 5.2-12	Cross-sectional details of the box-beams.....	167
Figure 5.2-13	Cross-sectional details of the box-beams at diaphragms.....	167
Figure 5.2-14	Longitudinal section details of box-beams.	168
Figure 5.2-15	Steel reinforcement cages containing Styrofoam within.....	169
Figure 5.2-16	Cross-sectional details of the end diaphragm.	170
Figure 5.2-17	Reinforcement of interior box-beams at the end diaphragm.....	170
Figure 5.2-18	Reinforcement of exterior box-beams at the end diaphragm.	171

Figure 5.2-19 Cross-sectional details of intermediate diaphragm.....	172
Figure 5.2-20 Reinforcement of interior box-beams at the intermediate diaphragm.	172
Figure 5.2-21 Reinforcement of exterior box-beams at the intermediate diaphragm.....	173
Figure 5.2-22 Reinforcements and oval-shape ducts at the transverse diaphragms locations.....	174
Figure 5.2-23 Instrumentation of the pre-tensioning steel strands.	175
Figure 5.2-24 Pre-tensioning operation at the live-end of the box-beam.	176
Figure 5.2-25 Conducting concrete slump test and casting the cylinders.....	178
Figure 5.2-26 Placement of concrete and curing process.....	179
Figure 5.2-27 Instrumentation on box-beams and shock de-tensioning of steel strands.....	181
Figure 5.2-28 Transportation of precast box-beams to the STC.	181
Figure 5.2-29 Plan view of the box-beams.	182
Figure 5.2-30 Aerial view of the four box-beams.	183
Figure 5.2-31 Box-beams placed side-by-side and adding superimposed dead loads.	183
Figure 5.2-32 Preparation of keyways before casting of shear-key.....	185
Figure 5.2-33 Construction of shear-key using FSSC grout.	185
Figure 5.2-34 Application of initial TPT forces and casting of deck slab.	186
Figure 5.2-35 Casting of deck slab concrete and curing process.	187
Figure 5.2-36 Cross-section of the completed box-beam bridge model.	188
Figure 5.2-37 Construction of additional exterior box-beam.....	189
Figure 5.3-1 Data acquisition system.....	190
Figure 5.3-2 Instrumentation of the bridge model before the test setup.	192
Figure 5.3-3 Layout of the strain gages installed on the deck slab.	193
Figure 5.3-4 Details of the unbonded TPT system.	195
Figure 5.3-5 Typical dead-end of TPT system.	196
Figure 5.3-6 Arrangements for strain distribution test.	197
Figure 5.3-7 Load distribution test setup.	198
Figure 5.3-8 Load distribution test with the application of TPT forces at five diaphragms. .	199
Figure 5.3-9 Load distribution test with the application of TPT forces at four diaphragms. .	200
Figure 5.3-10 Load distribution test with the application of TPT forces at three diaphragms.....	201

Figure 5.3-11 Load distribution test without applying TPT forces at any diaphragm.	202
Figure 5.3-12 Setup for cracking exterior shear-key C-C.	204
Figure 5.3-13 Setup for cracking interior shear-key B-B.	205
Figure 5.3-14 Separation of exterior beam B-4 by saw cutting through shear-key C-C.	207
Figure 5.3-15 Removal of the remaining grout from the bridge model.	207
Figure 5.3-16 Drilling of horizontal holes and attachment of Styrofoam gasket.	208
Figure 5.3-17 Placement of new beam and grouting the keyway.	208
Figure 5.3-18 Materials used and insertion of epoxy into the drilled holes.	209
Figure 5.3-19 Construction of formwork and casting of deck slab.	210
Figure 5.3-20 Experimental setup and instrumentation of the bridge model.	211
Figure 5.3-21 Ultimate load test setup.	211
Figure 6.2-1 Transverse strain distribution due to applying 80 kip at five diaphragms.	217
Figure 6.2-2 Transverse strain distribution due to applying 40 kip at five diaphragms.	218
Figure 6.2-3 Transverse strain distribution due to applying 20 kip at five diaphragms.	219
Figure 6.2-4 Transverse strain distribution due to applying 80 kip at four diaphragms.	220
Figure 6.2-5 Transverse strain distribution due to applying 40 kip at four diaphragms.	221
Figure 6.2-6 Transverse strain distribution due to applying 20 kip at four diaphragms.	222
Figure 6.2-7 Transverse strain distribution due to applying 80 kip at three diaphragms.	223
Figure 6.2-8 Transverse strain distribution due to applying 40 kip at three diaphragms.	224
Figure 6.2-9 Transverse strain distribution due to applying 20 kip at three diaphragms.	225
Figure 6.2-10 Transverse strains for shear-key A-A due to TPT force of 80 kip at different number of diaphragms.	229
Figure 6.2-11 Transverse strains for shear-key A-A due to TPT force of 40 kip at different number of diaphragms.	230
Figure 6.2-12 Transverse strains for shear-key A-A due to TPT force of 20 kip at different number of diaphragms.	231
Figure 6.2-13 Transverse strains for shear-key A-A due to applying different levels of TPT force at five diaphragms.	235
Figure 6.2-14 Transverse strains for shear-key A-A due to applying different levels of TPT force at four diaphragms.	236

Figure 6.2-15 Transverse strains for shear-key A-A due to applying different levels of TPT force at three diaphragms.	237
Figure 6.2-16 Transverse strains at point B-9 due to different levels of TPT force.	238
Figure 6.2-17 Transverse strains at point B-7 due to different levels of TPT force.	239
Figure 6.2-18 Transverse strains at point B-5 due to different levels of TPT force.	240
Figure 6.2-19 Transverse strains at point B-3 due to different levels of TPT force.	241
Figure 6.2-20 Transverse strains at point B-1 due to different levels of TPT force.	242
Figure 6.3-1 Bridge model in the uncracked stage with no external Load.	244
Figure 6.3-2 Deflection of the bridge model when loaded.	244
Figure 6.3-3 Cracks of deck slab at mid-span.	246
Figure 6.3-4 Cracks pattern of deck slab.	247
Figure 6.3-5 Load-deflection response of the bridge model while loading beam B-1.	249
Figure 6.3-6 Load-deflection response of the bridge model while loading beam B-2.	250
Figure 6.3-7 Load-deflection response of the bridge model while loading B-3.	250
Figure 6.3-8 Load-deflection response of the bridge model while loading beam B-4.	251
Figure 6.3-9 Load-deflection response for beam B-1 after repairs.	253
Figure 6.3-10 Load-deflection response for B-2 after repairs.	253
Figure 6.3-11 Load-deflection response for B-3 after repairs.	254
Figure 6.3-12 Load-deflection response for B-4 after repairs.	254
Figure 6.3-13 Effect of number of diaphragms on <i>PI</i> for loading beam B-1.	256
Figure 6.3-14 Effect of number of diaphragms on <i>PI</i> for loading beam B-2.	257
Figure 6.3-15 Effect of number of diaphragms on <i>PI</i> for loading beam B-3.	257
Figure 6.3-16 Effect of number of diaphragms on <i>PI</i> for loading beam B-4/5.	258
Figure 6.3-17 Load-deflection response for beam B-1 at different level TPT force.	260
Figure 6.3-18 Load-deflection response for beam B-2 at different level TPT force.	260
Figure 6.3-19 Load-deflection response for beam B-3 at different level TPT force.	261
Figure 6.3-20 Load-deflection response for beam B-4 at different level TPT force.	261
Figure 6.3-21 Load-deflection response for beam B-1 after repairs at different TPT forces.	263
Figure 6.3-22 Load-deflection response for beam B-2 after repairs at different TPT forces.	263
Figure 6.3-23 Load-deflection response for beam B-3 after repairs at different TPT forces.	264
Figure 6.3-24 Load-deflection response for beam B-4 after repairs at different TPT forces.	264

Figure 6.3-25 Effect of varying levels of TPT forces on <i>PI</i> for beam B-1	266
Figure 6.3-26 Effect of varying levels of TPT forces on <i>PI</i> for beam B-2	266
Figure 6.3-27 Effect of varying levels of TPT forces on <i>PI</i> for beam B-3	267
Figure 6.3-28 Effect of varying levels of TPT forces on <i>PI</i> for beam B-4/5.....	267
Figure 6.4-1 Load-deflection response of box-beam B-1 for different loading/unloading cycles.....	271
Figure 6.4-2 Load-deflection response of box-beam B-2 for different loading/unloading cycles.....	272
Figure 6.4-3 Load-deflection response of box-beam B-3 for different loading/unloading cycles.....	273
Figure 6.4-4 Load-deflection response of box-beam B-5 for different loading/unloading cycle.	274
Figure 6.4-5 Deflection of the bridge model at different levels of applied load.	275
Figure 6.4-6 Failure of bridge model.	276
Figure 6.4-7 Crushing of concrete near the location of the strain gages.....	280
Figure 6.4-8 Concrete compressive strains at the top surface of deck slab during ultimate load cycle.	281
Figure 6.4-9 Layout of transverse diaphragms and CFCC.....	282
Figure 6.4-10 Variation of TPT forces for the ultimate load cycle.....	283
Figure 6.4-11 Elastic and inelastic energy bands of the bridge model during the ultimate load cycles.....	284

LIST OF TABLES

Table 3.2-1 Box-beam depths for the investigated spans.....	27
Table 3.2-2 Post-tensioning tendons location (MDOT Bridge Design Guide 6.65.13, 2006).	30
Table 3.2-3 Details of box-beam reinforcement for different spans.....	34
Table 3.2-4 Material properties for prestressing steel strands.	34
Table 3.2-5 Material properties for CFCC.	36
Table 3.2-6 Material properties for the concrete in the deck slab.....	40
Table 3.4-1 Multiple presence factor, m (AASHTO LRFD 3.6.1.1.2, 2004).....	48
Table 4.2-1 Maximum principal stresses in the deck slab of 50 ft span bridge model under service loads.....	88
Table 4.2-2 Maximum principal stress in the deck slab of 62 ft span bridge model under service loads.....	95
Table 4.2-3 Maximum principal stress in the deck slab of 100 ft span bridge model under service loads.....	102
Table 4.2-4 Maximum principal stresses in the deck slab of 124 ft span bridge model under service loads.	109
Table 4.2-5 Maximum principal stresses in the deck slab for bridge models with different deck slab concrete strengths.	111
Table 4.3-1 Stress development in the deck slab due to surface loads in FE bridge models generated using 48 in. wide box-beams.....	144
Table 4.3-2 Stress development in the deck slab due to surface loads in FE bridge models generated using 36 in. wide box-beams.....	146
Table 5.2-1 Concrete mix proportions for beams.....	153
Table 5.2-2 Mechanical properties of the concrete mix.....	154
Table 5.2-3 Characteristics and mechanical properties of a typical seven-wire steel strand. ..	156
Table 5.2-4 Mechanical properties of the non-pretressing bars and stirrups.	157
Table 5.2-5 CFCC Quality Report (Tokyo Rope Mfg. Co., Ltd., 2007).	158
Table 5.2-6 Pre-tensioning forces and the corresponding elongations of steel strands.....	177
Table 5.2-7 Mechanical properties of FSSC.....	184

Table 5.2-8 Compressive strength of shear-key grout.	187
Table 5.2-9 Concrete mix proportions for deck slab.	187
Table 5.3-1 Elongation of CFCC at three different levels of TPT force.	195
Table 6.2-1 Rate of increase in the transverse strains in $\mu\epsilon/\text{kip}$	228
Table 6.2-2 Average transverse strains.	234

EXECUTIVE SUMMARY

Prestressed precast concrete box-beam bridges have numerous advantages over other types of bridges such as low life-cycle costs, quick and easy construction, and low depth-to-span ratio. Nevertheless, there are several problems associated with the performance of side-by-side box-beam bridges. One of the major distress types in the side-by-side box-beam bridges is the longitudinal cracks in the deck slab above the shear-keys between the adjacent box-beams. The crack development can cause secondary distresses associated with lack of transverse load distribution leakages, debonding, delamination, and corrosion of steel reinforcements. A frequent challenge in box-beam bridges is the misalignment of transverse post-tensioning (TPT) ducts, which arises as a result of differential camber between the adjacent box-beams. Furthermore, the replacement of a damaged beam is difficult with the use of bonded TPT steel strands in side-by-side box-beam bridges.

The use of transverse post-tensioning (TPT) force has been considered as a viable solution to the development of longitudinal cracks in the box-beam bridges (El-Remaily et al., 1996). To examine the influence of the level of TPT and the number of the transverse diaphragms on the performance of the bridge model in the transverse direction, experimental and numerical research program developed. The experimental program included the construction, instrumentation, and testing of one half-scale 30° skew side-by-side box-beam bridge model with effective span of 31 ft. The experimental bridge model consisted of four adjacent precast prestressed concrete box-beams interconnected using full-depth shear-keys, reinforced composite deck slab, and unbonded TPT carbon fiber reinforced polymer (CFRP). The numerical study included performing extensive finite element (FE) analysis using ABAQUS, which is a commercially available software package. A series of finite element models were generated to simulate a wide range of side-by-side box-beam bridges with different spans and different widths. Different loading cases were evaluated to establish the adequate number of diaphragms and the appropriate TPT forces, in order to prevent the development of longitudinal deck slab cracks. The experimental program consisted of load distribution test conducted during three different deck slab conditions of the bridge model. These conditions were uncracked, cracked, and the repaired deck slab. Transverse strain distribution test was conducted in the stage where the deck slab was uncracked. The cracked stage involved the

initiation of longitudinal cracks above the shear-key locations while the repaired stage involved the replacement of an assumed damaged exterior beam with a new one. The distribution of the transverse strain developed at the top surface of the deck slab and the deflection across the width of the bridge were examined for different combination of number of transverse diaphragms (five, four, and three) and the levels of TPT forces (20, 40, and 80 kip) at each transverse diaphragm. Once the load distribution test had been completed, the bridge model was loaded to failure to evaluate the response of the unbonded carbon fiber composite cables (CFCC) used for TPT strands and to assess the load-carrying capacity of the bridge model. The ultimate load test was conducted by applying an eccentric load using symmetrical two-point loading frame.

Analysis of the experimental results shows that the application of the TPT significantly improved load distribution among the side-by-side box-beams. Increasing the level of TPT forces generally improved the overall behavior of the bridge model in all the three cases studied. For this bridge model and load arrangements, the case of five diaphragms outperformed the three diaphragms case in terms of load distribution. Different arrangements of the TPT forces had insignificant influence on the transverse strains developed in the region between the diaphragms. From the ultimate load test results, it is noted that the TPT system coupled with the deck slab evenly distributed the eccentric load in the transverse direction until the complete failure of the bridge model. Furthermore, a close examination of the ten salvaged unbonded CFCC is clearly indicated that none of these strands experienced any rupture.

The numerical study revealed that the influence of the live load alone is not the major cause of the longitudinal cracks. However, combining the temperature gradient with the live load can lead to the development of longitudinal cracks between the adjacent beams. The adequate combination of number of diaphragms and TPT force level can delay the development of longitudinal cracks. The number of diaphragms is a function of the bridge span while the TPT force level is a function of the bridge width. Furthermore, using concrete of high strength in the deck slab can slightly reduce the amount of TPT forces required per diaphragm. The developed recommendations are summarized in design charts relating the number of the diaphragms to the bridge span and the TPT force level to the bridge width.

ACKNOWLEDGEMENTS

The authors would like to express their appreciation to the Michigan Department of Transportation (MDOT) in conjunction with the U.S. Federal Highway Administration (FHWA) for sponsoring this research project under Contract No. 2004-0105. The technical advice and directions provided by Roger Till, Steven Beck, and the members of the Research Advisory Panel of MDOT have been greatly helpful for the successful completion of this investigation. The staff of Center for Innovative Materials Research (CIMR), Lawrence Technological University, Charles Elder, Moheb Labib, Delali Noamesi, Prasadu Penjendra, Chenglin Wu, Charles Aziabor, Kapil Patki, Andrew Weller, Kendall Stevens, Lawrence Bukowski, and Tony Magnan extended their tremendous efforts and contributions. The carbon fiber composite cable (CFCC) for transverse post-tensioning were supplied by the Tokyo Rope Mfg. Co. Ltd., Japan. The opinions expressed in this project report are those of the authors and do not necessarily reflect the views of the sponsors.

CHAPTER 1: INTRODUCTION

1.1 Introduction

According to the United States Federal Highway Administration's 2005 National Bridge Inventory data, about 25% of the nation's 595,625 bridges are structurally deficient or functionally obsolete, as reported in the Better Roads Magazine, May 2007 issue. Such high number of structurally or functionally deficient bridges calls for weight limits, rehabilitation, or withdrawal and replacement. Corrosion of steel reinforcements, resulting from aggressive environmental conditions and the use of deicing salts, has been one of the major causes for deterioration of concrete bridge structures, as shown in Figures 1.1-1a and Figure 1.1-1b.

In Michigan State, the percentage is higher than the average 28% of Michigan's 10,825 bridges are structurally deficient or functionally obsolete. It has been reported that in Michigan, bridge deterioration is primarily the combined result of 1) use of deicing salts leading to corrosion of conventional steel reinforcement, 2) repeated freeze and thaw cycles, 3) development of longitudinal cracks between the side-by-side box-beams allowing ingress of water, which accelerates rate of corrosion, 4) uneven load distribution giving rise to dissimilar deterioration of beams, and 5) heavy traffic volume and axle loads (Better Roads Magazine, May, 2007).

Prestressed concrete bridges make up a major portion of the bridges constructed in Michigan and USA where the typical cross-sections used are I- or T-sections, and spread or side-by-side box-beams. Prestressed concrete box-beams are commonly used in bridge construction due to their many advantages as follows.

1. High torsional stiffness making the box-beam sections ideal for curved bridge alignments and for segmental bridge construction.
2. High span-to-depth ratios making a suitable choice for longer spans.
3. Structural stability and good aesthetic appearance due to monolithic construction.



(a) Deterioration and concrete spalling



(b) Deterioration and leakage

Figure 1.1-1 Deterioration of concrete due to leakage and corrosion.

However, side-by-side box-beam bridges are prone to the development of longitudinal cracks in the deck slabs where the cracks are observed above the longitudinal shear-key joints between adjacent box-beams. Currently, the side-by-side box-beam bridges are designed with transverse post-tensioning (TPT) arrangements to limit the development of longitudinal deck cracking as well as limit any differential movement between the adjacent box-beams, once the cracks have formed. However, the current design of the TPT arrangement is not adequate in preventing deck cracking. Typical results of deck cracking observed over side-by-side box-beam is seen in Figure 1.1-2. The presence of the longitudinal cracks above the longitudinal shear-key joint allows water and deicing solutions to saturate the concrete near the joints. It is well known that the presence of chloride leads to accelerated corrosion of the reinforcing and prestressing steel. Furthermore, the seepage of water through the shear-key during freezing conditions allows for the formation of icicles below the bridge surface. The unexpected falling of icicles can pose a high risk for vehicles moving under the bridges.



Figure 1.1-2 Deterioration due to lack of adequate post-tensioning in transverse direction.

Several issues are addressed in this report to improve the performance of prestressed concrete side-by-side box-beam bridges. These issues include: 1) replacement of

interior/exterior damaged bridge beams due to deterioration or high load impact (Figure 1.1-3), 2) longitudinal cracks in the deck slabs between the box-beams due to lack of TPT and joint detail (Figure 1.1-4), 3) unbonded TPT (Figure 1.1-5 and Figure 1.1-6), 4) deterioration of concrete and corrosion of steel strands resulting from leakage (Figure 1.1-7), and 5) misalignment of TPT ducts due to differential camber of box-beams of skew bridges.



Figure 1.1-3 Damaged exterior prestressed concrete box-beam due to impact.



Figure 1.1-4 Longitudinal cracks in deck slab along shear-keys between box-beams.



Figure 1.1-5 Close-up view of field application of transverse diaphragm for unbonded CFRP strand.



Figure 1.1-6 Details of seven transverse diaphragms for unbonded CFRP post-tensioning strands.



Figure 1.1-7 Corrosion of longitudinal prestressing strands.

1.2 Project Objectives

The main objective of this study is to determine the adequate TPT arrangement, which would delay and reduce the development of longitudinal deck cracking in side-by-side box-beam bridges. The results and recommendations of comprehensive numerical and experimental investigations would provide MDOT engineers guidance in developing revised design specifications for the TPT arrangement for side-by-side box-beam bridges. These design specifications would provide strategies for the construction and performance issues outlined in Section 1.1. The following tasks have been conducted to achieve the project objectives. The tasks were:

1. Conduct a numerical analysis to determine the adequate number of transverse diaphragms and the effective level of TPT forces applied with unbonded CFRP strands in order to avoid longitudinal cracking.
2. Construct, instrument, and test a one-half scale 30° skew box-beam bridge model with transverse diaphragms located at the two supports, quarter-span sections, and mid-span section.
3. Investigate the suitability and effectiveness of using unbonded CFCC for TPT.
4. Develop an adaptable construction approach to address the issue related to misalignment of transverse ducts due to differential camber experienced in skew box-beam bridges.
5. Recommend a suitable rehabilitation construction methodology to allow the replacement of a deteriorated/damaged box-beam within any part of the box-beam bridge.
6. Establish recommendations for revised construction and design specifications for side-by-side box-beam bridges.

1.3 Report Organization

This numerical and experimental research project on skewed prestressed concrete box-beam bridge models addresses the provision of adequate numbers of transverse diaphragms and their effective level of TPT forces. This report documents these efforts in the following chapters:

Chapter 2: This chapter presents a comprehensive review of the past research work conducted on variety of prestressed concrete bridges with particular focus on the performance of side-by-side box-beams with respect to longitudinal deck cracking.

Chapter 3 and 4: These chapters present the details of the finite element analysis of skewed prestressed concrete box-beam bridge. Furthermore, recommendations have been made for the TPT arrangement for side-by-side box-beam bridges with spans ranging from 50 ft to 120 ft and widths ranging from 24 ft to 72 ft. The TPT arrangement included the levels of TPT force, and the number of transverse diaphragms.

Chapter 5: This chapter presents the details of the experimental program for a 30° skewed prestressed concrete box-beam bridge model including details of the construction, instrumentation, test setup, and test procedures.

Chapter 6: This chapter presents the discussion of the experimental results.

Chapter 7: This chapter presents the project conclusions and recommendations.

CHAPTER 2: LITERATURE REVIEW

2.1 Introduction

This chapter presents a comprehensive literature review conducted on the use of transverse post-tensioning (TPT) in bridges with particular focus on side-by-side box-beam bridges. Precast prestressed concrete members are widely used in the construction of bridges due to their constructional, structural, and field advantages. The use of box-beam bridges in USA has increased gradually since the year 1955 due to distinctive advantages (Taly, 1998; and Aktan et al., 2004):

1. High span-to-depth ratio of box sections provide a slender and aesthetically pleasing appearance.
2. Monolithic construction imparts structural stability as well as enhanced appearance;
3. High torsional stiffness of box-beam sections make them ideal for curvilinear and segmental bridge construction.
4. High industry acceptance of box-beam bridges due to their simple design, rapid construction, and low life-cycle cost.

However, as discussed in Chapter 1, the performance issues and construction challenges associated with the current design details and construction practices of precast prestressed concrete box-beam bridges warrants an in-depth review of the factors that affect these issues and challenges. The service life performance of side-by-side box-beams is measured in terms of the load distribution between the girders when subjected to vehicle loading, the presence or absence of longitudinal deck cracking, and the deterioration of the concrete and reinforcing material. These measures are affected by TPT force level, number of transverse diaphragms, shear-key design, bonded versus unbonded post-tensioning strands, and skew angle.

Significant experimental, field, and numerical investigations have been performed over the last two decades, providing an improved understanding on the interaction between the measures and the factors. One of the key findings was that TPT could be used as a mitigating design feature to control deck and shear-key cracking. However, a significant portion of the research was directed towards bridge systems other than side-by-side box-beam bridges.

Therefore, this literature review synthesizes the general knowledge as it pertains to side-by-side box-beam bridges with TPT arrangements through the beam sections. Emphasis has been placed on features that overcome some of the prominent performance problems such as cracking in skewed side-by-side box-beam bridges.

Service life performance and the durability/longevity of bridges have been regarded as crucial factors in bridge management nationwide (Ramey and Wright, 1997a and 1997b). Premature and accelerated distress development in bridge decks, in particular, was often observed where aggressive weather and heavy traffic conditions prevailed. Hence, aspects associated with these loading and environmental conditions should be integral parts of a design and bridge management program (Ramey et al., 1997a and 1997b). Particular performance issues for box-beam bridges were reported by Aktan et al. (2004). Evaluation of 15 side-by-side prestressed concrete box-beam bridges with skew angles $\leq 30^\circ$ indicated that the major distresses were related to beam moisture, shear-key moisture, beam cracking, spalling, shear-key cracking, and deck condition. The study recommended 1) inspecting the concrete cover of the prestressing tendon near the top of the bottom flange, and 2) developing detailed finite element models to represent the entire bridge system as a way to analyze shear-key cracking, movement between adjacent beams, and structural capacity. Furthermore, the study found a need to confirm the effectiveness of various employed maintenance and repair techniques.

In 1998, the Ohio Department of Transportation (ODOT) constructed a high performance concrete (HPC) side-by-side box-beam bridge (Greuel et al., 2000). In this bridge, an experimental shear-key was utilized at mid-depth of the cross-section whereas the beams were tightened together using non-prestressed threaded rods located transversely through diaphragms at the ends and quarter-spans of the bridge. After constructing the entire bridge, it was subjected to eccentric load using four ODOT trucks filled with gravel to record load of 30 kip for each truck. It was reported that while subjecting the bridge to eccentric load, the deflection was larger on the loaded side than the opposite side of the bridge width. However, the side-by-side placed beams acted in unison, sharing the applied truck load, as evident from the live load distribution test.

Badwan and Liang in 2007, reported an analysis method, based on grillage analogy (skeleton structure with transverse loads), for calculating the required TPT stress for a deck

built with precast concrete multi-beams. The researchers concluded that the effect of skew angle was significant when the skew angle was greater than 30°. Furthermore, it was found that the required post-tensioning stress for optimum design of a precast concrete multi-beam deck was decreased with increase in skew angle. The tests were conducted with maximum skew angle of 45°.

2.2 Transverse Post-Tensioning

For decades, TPT has been used as a mitigating design feature to control deck and shear-key cracking (Moll, 1984; Phipps et al., 1985; Poston et al., 1985 and 1989). Analytical and experimental investigations indicated overall improved bridge performance in terms of strength and serviceability when applying substantial TPT forces through the deck of a slab-girder bridge model. This placed the majority of the deck slab in compression counteracting any tensile forces developed through loading. Poston et al. (1985, 1989) also concluded that transverse prestressing of a slab-girder or box-girder bridge effectively developed compressive stresses.

Thoman et al. (1984) conducted load tests on a single-cell box girder bridge with cantilever deck. The bridge incorporated TPT in the bridge deck. The experimental results were in agreement with the analytical models used to predict the behavior of the structure through the case study on the transverse cantilever decks of the bridge. Lately, Csagoly (1997) showed experimentally that post-tensioning prevented the formation of transverse surface cracking and decreased the tendency for longitudinal surface cracking when applied in bridge decks. Roschke and Pruski (2000) constructed a large, two-span $3/10$ scale model of a post-tensioned slab bridge in a laboratory, where in addition to uniformly distributed longitudinal post-tensioning a band of transverse tendons was placed in a narrow region directly above the supporting columns. The transverse strain distribution due to prestressing in the transverse direction was compared with the finite element results. It was concluded that the experimental and finite element results matched closely.

2.3 Finite Element Modeling of Transverse Post-Tensioning Arrangements

A simple mechanical model was developed and verified by Kaneko et al. (1993a and 1993b) for the analysis and design of plain and fiber reinforced concrete shear-key joints. The basic feature of the study was to identify two main fracture mechanisms for shear-off failure of the key joints such as single curvilinear cracking and development of multiple diagonal cracks. An experimental investigation was also conducted and good agreement was obtained between the experimental and numerical analysis results.

In a finite element study carried out by Issa et al. (1998), the main objective was to determine the amount of longitudinal post-tensioning required to secure the tightness of the transverse joints between the precast concrete bridge deck panels, and keep them in compression. Two finite element models analyzed were simply supported model and three-span models. The models were subjected to the load of an AASHTO HS-20 truck as a live load. The analysis revealed that for simply supported spans, the required longitudinal post-tensioning should not be less than 200 psi to secure the tightness of the transverse joints between the precast concrete bridge deck panels for simply supported bridges. The longitudinal post-tensioning should not be less than 450 psi to maintain transverse joint integrity at interior negative moment regions over supports in compression.

Experimental tests and finite element analyses of different bridges conducted by Barr et al. (2001) revealed that the use of end diaphragms, increased skew angle, and load type (truck and lane) significantly affected the live load distribution factors. On the other hand, continuity and intermediate diaphragms had the least effect. Earlier work by Sithichaikasem and Gamble (1972) as well as Stanton and Mattock (1986) contradict these findings. For the exterior girders, the intermediate diaphragms slightly increased the live load distribution factor at low skew angles. At high skew angles ($\geq 30^\circ$), the diaphragms were slightly beneficial. At larger skew angles, the live load distribution factor decreased with increasing skew.

2.4 Shear-Key Performance

The longitudinal grouted shear-key connection between side-by-side precast, prestressed concrete box-beams enables the shear load transfer between the adjacent elements. Different types of non-shrink grouts may be used to fill the keyways. The load distribution amongst the

adjacent girders is thus dependent on the performance of shear-keys. Moreover, failure of a shear-key leads to uneven live load distribution, stressing the individual girders excessively, which results in the formation of longitudinal cracks giving a path for water to seep through, thereby increases the risk of accelerated corrosion of the reinforcing steel. For determining transverse shear intensity in the shear-keys of multi-beam bridges due to design vehicle loads, a simplified method was presented by Bakht et al. (1983). It was shown that the behavior of multi-beam bridges could be characterized by a single, dimensionless parameter, without relying on any empirical approach. Later, connection response was modeled by linear and rotational springs resisting relative displacement between adjacent beams of a prestressed precast skewed multi-beam double-tee bridge by Jones and Boaz (1986).

2.4.1 Location of Shear-Key and Grout Material

Huckelbridge et al. (1995) and Huckelbridge (1996) investigated the in-situ performance of the grouted shear-keys, located at the longitudinal joints between adjacent girders of multi-beam prestressed box bridges. All the bridges tested, exhibited relative displacements across at least some of the joints, which indicated a fractured shear-key. The study proposed to locate the shear-key at the neutral axis level of the cross-section. With the use of such new shear-key design, El-Esnawi (1996) observed that the static shear load capacity was almost tripled from the current shear-key design with the same grouting material, and fatigue life of the new shear-key design was extended to over 8,000,000 cycles. Gulyas et al. (1995) made a comparative laboratory study on composite specimens for vertical shear, longitudinal shear, and direct tension, using two different grouting materials such as non-shrink grouts and mortars of magnesium ammonium phosphate. The results obtained indicated significant differences in performance between these two materials, which necessitate proper selection of grout material for constructing shear-keys.

Hlavacs et al. (1996) used a full-scale portion of a side-by-side box-beam bridge to test the performance of grouted shear-keys under environmental and cyclic loads. The shear-keys were grouted between the beams twice, first in the autumn season and second in the summer season. The beams were subjected to tests after each grouting in order to investigate the behavior of shear-keys. In the first test, shear-keys that were grouted in autumn cracked soon after casting, before any load had been applied. Data from instruments embedded in the beams and shear-

keys showed large discontinuities in strain caused by freezing temperatures in the following winter. Moreover, the strains caused by temperature were much larger than strains occurring under loads corresponding to the weight of an HS20-44 truck. The beams were subjected to 41,000 cycles of loading, simulating HS20-44 wheel loads. No new cracking occurred from the loading, but cracks caused by temperature propagated under loads. In the second test, high temperature caused by the sun heat on the top of the beams again caused large thermal strains, which cracked the shear-keys. These cracks were subjected to 10,000,000 cycles of the load corresponding to an HS20-44 wheel load. As in the first test, the load itself did not cause any cracks but the existing thermal cracks propagated under the load.

2.4.2 Thermal Stresses

The thermal cycles are believed to have significant influence on the load-carrying capacity of the joint formed at the shear-key locations. Not many studies have been conducted on the thermal effect owing to the difficulties in simulating it in an experimental setup. Miller et al. (1999) had studied three different shear-key configurations under thermal effects. The three shear-keys differed in their locations within the section and in the materials used. It was concluded that the shear-keys located towards the deck surface cracked primarily due to the thermal stresses caused by daily heating and cooling. The shear-keys provided at mid-depth of the section were found less susceptible to the thermal stresses. The cracks developed due to the thermal stresses initiated the cracking process which was further propagated by the live load applied. Notably, the thermal cracks were found to be more pronounced at the support locations than at the mid-span locations.

2.4.3 Construction Practices

Lall et al. (1998) studied performance of full-depth shear-keys and transverse tendon systems in adjacent prestressed box-beam bridges. The researchers recommended providing higher TPT forces and two tendons over the depth of the beam at each post-tensioning location. Proper grouting during the shear-key installation was shown to be essential, emphasizing sandblasting, pre-wetting of keyway surfaces and maintaining proper water cement ratio in the grout. Miller et al. (1999) studied different shear-key configurations and tests were conducted on a full-scale, four-beam assembly that represented part of a bridge. The mid-depth shear-key was found less

susceptible to the stresses developed and was found to be more resistant to cracking. The epoxy shear-keys did not crack. However, it is evident that further studies are warranted in order to arrive at the appropriate shape of shear-key and its location by investigating the behavior of shear-keys in transmission of forces across the adjacent bridge girders.

Issa et al. (2003) studied the performance of transverse joint grout material in precast concrete bridge deck systems. The study was performed on 36 full-scale specimens fabricated and tested under vertical shear, direct tension, and flexural capacity. Different grout materials were examined for the shear-key connection such as Set 45, Set 45 HW, Set Grout, and polymer concrete. The connected surfaces were sandblasted, cleaned from dust, dried, treated chemically with hydrochloric acid, HCL (10% solution) to eliminate carbonation, and then washed by water. The researchers recommended high quality control during the construction for such joints. The study revealed that polymer concrete was the best material for the transverse joints in terms of strength, bond, and mode of failure as compared to the rest of the Set grouts. The Set grouts however facilitated ease of construction.

2.5 Transverse Diaphragms

As mentioned erstwhile, research supports the use of post-tensioning of transverse beams, also denoted as diaphragms, in addition to or replacement of the transverse prestressing of the deck slab (El-Remaily et al., 1996; Ebeido and Kennedy, 1996a, 1996b). The transverse diaphragms help improve integrity of the side-by-side box-beam bridges through the post-tensioning applied through it, i.e. it help increase live load distribution evenly amongst the beams. The MDOT Bridge Design Guide 6.65.13 (2006) recommends the locations of post-tensioning tendons to be provided in prestressed concrete box-beam bridges.

The influence of intermediate transverse diaphragms on the distribution of reaction on the pier supports was investigated by Ebeido and Kennedy (1996a, 1996b) experimentally and through finite element analyses. It was found that the presence of intermediate transverse diaphragms played an important role in the distribution of shear forces at the pier supports, making the shear distribution more uniform thereby avoiding localization of forces. Such even distribution of live loads amongst adjacently placed beam in a bridge avoids faster deterioration of a particular beam, thereby delaying the need for replacement of the deteriorated beam. The

connection achieved through the transverse diaphragms was observed to improve bridge stiffness, load distribution, and increase ultimate load-carrying capacity.

The effect of arrangement of internal transverse diaphragms and skew angle was also investigated by Khaloo and Mirzabozorg (2003) using finite element models. The variation of defined load distribution factor (DF) with different arrangements of transverse diaphragms is reproduced here in Figure 2.5-1, for bridges with skew angle, $\theta = 60^\circ$ and three different I-girder spacing, S . Four different arrangements for internal transverse diaphragms of rectangular cross-sections were considered, designated with system type numbers 1 through 4. In system type number 1, the models did not include any internal transverse diaphragms. The internal transverse diaphragms, located at approximately each third point of the span length, were parallel to the supporting lines of the decks in system type number 2. The locations of the internal transverse diaphragms were based on AASHTO (1996) code and provided perpendicular to the longitudinal girders in system type number 3. Lastly, in system type number 4 the spacing between the internal transverse diaphragms was about 5 m, provided perpendicular to the longitudinal girders. Two standard trucks HS20-44 were used, placed side-by-side on the decks with $S = 1.8$ and 2.4 m, while for the decks with $S = 2.7$ m girder spacing, three trucks were used side-by-side. It was concluded that the effect of orientation of the internal diaphragms relative to the supporting lines and the girders on the load distribution was significant. Systems 3 and 4 showed significantly improved performance. In addition, the effect of spacing between internal transverse diaphragms perpendicular to the longitudinal girders might be neglected, such that the maximum difference between systems 3 and 4 is 7-10%.

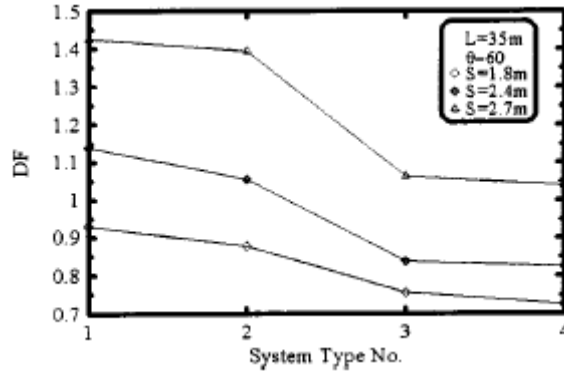


Figure 2.5-1 Effect of number of internal transverse diaphragms on the load distribution factor when skew angle is 60° (Khaloo and Mirzabozorg, 2003).

The contribution of intermediate diaphragms in enhancing precast bridge girder performance was investigated by Green et al. (2004) through modeling of the Florida Bulb Tee 78 precast concrete bridge girders. It was shown that the presence of intermediate diaphragms helped in stiffening of the precast bridge girders and thereby reduced maximum girder deflections. El-Remaily et al. (1996) reported an in-depth study on the design of TPT in adjacent precast prestressed concrete box girder bridges. They observed that post-tensioned transverse diaphragms serve as the primary mechanism for the distribution of wheel loads across the bridge. The amount of post-tensioning required at each diaphragm was shown to depend on the bridge geometry and loading, and a chart had been developed for the determination of the required amount of TPT (Figure 2.5-2). In general, it is observed that the level of post-tensioning recommended by the researchers is significantly higher than that suggested by the current MDOT Specifications. The researchers suggested use of a full-depth vertical shear-key at each diaphragm and the post-tensioning distributed equally between the top and bottom of the diaphragm. The authors recommended performing a detailed grid analysis for situations where large skew is present, and accurate results are needed.

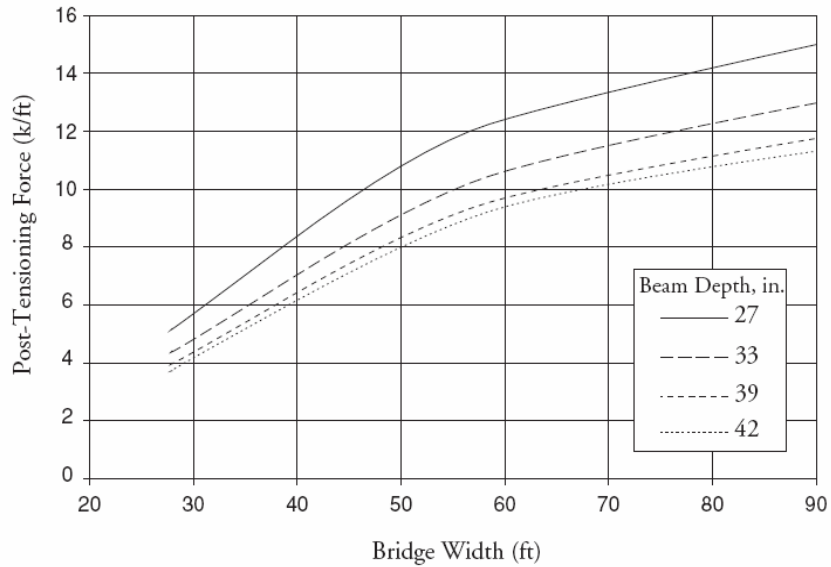


Figure 2.5-2 Design chart for effective post-tensioning force (El-Remaly et al., 1996).

Indented transverse pre-tensioning strands were shown to provide satisfactory prestress transfer by Yamane et al. (1998). In addition, the grouted post-tensioned transverse joints between precast panels were shown to exhibit satisfactory performance. For a deck replacement project, it was also advised to develop a scheme to maintain continuity at the existing-to-new deck joint to avoid edge loading when the deck remains temporarily open to the traffic.

2.6 Load Distribution

The provision of shear-key, transverse prestressing, and deck slab facilitates the distribution of live loads amongst the adjacently placed box-beams in bridges. The effective transmission of loads evenly across the entire width of bridge reduces chances of differential movement among the side-by-side placed beams and relative joint opening at the beam bottom, thereby hindering development of longitudinal cracks and hence ensures improved performance and durability. The distribution of truck wheel loads and performance of joints between the two adjoining members in multi-beam precast bridges were investigated by Stanton and Mattock (1986). The report presented different types of geometric shapes of keys, connection methods such as a grouted key, welded steel connectors etc. and calculated the shear forces transmitted between

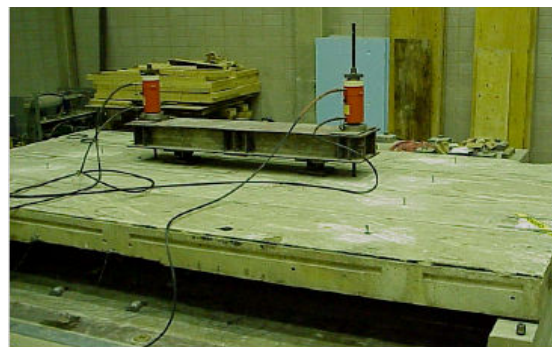
the members. They concluded that the grouted keyway was much stiffer than the steel connectors.

Abendroth et al. (1989) and Ebeido and Kennedy (1996a) had emphasized the role of transverse diaphragms in live load distributions and bridge load-carrying capacities. Transverse diaphragms tie the beams together to facilitate construction, transfer lateral loads (such as wind load), and improve vertical load (such as traffic load) distributions. It was concluded that both the span and support girder moments were decreased significantly with increases in the skew angle of the bridge, especially for skew angles $>30^\circ$. Moreover, the skew angle was shown to have more influence on the design of interior girders than the exterior girders. The presence of intermediate transverse diaphragms was shown to enhance load distribution characteristics of the bridge.

Service load tests were performed by Klaiber et al. (2001) on four deteriorated precast concrete deck bridge panels; two with shear-keys in place and two without. Based on the field results, it was determined that these bridges had sufficient lateral load distribution and adequate strength when shear-keys were properly installed between the adjacent panels. The measured lateral load distribution factors were larger than AASHTO values when the shear-keys were not installed. Since some of the reinforcement had hooks, deterioration of the reinforcement had a minimal effect on the service level performance of the bridges when there was minimal loss of cross-sectional area. Laboratory tests were performed on the precast concrete deck bridge panels obtained from three bridge replacement projects, as shown in Figure 2.6-1.



(a) Load distribution test



(b) Ultimate load test

Figure 2.6-1 Reported experimental program by Klaiber et al. (2001).

Twelve deteriorated panels were loaded to failure in a four-point bending arrangement (Klaiber et al., 2001). Although the panels had significant deflections prior to failure, the experimental capacity of eleven panels exceeded the theoretical capacity. Experimental capacity of the twelfth panel, an extremely distressed panel, was only slightly below the theoretical capacity. Service tests and an ultimate strength test were performed on a laboratory bridge model consisting of four joined panels to determine the effect of various shear connection configurations. These data were used to validate a finite element model of the precast concrete deck bridge providing more accurate live load distribution factors for use in rating calculations.

Results of structural load tests were performed on the Bridge Street Bridge, the first prestressed concrete bridge in the United States, reinforced almost entirely with CFRP (Grace et al., 2005). Based on the results from load tests, it was concluded that the applied loads per lane were effectively distributed to all four beams of each bridge span; the three spans of the bridge exhibited similar load distribution behavior; the actual load distribution behavior was consistent with the distribution factors derived from the provisions of the AASHTO (2004) Specifications, and that the provisions of the AASHTO Standard or LRFD Specifications could be used to predict the load distribution behavior of bridge superstructure.

2.7 Level of Prestressing

The extent of prestressing provided in the transverse direction affects the stiffness of the bridge and governs the structural behavior, and importantly the development of cracks under service load conditions. Many State DOTs recommend the use of prestressed transverse diaphragms. A study by Cai and Sahawy (2004) demonstrated the effect of the transverse diaphragms on load distribution factor (LDF) and maximum strain for different skew angles (see Figure 2.7-1) in bridges with I-girders. The normalization is made with the case when no diaphragm was provided. From the Figure, it is observed that the diaphragms had significant effect on LDF and maximum strain developed. However, this effect diminished with the increased skew angle. Increasing the number of diaphragms did not have much effect on LDF and maximum strain. They concluded that an increase of the diaphragm stiffness could significantly reduce both the strains developed and the load distribution. A full stiffness can be achieved by

prestressing the diaphragms, which also can prevent cracking and ensure the continuity of the diaphragms across the beams. Later a formula was proposed by Cai (2005) to quantify the intermediate diaphragm effect on live load distribution, and the results were compared with AASHTO (American Association of State Highway and Transportation Officials) LRFD (Load and Resistance Factor Design) load distribution factors.

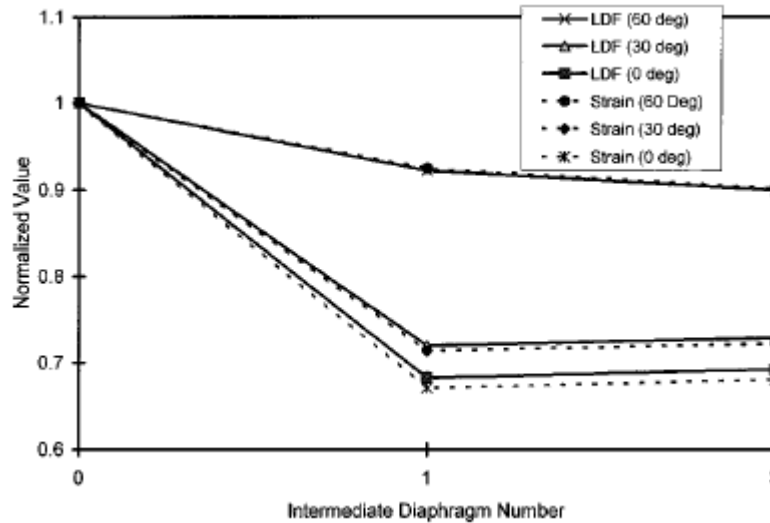


Figure 2.7-1 Diaphragm effects on load distribution factors (Cai and Sahawy, 2004).

Nevertheless, contradictory observations from the field studies of cracked bridge decks were reported by Chamberlain and Kreger (1999) - that the transverse post-tensioned strands were not successful in making the box girders act compositely. As the study was focused on field observations, no data is available to know if the increased level of TPT or increased number of transverse diaphragms would help the beams act in unison sharing the live load uniformly.

2.8 CFRP Bonded and Unbonded Transverse Prestressing

The use of fiber reinforced polymers (FRPs) in bridges has been started owing to its corrosion resistant properties and higher strength to weight ratio. A substantial amount of research work has been reported on the performance of FRPs when used for construction applications. A state-of-the-art paper by Bakis et al. (2002) presents a concise historical background, accomplishments of the investigations and research progress made so far on FRPs.

Furthermore, FRPs implemented successfully in real-life bridge construction projects were also reported by Grace et al. (2002).

Carbon fiber reinforced plastic tendons were used by Braimah et al. (1998) for transverse prestressing of a bridge model, and tested under simulated concentrated wheel loads. The test results showed that transverse prestressing considerably enhanced the punching failure loads of the deck slabs resting on steel I-beam girders. Grace and Abdel-Sayed (1998) discussed the comparative effectiveness of fully bonded and completely unbonded applications of the carbon fiber reinforced polymer (CFRP) tendons. The bridge models in this study consisted of CFRP rods grouted and ungrouted in the transverse direction. It was concluded that ductility of the bridges could be increased by keeping the transverse tendons unbonded.

Later, Marshe and Green (1999) described an experimental investigation on the punching behavior of composite bridge decks transversely prestressed with CFRP tendons. Their investigation provided information on the usefulness of transverse prestressing using CFRP, and the consequent effects. The transverse prestressing of the deck slab improves the compressive membrane action and allows a reduction in the slab thickness, however with a reduced thickness durability is a concern with steel prestressing tendons. By using FRP prestressing tendons, the durability of the bridge deck slab would be improved. The feasibility of using CFRP tendons to prestress the composite bridge decks in transverse direction was demonstrated by Marshe and Green (1999), and the CFRP prestressed bridge deck showed better overall structural performance than the steel prestressed deck.

2.9 Effect of Skew Angle on Load Distribution

In many bridge construction projects, due to the practical difficulties in providing a right-angled alignment of the bridges, skew alignments become inevitable. However, the load distribution amongst adjacent bridge girders is significantly influenced by the skew angle. El-Ali (1986); Bishara et al. (1993); and Khaloo and Mirzabozorg (2003) showed that the increase in skew angle reduced the ability of the bridge system to distribute the load between individual girders.

The ratio of distribution factor at any skew angle to the distribution factor at zero skew, illustrating the effect of skew, is shown in Figure 2.9-1 (Barr et al., 2001). Model 1 was a

simply supported, single-span model of span 80 ft with only the deck and girders modeled. This model did not account for lifts (the layer of concrete between the top of the girder and the bottom of the deck), intermediate diaphragms, end diaphragms, or span continuity. Model 2 was the same as model 1, but the lifts were included between the girders and deck. In model 3, intermediate diaphragms were added, and in model 4 end diaphragms were added. Model 5 was the same as model 4, but spans 80 ft were added and the three spans were made continuous. The skew angle of each model was varied between 0 and 60° to evaluate the effect of skew. It was concluded that skew had little effect for an angle of 20°, and for some models, the live load distribution factor actually increased slightly. However, at larger skew angles, the live load distribution factor decreased with increasing skew. In general, the interior girders were more affected by skew than were the exterior girders.

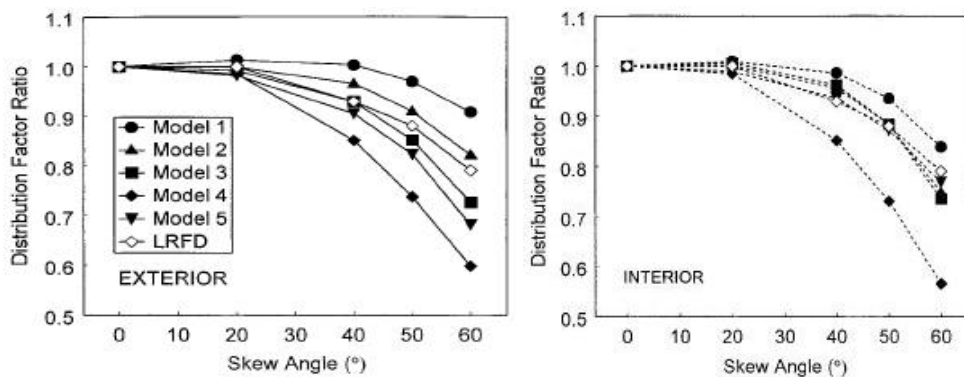


Figure 2.9-1 Effect of bridge skew angle on load distribution factor (Barr et al., 2001).

It was shown by Green et al. (2004) that the presence of intermediate diaphragms helped in reduction of the maximum girder deflections; however, such reductions were shown to decrease with the increased skew angles. The addition of intermediate diaphragms had an overall effect of reducing the deflections by about 19% for straight bridges, about 11% for 15-30° skew bridges, and about 6% for 60° skew bridges.

The paper by Huang et al. (2004) presented a study on the transverse load distribution in highly skewed (60°) bridges. Finite element analyses of the bridge were conducted to investigate the influence of model mesh, transverse stiffness, diaphragms, and modeling of the supports. The AASHTO (1998) formulas for transverse load distribution were shown to be

conservative for positive bending, and not conservative for negative bending for slab-on-steel girder bridges with skews as large as 60° . However, it is necessary to conduct similar investigations on precast prestressed bridges to verify the applicability of similar observations made on slab-on-steel girder bridges.

2.10 Summary

In summary, the above literature review brought about several interesting observations regarding the provision of transverse prestressing in precast prestressed bridges systems, and regarding performance of the shear-keys. Although providing transverse prestressing to the deck slab was recommended during earlier research, later it was shown more preferable to provide transverse prestressing to the transverse diaphragms. However, the extent of prestressing to be provided in the transverse direction was not suggested by any of the researchers. In their code recommendation, MDOT adopted post-tensioned transverse diaphragms to be provided in precast prestressed bridges. However, the number of diaphragms and prestressing force have not been optimized using experimental or numerical evidence. This calls for further research to be conducted so as to determine the most effective number of transverse diaphragms and prestressing force levels to be provided. Moreover, the severe problems associated with the development of premature longitudinal cracks on the deck slab along the joints between side-by-side box-beams could possibly be either reduced or delayed, if not eliminated altogether through adequate TPT arrangements. Load distribution studies for skewed precast prestressed bridges are also necessary because no particular study has been carried out for these types of bridges.

CHAPTER 3: NUMERICAL METHODOLOGY

3.1 Introduction

The development of the longitudinal cracks in side-by-side box-beam bridges was investigated through an in-depth finite element analysis (FEA) to determine the adequate transverse post-tensioning force level and number of diaphragms required to eliminate cracking. The FEA was conducted using the commercial software package ABAQUS 6.6.1. In this chapter, a detailed explanation of the modeling technique is presented first by defining: the finite element (FE) model components, material properties, elements types, boundary conditions, analysis steps, and all the assumptions that have been used through the process of modeling to simulate the response of side-by-side box-beam bridges under service loads. Then, the results of the numerical analysis are presented and discussed. Finally, recommendations are provided for MDOT engineers to formulate revised design Specifications for transverse post-tensioning (TPT) arrangements for typical side-by-side box-beam bridges.

According to MDOT Bridge Design Guide 6.65.13 (2006) for the transverse post-tensioning details, box-beam bridges are categorized by their spans. There are four categories: bridges with spans up to 50 ft, bridges with spans over 50 ft but not more than 62 ft, bridges with spans over 62 ft but not more than 100 ft, and bridges with spans over 100 ft. For each of these categories, the number of diaphragms is specified in the Bridge Design Manual. In this FE study, the results of the longest span of each category were used as a guideline for the entire category; four models of spans 50, 62, 100, and 124 ft were generated. The last span was an example for bridges with spans over 100 ft. The required box-beam depth and reinforcement details were justified based on flexural design specifications for each bridge performed according to the AASHTO LRFD (2004).

3.2 Components of the Bridge Model

The FE models simulated side-by-side box-beam bridges with superstructure composed of:

1. Box-beams reinforced with prestressing strands and reinforcing bars.

2. Unbonded transverse post-tensioning carbon fiber composite cables (CFCC) with end bearing nuts or plates.
3. Deck slab of 6 in. thick reinforced with one layer of reinforcement at the mid-thickness.
4. Elastomeric bearing pads (supports).
5. Non-shrink grout material in the shear-keys connecting the adjacent box-beams.

The following subsections provide the details of modeling each component.

3.2.1 Box-Beams

The cross-sections of the box-beams were selected from MDOT Bridge Analysis Guide (2005), as shown in Figure 3.2-1, Figure 3.2-2, and Figure 3.2-3. Box-beams are commonly manufactured in widths of 36 and 48 in., and depths ranging from 17 to 60 in. Beams with depths of 12 and 17 in. are manufactured only in a width of 36 in. Other shallow box-beams are manufactured in both widths. Beams deeper than 42 in. are manufactured only in a width of 48 in. The FE models were initially generated using beams of a width of 48 in. and depth satisfying the flexural requirement for the span (Table 3.2-1). Later on, the models were regenerated using box-beams of a width of 36 in. to make the results of the analysis more comprehensive.

In the transverse direction, each box-beam was provided initially with two end blocks of a width of 24 in. each, and interior diaphragms of a width of 14 in. each (MDOT Bridge Design Guide 6.65.13, 2006). The number and spacing of the interior diaphragms varied according to the span, as shown in Table 3.2-2 (MDOT Bridge Design Guide 6.65.13, 2006).

Box-beams and the transverse diaphragms were meshed using a brick element (C3D8R). This is a three dimensional element with eight nodes, as shown in Figure 3.2-4. Each node has three transitional degrees of freedom (U_x , U_y , U_z). A typical mesh for a single box-beam is shown in Figure 3.2-5 with a maximum element size less than 10 in.

Concrete properties for box-beams

A continuum, plasticity-based, damage model for concrete was used to model the material behavior. The concrete damaged plasticity model uses concepts of isotropic damaged elasticity in combination with isotropic tensile and compressive plasticity to represent the inelastic

behavior of concrete. It assumes that the two main failure mechanisms are tensile cracking and compressive crushing of the concrete material. Consequently, the concrete material was defined by its uniaxial compressive and tensile performance in addition to the elastic properties.

Table 3.2-1 Box-beam depths for the investigated spans.

Span (ft)	Box-beam depth (in.)
50	27
62	33
100	39
124	54

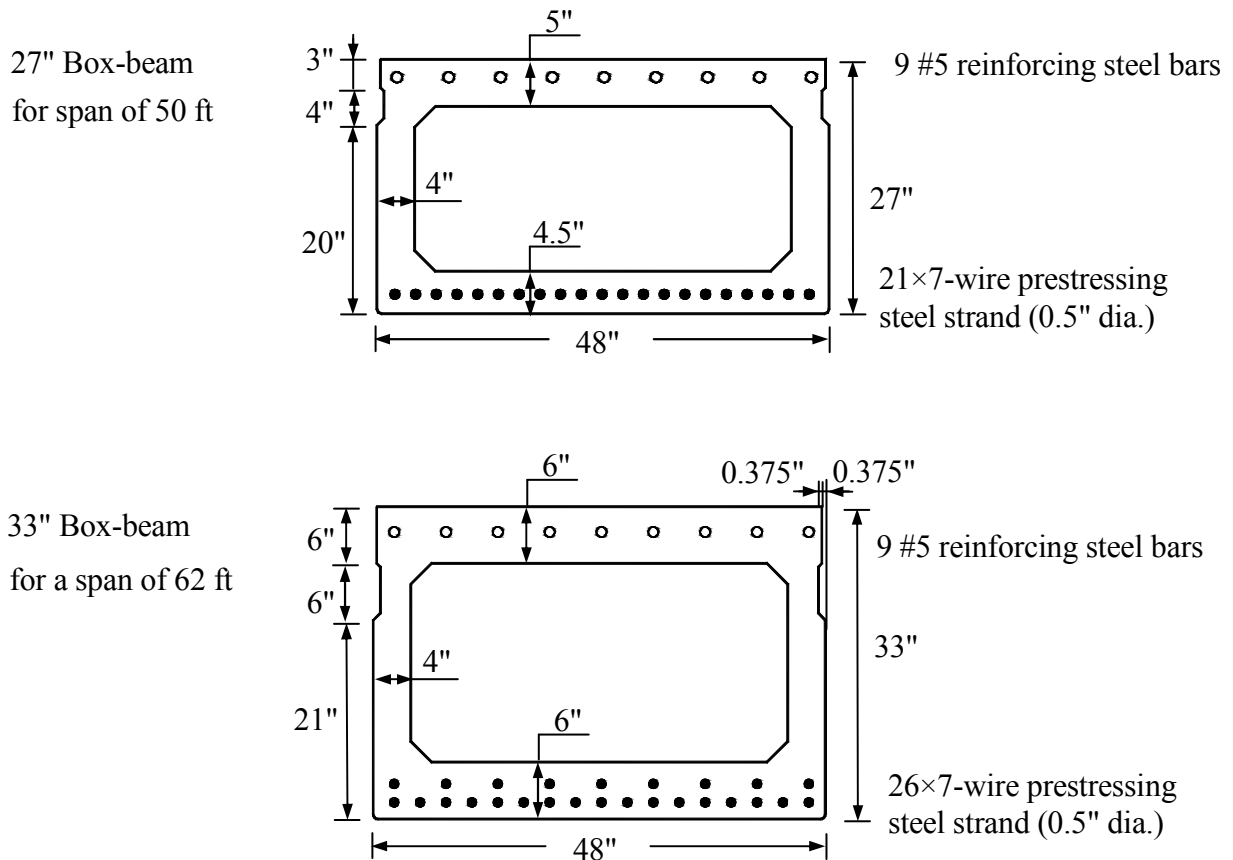
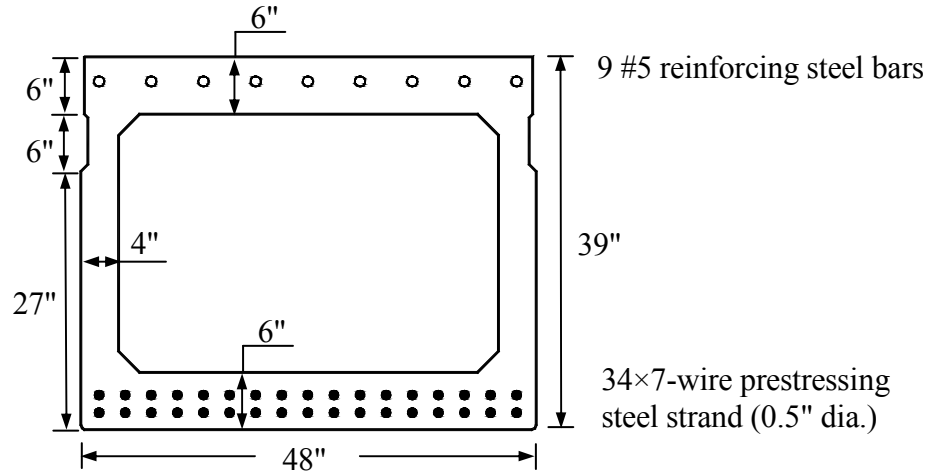


Figure 3.2-1 Cross-sectional details for box-beams.

39" Box-beam
For span of 100 ft



54" Box-beam
for span of 124 ft

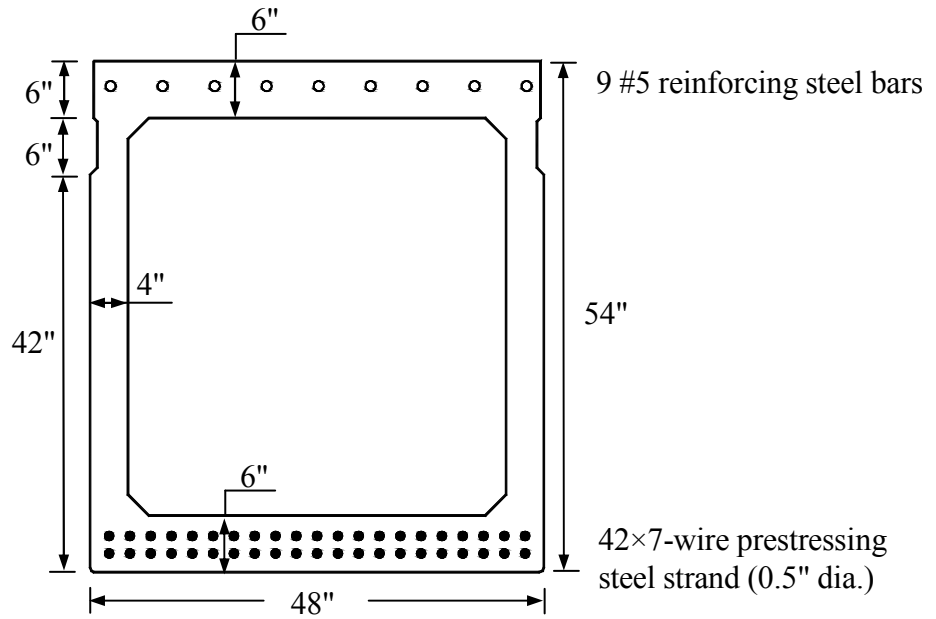
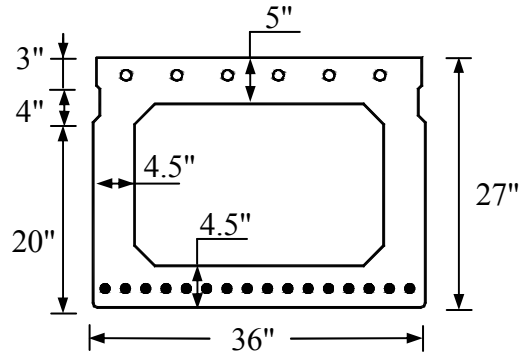


Figure 3.2-2 Cross-sectional details for box-beams (continued).

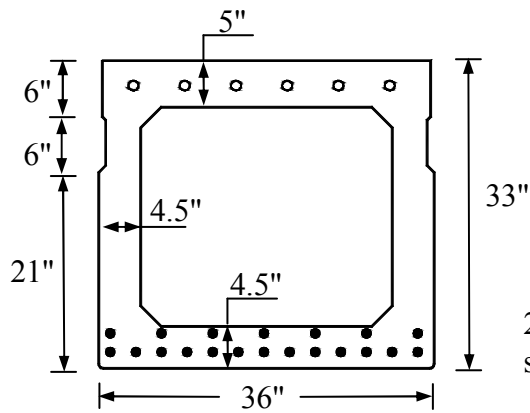
27" Box-beam
for a span of 50 ft



6 #5 reinforcing steel bars

16×7-wire prestressing
steel strand (0.5" dia.)

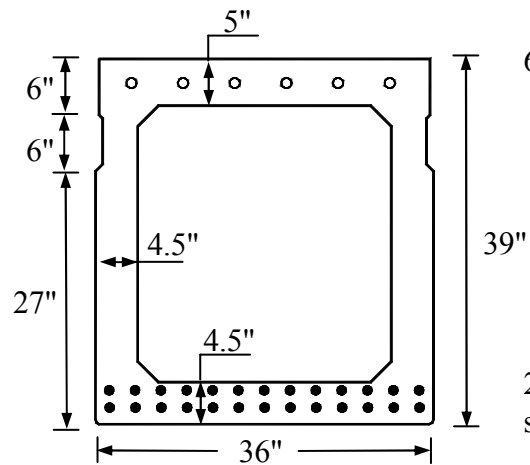
33" Box-beam
for a span of 62 ft



6 #5 reinforcing steel bars

20×7-wire prestressing
steel strand (0.5" dia.)

39" Box-beam
for a span of 100 ft



6 #5 reinforcing steel bars

26×7-wire prestressing
steel strand (0.5" dia.)

Figure 3.2-3 Cross-sectional details for box-beams (continued).

Table 3.2-2 Post-tensioning tendons location (MDOT Bridge Design Guide 6.65.13, 2006).

Span Length, ft	Locations
Up to 50	2 @ center of span (11 ft apart); 1 @ each end of beam
Over 50 to 62	1 @ each quarter point; 1 @ center of span; 1 @ each end of beam
Over 62 to 100	2 @ center of span (11 ft apart); 1 @ each quarter point; 1 @ each end of beam
Over 100	1 @ each end of beam with 5 equally spaced between

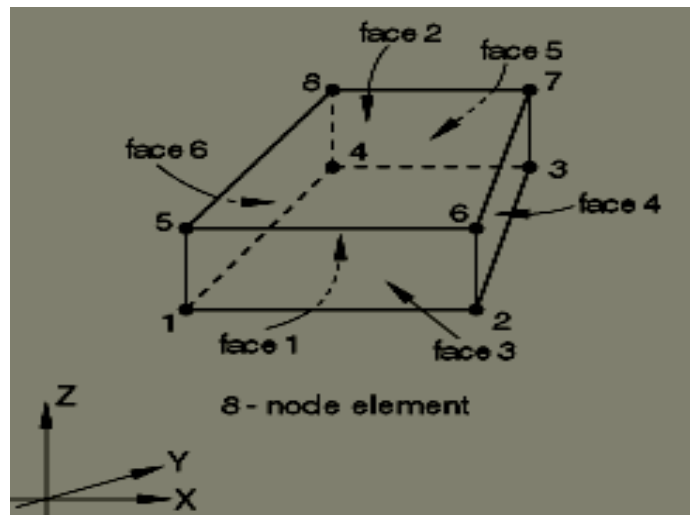


Figure 3.2-4 Brick element used in modeling box-beams (ABAQUS Manual, 2006).

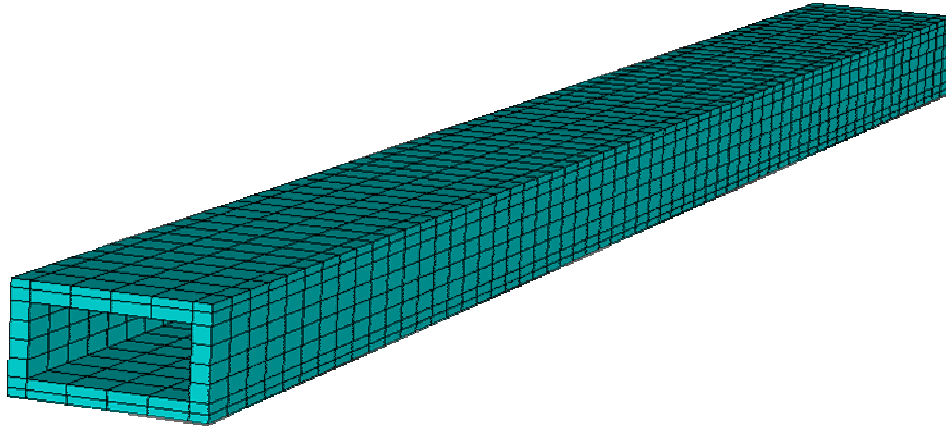


Figure 3.2-5 Three dimensional view for box-beam sides.

For the compressive stresses, as shown in Figure 3.2-6, the material model response is linear until the value of initial yield; the initial yield usually occurs at stress equal to 60% of the concrete ultimate strength and then the material begins the plastic response, which is typically characterized by stress hardening followed by strain softening beyond the ultimate stress.

For the tensile stresses, as shown in Figure 3.2-7, the stress-strain response follows a linear elastic relationship until reaching the value of the cracking stress, which corresponds to the onset of localized cracking in the concrete material. Beyond the cracking stress, the formation of cracks is represented macroscopically with a softening stress-strain response, which includes strain localization in the concrete structure. The stress-strain curves for the concrete were adapted from Nawy (2003) for concrete with compressive strength of 7,800 psi.

Based on available experimental results for tests performed in LTU using cylinders made of concrete with similar strength and having a maximum aggregate size of 3/8", the modulus of elasticity was taken equal to 4,270 ksi. The test was performed according to ASTM C469 up to stress equal to 40% of the ultimate strength. The points on the stress-strain curve and the experimentally determined modulus of elasticity were in good agreement. In addition, Poisson's ratio (ν) was obtained from experimental results as 0.15.

The modulus of rupture (f_r) was calculated as 530 psi [$0.19\sqrt{f'_c}$ for prestressed concrete, AASHTO LRFD (2004) Table 5.9.4.2.2.-1]. The term "modulus of rupture" in the finite

element analysis indicates the maximum allowable tensile strength in the concrete and not necessarily as defined by AASHTO LRFD (2004) 5.4.2.6.

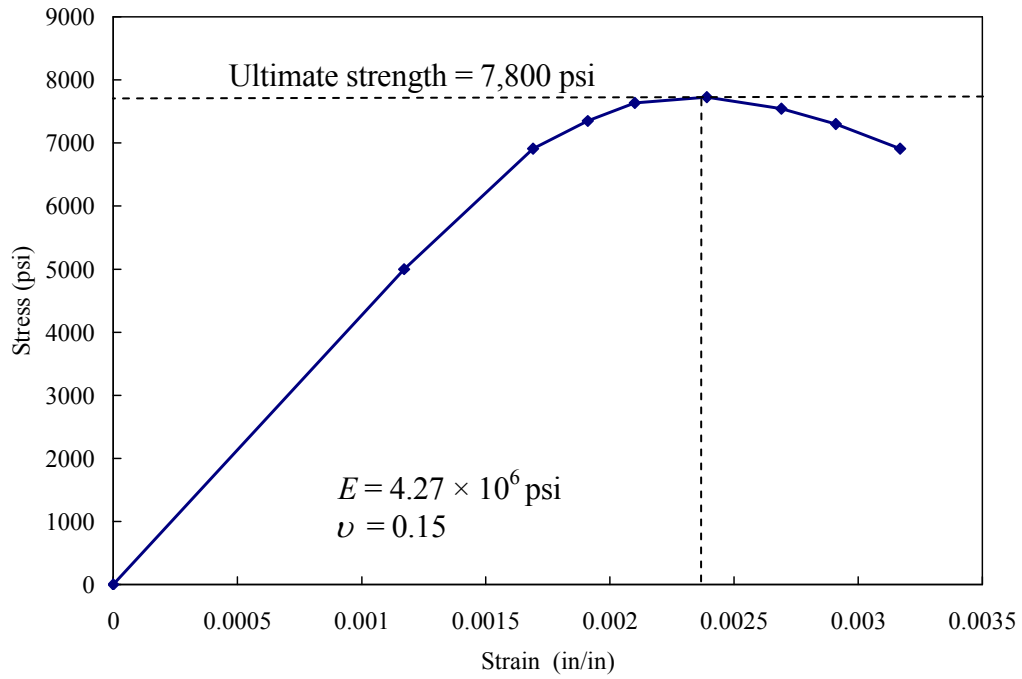


Figure 3.2-6 Compressive behavior for the concrete material in the box-beams (Nawy, 2003).

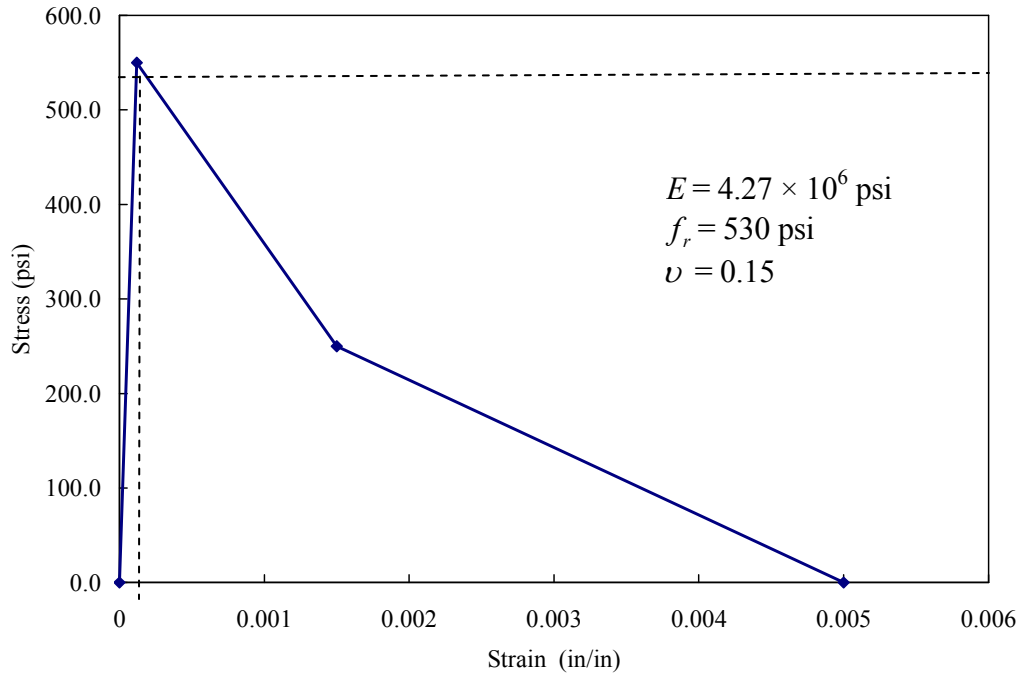


Figure 3.2-7 Tensile behavior for the concrete material in the box-beams (Nawy, 2003).

3.2.2 Box-Beam Reinforcement

Each box-beam was reinforced with bottom reinforcement composed of steel prestressing strands of a cross-sectional area of 0.153 in² each (seven-wire strand of 0.5 in. diameter). The number of strands per beam in the different bridge models varied according to the flexural design of each span (AASHTO LRFD, 2004). In addition, spans of 100 and 124 ft required some strands to be debonded for certain distances at the beam ends in order to prevent development of excessive tensile stresses in these end sections. Table 3.2-3 shows the number of strands for each beam and the number of debonded strands along with the debonded length as determined from the analysis. In addition, top flange reinforcement composed of nine reinforcing steel bars #5 (cross-sectional area of 0.3 in²) was provided.

All the reinforcement was modeled with a two-node linear 3D truss element (T3D2) with each node having three degrees of freedom (U_x, U_y, U_z). Truss elements were embedded inside the host elements - concrete brick elements. The translational degrees of freedom of the embedded element nodes were constrained to the interpolated values of the corresponding degrees of freedom of the host element nodes.

Material properties for the longitudinal prestressing strands

The stress-strain curve for the strands shown in Figure 3.2-8 shows the stress-strain curve for the strands (Nawy, 2003). The material responds linearly up to the yield stress, and then it behaves nonlinearly up to failure with an ultimate tensile strain of 5%. In addition, the material properties for prestressing steel strands are shown in Table 3.2-4. The input parameters to be used in ABAQUS are the stress and strain coordinates associated with the point of yielding and ultimate failure.

Table 3.2-3 Details of box-beam reinforcement for different spans.

Span (ft)	No. of Strands	No. of De-Bonded Strands	Length of De-Bonding (in.)
50	21	–	–
62	26	–	–
100	34	5	15
124	42	12	44

Table 3.2-4 Material properties for prestressing steel strands.

Ultimate tensile strength (psi)	270,000
Yield strength (psi)	230,000 (85% of the ultimate strength)
Modulus of elasticity (psi)	$27,500 \times 10^3$
Poisson's ratio	0.3

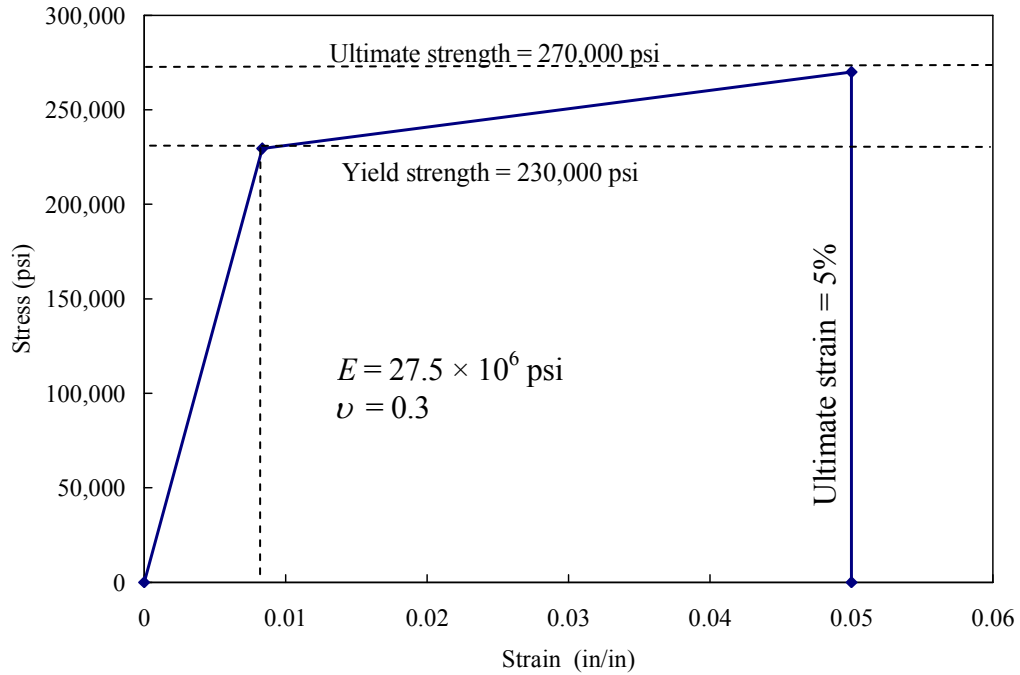


Figure 3.2-8 Stress-strain curve for prestressing steel strands (Nawy, 2003).

3.2.3 Transverse Post-Tensioning Strands (TPT Strands)

The same 2-node truss element (T3D2) was used to model the transverse unbonded post-tensioning strands, which functioned as ties confining the box-beams transversely. The end nodes of the transverse strand were tied to steel plates acting as end bearing plates. The steel plates were tied to the exterior sides of the external box-beams; however, the interior nodes of the post-tensioning strands were not tied to the surrounding objects. The steel plates in this connection were provided to distribute the post-tensioning force on the concrete surface and prevent any concrete crushing. Figure 3.2-9 shows the strands with their end bearing plates.

In the FE models, the unbonded transverse strands were modeled as cables made of carbon fiber composite cables (CFCC). The number of tendons per diaphragm was determined based on the depth of the box-beam; for box-beams of a depth of 12 in., one tendon should be placed 5.5 in. below the top of the beam. For beam depth: 17, 21, and 27 in., one tendon should be placed at the middle of the beam. For beam depths of 33 in. and over, two tendons should be placed at the third points of the beams depth. In addition, a TPT force of 104,500 lb per

diaphragm was provided initially based on the specifications provided by MDOT Bridge Design Guide (2006).

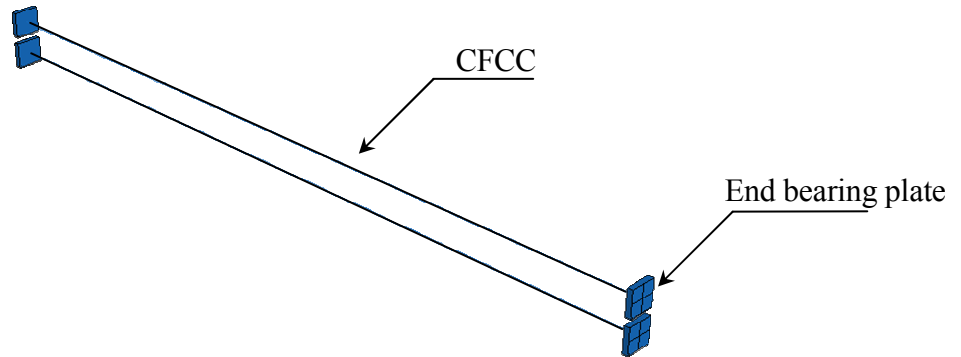


Figure 3.2-9 CFCC with end bearing plates.

Material properties of CFCC

The CFCC was defined in the model as an elastic-plastic material with its yield strength equal to its ultimate strength - the material behaved linearly up to failure. The CFCC was defined in the analysis with properties, as shown in Table 3.2-5.

Table 3.2-5 Material properties for CFCC.

Ultimate tensile strength (psi)	350,000
Modulus of elasticity (psi)	19.8×10^6
Ultimate strain (at failure)	1.62%

3.2.4 Deck Slab

The main study was performed using bridge models with 6 in. thick deck slabs as required by the current MDOT Specifications. The 8-node linear brick element (C3D8R) was used to mesh the slab with special attention; the slab thickness was 6 in.; yet, it was divided into three layers of elements (Figure 3.2-10). This meshing technique provided a good distribution for the stresses that were developed in the slab because of the relative movements between the box-beams.

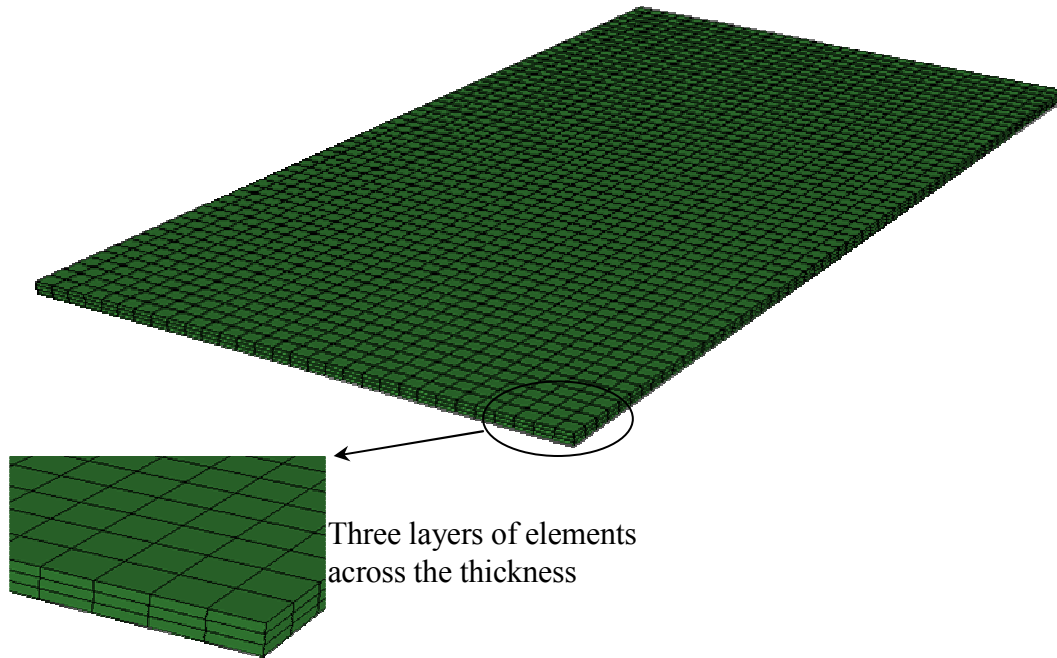


Figure 3.2-10 Deck slab FE mesh.

Being cast in place, the deck slab should not be influenced by the pre-tensioning force or the dead loads, which influence the box-beams only; however, it should be influenced along with the beams by the superimposed dead loads and service loads. Therefore, in the FE model, the connection between the deck slab bottom surface and the box-beams top surface was established in a later step of the model development. The deck slab was added as to simulate the construction sequence for this type of bridges. Figure 3.2-11 shows the procedure of integrating the deck slab to the whole model. This procedure can be summarized in the following steps:

1. The box-beams were analyzed first without the deck slab under the pre-tensioning forces, box-beams dead load, shear-key dead load, first stage of TPT force, and slab dead load.
2. Due to the aforementioned loads, the beams exhibited displacement (upward or downward). This deflection was deducted from the slab thickness in a separate computer analysis run. A modified deck slab of varying thickness resulted from the

- analysis. The modification was only geometrical; the slab bottom surface exhibited artificially the same deflection of the beams without developing stresses in the slab.
3. The modified deck slab was added to the box-beams along with its reinforcement.
 4. The complete model was then analyzed from the beginning starting from applying pre-tensioning force, box-beams dead load, shear-key dead load, first stage of TPT force, and slab dead load.
 5. After applying the slab dead load, the beams exhibited the same deflection they exhibited before in Stage 2. As a result, the beams' top surface closely approached the artificially-deflected slab bottom surface. The virtual connecting elements - tie-elements were created between the top surface of the box-beams and the bottom surface of the slab and the model started to act as a one unit.
 6. After establishing the contact between the slab and the beams, the whole model was subjected to time dependent losses, superimposed dead load, and service load.

By these steps of analysis, exact simulation of the sequence of construction for side-by-side box-beam bridges was possible.

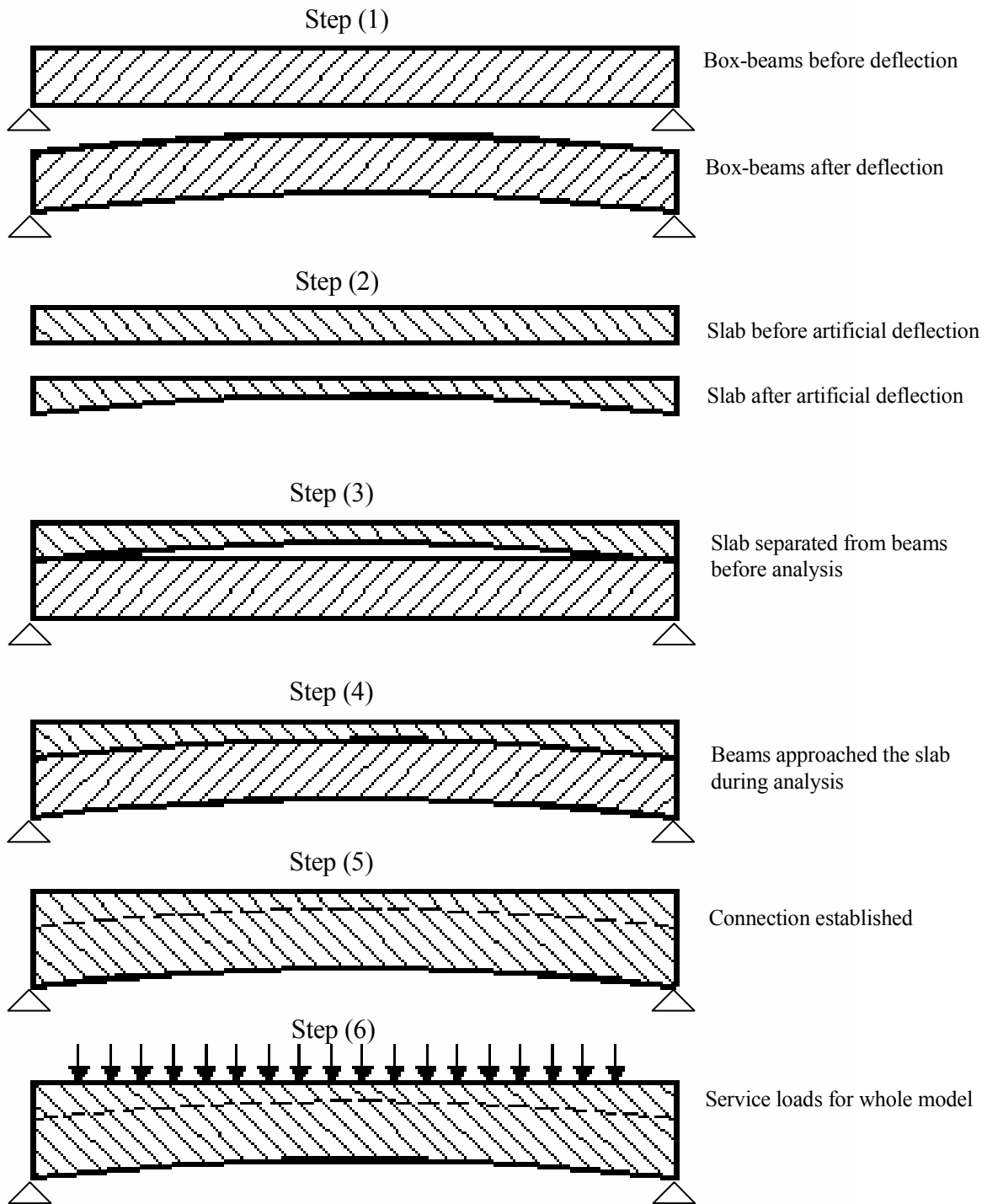


Figure 3.2-11 Deck slab connection with box-beams.

Properties of concrete in deck slab

A concrete with design compressive strength of 4,000 psi is usually used in the deck slabs (MDOT Bridge Design Guide 6.41.01, 2006); yet, replacing deck slabs is the most common rehabilitation task in bridge engineering because it is the major component exposed directly to the truck loading and the environmental conditions that can accelerate the concrete deterioration and reduce the strength and stiffness. Although there is no specific guide that can give an estimate for the strength loss in the deck slab over time, strength of 3,000 psi in this study was considered a fair estimation of the concrete ultimate strength in the deck slab towards the end of service life. The analysis was performed for three classes of deck slabs: deteriorated deck slab with concrete compressive strength of 3,000 psi, recently-constructed deck slab with concrete compressive strength of 4,000 psi, and special-quality deck slab with concrete compressive strength of 5,000 psi.

For concrete with strengths of 4,000 and 5,000 psi, the modulus of rupture was taken as $0.23\sqrt{f'_c}$ [AASHTO LRFD (2004) C5.4.2.7]. The maximum tensile strength of the concrete is required parameter in the finite element analysis and not the modulus of rupture. For deteriorated concrete, the value of the compressive strength (3,000 psi) was estimated based on available field tests for deteriorated decks (Kwasniewski et al., 2000). Note that the value of the compressive strength of the concrete is not of great influence on the analysis. The combination between the tensile strength of the concrete and the modulus of elasticity plays the key role in developing the cracks under the applied loads. The values of the modulus of elasticity and tensile strength of the deteriorated deck slab were selected after several trials to provide an upper limit for the required post-tensioning force.

Table 3.2-6 Material properties for the concrete in the deck slab.

Material Prop. Class of Slab	Ultimate Strength f'_c (psi)	Modulus of Elasticity (psi)	Modulus of Rupture (psi)	Poisson's Ratio
Deteriorated	3,000	3.00×10^6	350	0.15
Recently-constructed	4,000	3.83×10^6	460	0.15
Special-quality	5,000	4.30×10^6	514	0.15

3.2.5 Deck Slab Reinforcement

To satisfy the minimum reinforcement required by AASHTO LRFD (2004) Section 5.10.8, the slab was provided with a single layer of reinforcement (Figure 3.2-12). The layer was composed of Grade 60 steel bars #5 @ 12 in. in both longitudinal and transverse directions. The stress-strain curve for the steel used is shown in Figure 3.2-13 with a modulus of elasticity of 29,000 ksi, yield strength of 60,000 psi, and ultimate strength of 90,000 psi. The 2-node truss element (T3D2) was also used to model the reinforcement layer.

It should be noted that While developing the finite element model, trials have been made to study the effect of changing the deck reinforcement on eliminating the longitudinal deck cracks but the finite element analysis showed that the deck reinforcement was of negligible influence on the longitudinal deck cracking when provided at the mid-depth of the deck slab. The final arrangement of the deck reinforcement in the finite element models was selected save some of the CPU memory for more important details.

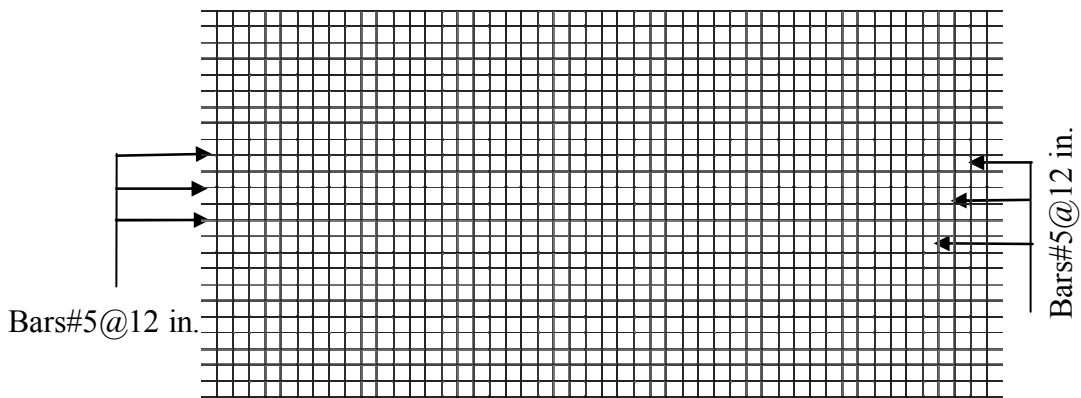


Figure 3.2-12 Deck slab reinforcement.

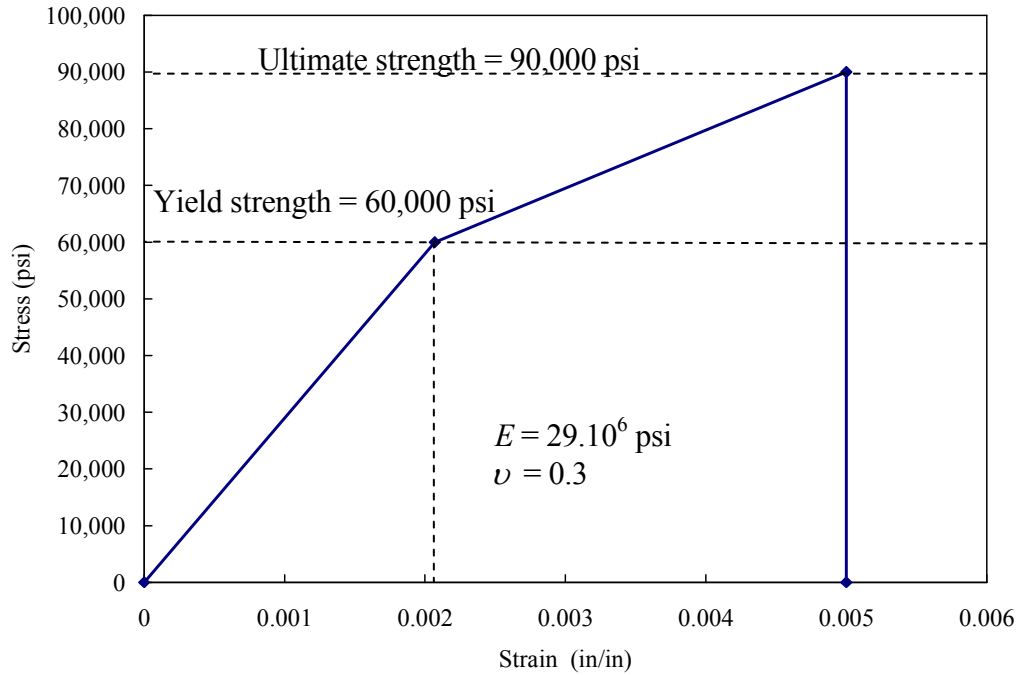


Figure 3.2-13 Idealized stress-strain curve for reinforcement bars.

3.2.6 Elastomeric Bearing Pads

The end supports were provided for the box-beams as steel-reinforced elastomeric bearings. The bearings were composed of alternate layers of steel reinforcement and elastomer bonded together, as shown in Figure 3.2-14. The elastomer - rubber -was defined in the FEA as a hyper-elastic material of ultimate uniaxial tensile stress of 2,500 psi and ultimate uniaxial tensile strain of 400% (complies with ASTM D412). Both of the reinforcement and the elastomer layers were modeled with 8 node linear brick elements (Figure 3.2-15) however the elements functioned differently during the FE analysis: the reinforcement layers were modeled with an element identified in ABAQUS library as C3D8R. This element is controlled by the reduced integration during the analysis (identified by the letter R at the end of the name). The elastomer layers, on the other hand, were modeled with an element identified as C3D8H. This element is controlled by hybrid formulations that can deal with the elastomer material behavior (identified by the letter H). The ABAQUS manual for element types provides a detailed description for both elements and their functions.

The length, width, and thickness of the bearing pads were calculated for the FEA according to AASHTO LRFD (2004) Section 14.7.6. The width of the bearing was fixed to 45 in. when used with 48 in. wide box-beams and to 33 in. when used with 36 in. wide box-beams. Furthermore, the length varied according to the bridge span. For the 50 ft span, the length was taken equal to 8 in. and for the 62, 100, and 124 ft spans, the length was taken equal to 10 in. In addition, the total thickness of the bearing was taken as 2.075 in. divided into:

1. Three steel layers of thickness 0.125 in. each.
2. Two interior elastomer layers of thickness 0.6 in. each.
3. Two exterior elastomer layers of thickness 0.25 in. each.

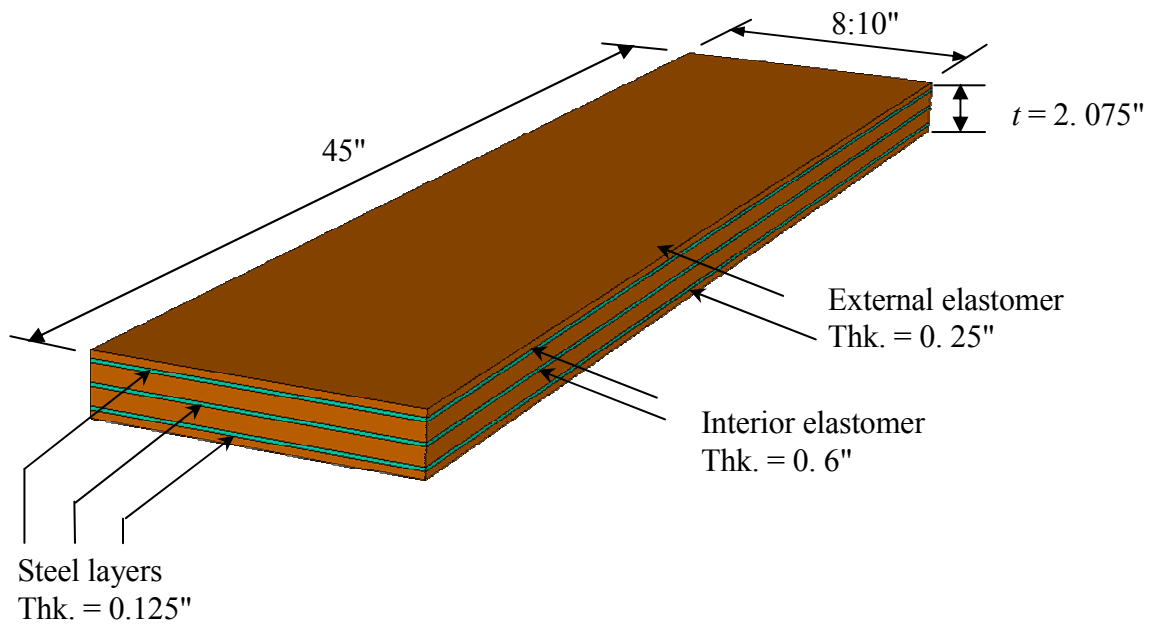


Figure 3.2-14 Elastomeric bearing pad for one beam.

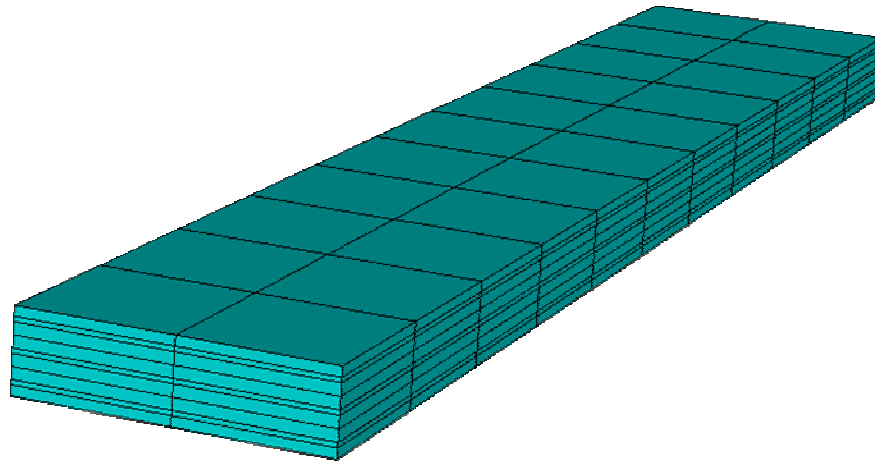


Figure 3.2-15 Meshing of the bearing pad.

3.2.7 Shear-Keys

Typically, shear-keys in side-by-side box-beams bridges serve as connectors between the box-beams to transfer the shear and prevent differential movement under service loads. In the transverse design of adjacent box-beam bridges, PCI Design Manual 8.9.3.6 (2003) refers to AASHTO LRFD (2004) Section 5.8.4, for checking the transfer shear in the vertical plane through the joints, and according to AASHTO LRFD (2004) Section 5.8.4, the interface shear transfer, in general, shall be considered across a given plane at:

1. An existing or potential crack,
2. An interface between dissimilar materials, or
3. An interface between two concretes cast at different times.

The second and third cases represent the interface plane between shear-keys and box-beams. Therefore, the nominal shear resistance of this interface plane shall be taken according to AASHTO LRFD (2004) Section 5.8.4.1-1 as:

$$V_n = cA_{cv} + \mu[A_{vf}f_y + P_c]$$

where

$$V_n = \text{nominal shear resistance (kip)}$$

A_{cv} = area of concrete engaged in shear transfer (in²)

A_{vf} = area of shear reinforcement crossing the shear plane (in²)

f'_c = specified 28-day compressive strength of the weaker concrete (ksi)

f_y = yield strength of reinforcement (ksi)

c = cohesion factor (ksi)

μ = friction factor

P_c = permanent net compressive force normal to the shear plane (kip)

The nominal shear resistance V_n used in the design shall not be greater than the lesser of “ $V_n \leq 0.2f'_c A_{cv}$ ” or “ $V_n \leq 0.8A_{cv}$ ”.

The equation provided in AASHTO LRFD (2004) primarily splits the nominal shear capacity into two separate components:

1. Cohesion between the two surfaces with a cohesion factor, c .
2. Friction between the two surfaces with a friction factor, μ .

These factors are determined in AASHTO LRFD (2004) Section 5.8.4.2.

1. For concrete placed against clean, hardened concrete with a surface intentionally roughened to an amplitude 0.25 in.: $c = 0.1$ ksi, $\mu = 1.0\lambda$ ($\lambda = 1.0$ for normal weight concrete).
2. For concrete placed against clean hardened concrete and free of laitance but not intentionally roughened: $c = 0.075$ ksi, $\mu = 0.6\lambda$

However, shear-key connections are somewhere in between the aforementioned boundaries as the box-beam concrete surface is not intentionally roughened to an amplitude of 0.25 in. but at the same time, it has a groove of a depth of 0.25 in. in the box-beam side to be filled with the grout material. In addition, there is no reinforcement going through the connection; therefore, the friction component is a function only of P_c , which is the transverse post-tensioning force.

The coefficient of friction was taken as 0.7; however, the coefficient of cohesion, which represents the bond capacity between connected surfaces, was taken as 0.0 in the full-scale models, because:

1. In the PCI Design Manual 8.9.3.7 (2003), even though full-depth grouting of the shear-key was recommended, the shear-key is not considered a structural member transferring shear between the box-beams.
2. The transverse post-tensioning and the deck slab (reinforced structural overlay) are the available techniques that AASHTO LRFD (2004) Section C4.6.2.2.1 recommends to develop the interconnection between box-beams. It does not specify the bond capacity for the grout material.
3. Since it is a cold joint, the shear-key connection usually fails in bond between the surfaces unless special precautions are applied (Issa et al., 2003). Some of these precautions require higher quality control, which might not be available on the site while pouring the grout of the shear-keys.
4. To simulate the actual behavior for a cohesive connection, a very small element size must be used in meshing the connecting parts. Yet, a mesh that is too fine makes the analysis intractable. A coarser mesh leads to an overly high estimate for the joint capacity.

3.3 Construction Loads

Construction loads included the prestressing forces, dead loads, transverse post-tensioning force, and superimposed dead loads. Except for superimposed dead loads and time dependent losses in longitudinal prestressing strands, all construction loads were applied to the box-beams before integrating the deck slab into the model.

Prestressing forces were modeled as concentrated forces acting at the ends of the prestressing strands. Each strand was provided with an initial prestressing force of 28,500 lb, which dropped to 25,000 lb after deducting the time dependent losses. The time dependent losses were calculated according to Section 5.9.5.3 of AASHTO LRFD (2004), and applied at a later stage after integrating the deck slab to the model.

Dead loads of box-beams and deck slab were calculated assuming the concrete of unit weight of 150 lb/ft³ and applied as a distributed load on the box-beams.

Transverse post-tensioning (TPT) force was applied as a bolt load (post-tensioning load from ABAQUS load library) through the post-tensioning CFCC which were tied to the beams exterior sides with steel bearing plates of dimensions of 10 in. × 10 in. × 2 in. each.

Superimposed dead loads included the weight of a wearing surface (25 lb/ft²) and the weight of the barriers. Type 4 barriers with a weight of 475 lb/ft were provided at both sides of the bridge model. The superimposed dead loads were applied at the top surface of the deck slab after the deck slab was integrated to the FE model (recall Figure 3.2-11).

3.4 Load Combinations

According to AASHTO LRFD (2004) Section 3.4 for load factors and load combinations, the deck slab cracking was investigated by combining the loads according to Service I, which permits combining: dead loads (DC), wearing surface dead loads (DW), live loads (LL), impact allowance (IM), wind load (WS), wind on live load (WL), shrinkage (SH), creep (CR), uniform temperature (TU), temperature gradient (TG), and some additional types of loads not relevant to the current case of analysis.

Out of the aforementioned loads, TU does not create internal stresses in simply supported structures. It is primarily provided for the design of the support movement (AASHTO LRFD, 2004 Section 3.12.2). In addition, CR is not believed to develop cracks in the deck slab, which experiences compressive stresses most of the time. Furthermore, WS and WL would not be considered in analysis because it is not recommended to combine thermal gradient with high wind forces (AASHTO LRFD, 2004 Section C3.4.1). Finally, SH can not be blamed for the longitudinal cracks as the crack pattern due to shrinkage, regardless of the shrinkage value, is different from what is usually reported in the side-by-side box-beam bridges. In other words, TU, WS, WL, CR, and SH would not be included in the acknowledged load combination when checking deck slab longitudinal cracks.

The remaining loads -DC, DW, LL, IM, and TG -were combined together according to AASHTO LRFD (2004) to create the maximum influence on the deck slab. The AASHTO LRFD (2004) allows load factor of 1.00 for dead loads and superimposed dead loads when they are considered in Service I load combination. However, load factors for live loads, impact allowance, and temperature gradient need further consideration.

Section 3.6.1.2.1 of AASHTO LRFD (2004) provides new vehicular loading labeled as HL-93 and consists of a combination of a design truck or tandem in addition to a design lane load (Figure 3.4-1). Each design lane under consideration shall be occupied by either design

truck or tandem, along with the lane load. The load shall be assumed to occupy 10 ft transversely within a design lane (Figure 3.4-2). Furthermore, the maximum live load effect shall be determined by considering each possible load combination of number of loaded lanes multiplied by the corresponding multiple presence factor as provided by Section 3.6.1.1.2 of AASHTO LRFD (2004) (Table 3.4-1) to account for the probability of simultaneous lane occupation by the HL-93 live load. To account for the dynamic effect of the moving loads, AASHTO LRFD (2004) Section 3.6.2 specifies a percentage of the static load of the truck or the tandem, but not the lane load, to be added to the original load as a dynamic allowance. The limit shall be taken as 75% for the purpose of designing the deck slab joints and 33% for designing other bridge components. It is not specified clearly in Section 3.6.2 whether 75% is applicable for the design of the transverse deck joints only or it is applicable for the design of both transverse and longitudinal deck joints. In the FE analysis, the impact allowance was taken equal to 75% based on the calibration of a full-scale bridge model (Bebawy, 2007).

Table 3.4-1 Multiple presence factor, m (AASHTO LRFD 3.6.1.1.2, 2004).

Number of loaded lanes	Multiple presence factor (m)		
	ADTT ¹ > 5,000	100 ≤ ADTT ≤ 1,000	ADTT < 100
1	1.20	1.14	1.08
2	1.00	0.95	0.90
3	0.85	0.81	0.73
> 3	0.65	0.62	0.59

¹ ADTT: Average daily truck traffic

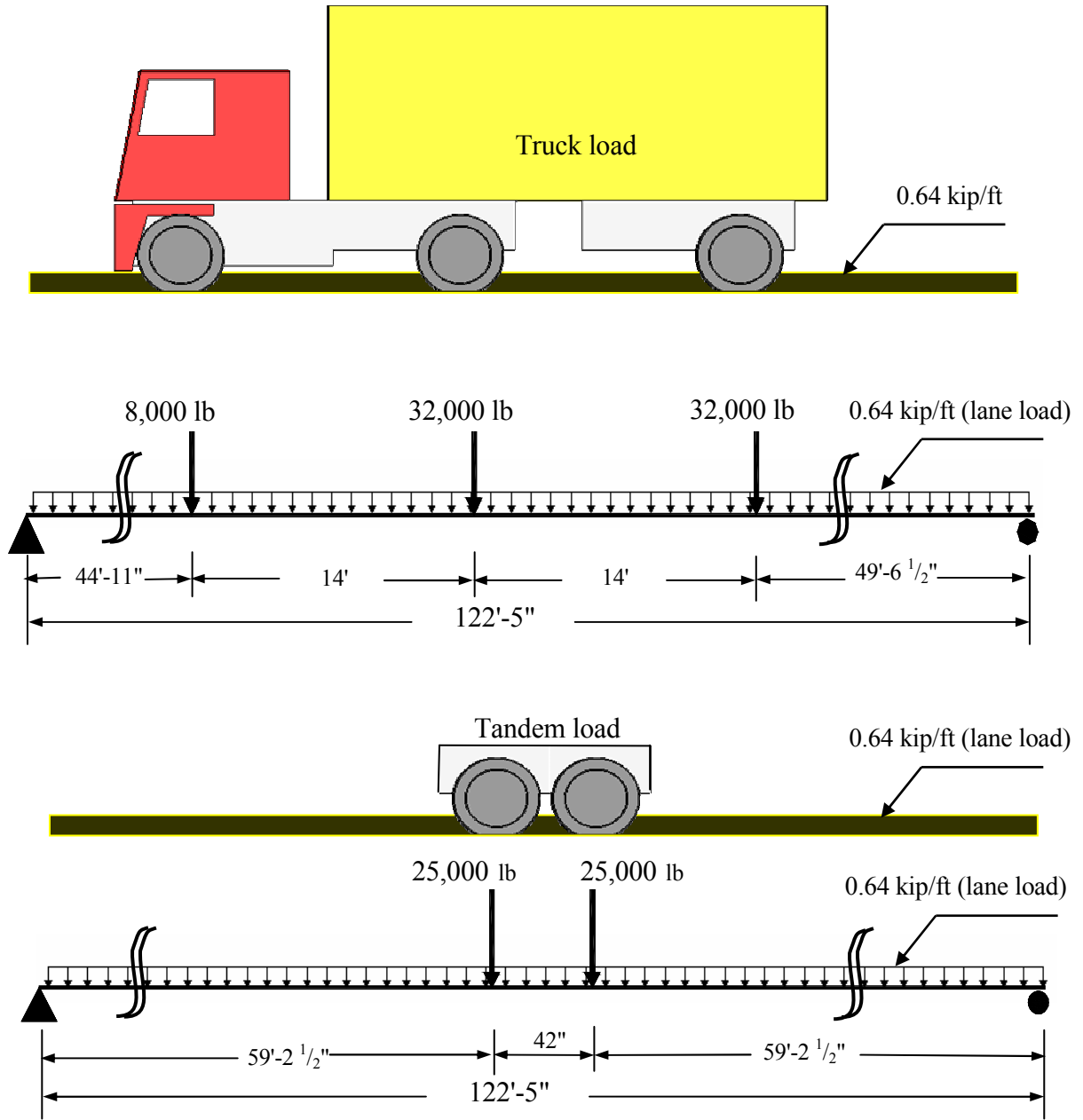


Figure 3.4-1 AASHTO LRFD HL-93 load (longitudinal direction).

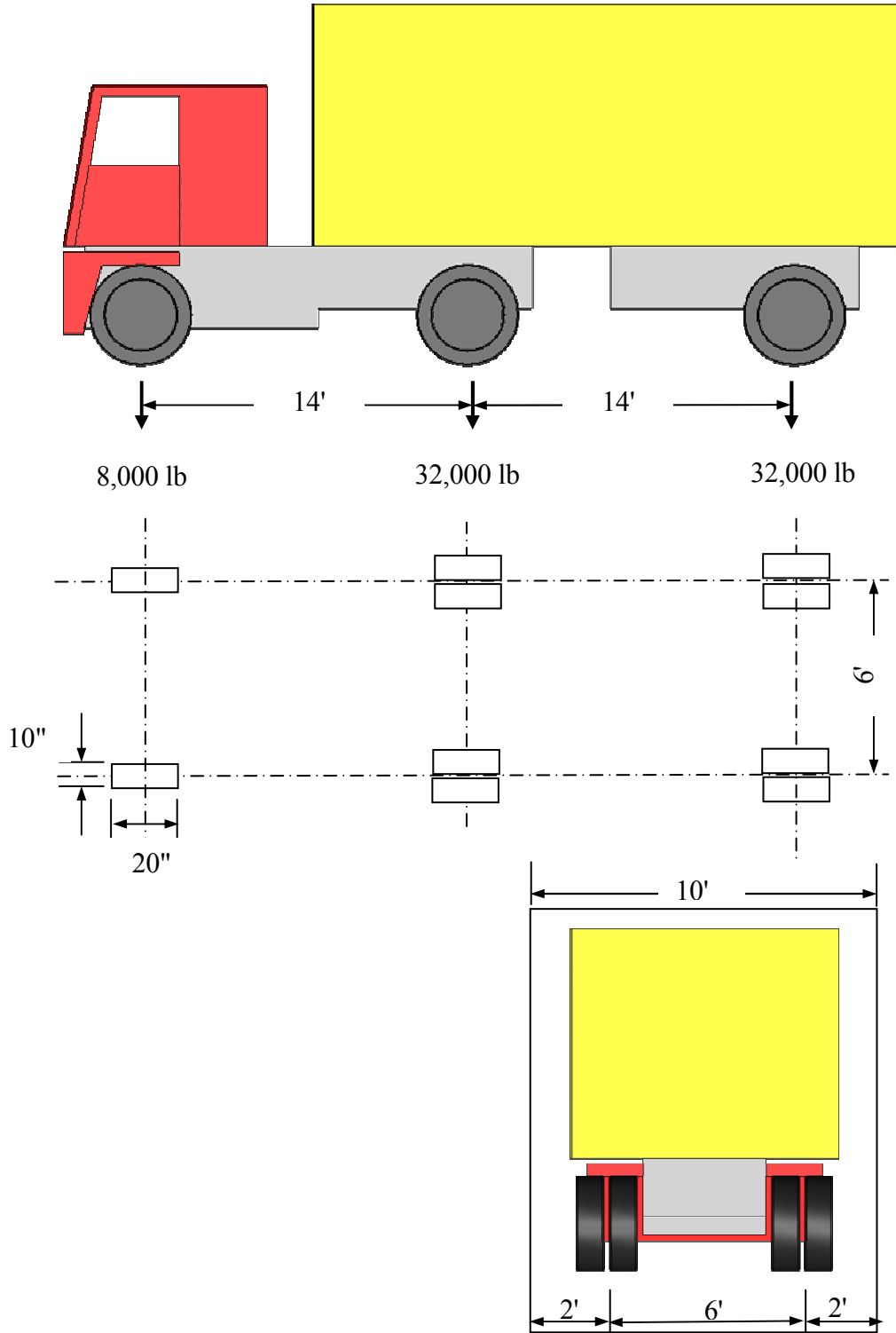


Figure 3.4-2 Truck in AASHTO load HL-93.

Temperature gradient

When exposed to sunlight during the daytime, the top fibers of the bridge experience higher temperatures than the bottom fibers, defined herein as positive gradient, and when the temperature drops down during the night, the top fibers experience lower temperatures than what the bottom fibers experience, defined herein as negative gradient. The variation of the temperature over the cross-section of the bridge is usually highly nonlinear. For simplicity, AASHTO LRFD (2004) Section 3.12.3 provides a general bi-linear configuration for the positive temperature gradient (Figure 3.4-3). The negative temperature gradient can be obtained from the same figure by multiplying the temperature values by -0.2 for decks with asphalt overlay and -0.3 for plain concrete.

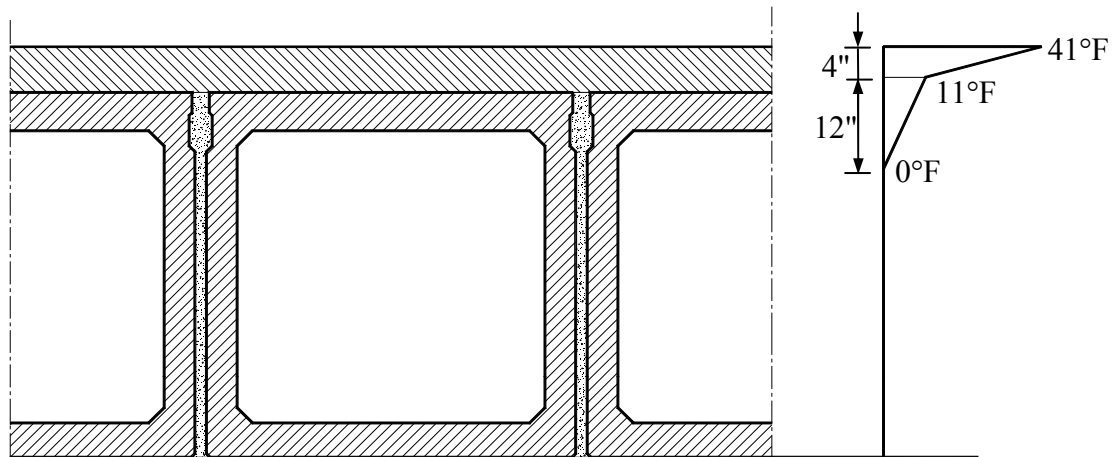


Figure 3.4-3 Typical positive temperature gradient over the bridge depth in Michigan.

3.5 Analysis Calibration

One essential step before conducting any of the study objective is to check the validity of the finite element analysis. This can be done by generating a numerical model for a small-scale experimental model or a full-scale prototype, and comparing the response of the FE model with that of the experimental/existing prototype. This finite element analysis has been verified for accuracy using two approaches:

1. By simulating an experimental half-scale bridge model built at Lawrence Technological University (Labib, 2007), and

2. By simulating an existing side-by-side box beam bridge built in south-east Michigan in 1999.

Simulating the existing bridge model can be found somewhere else (Bebawy, 2007 and Grace et al., 2007). In general, the analysis of this bridge yielded the following conclusions:

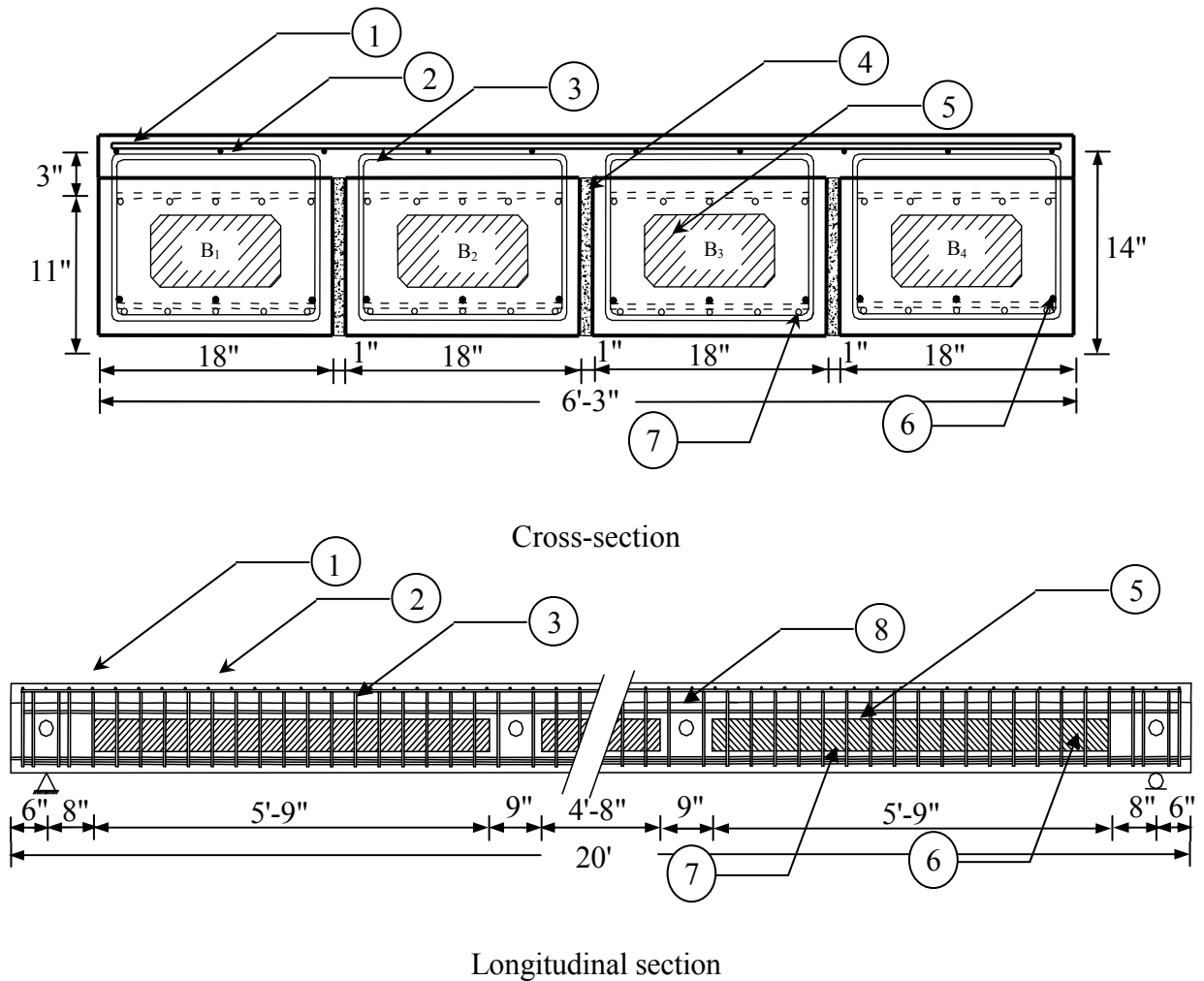
1. Traffic loads do not appear to be the key factor in developing longitudinal cracks in the slab. The positive temperature gradient is the major contributing factor in the initiation of the longitudinal cracks in the deck slabs in side-by-side box beam bridges.
2. To avoid the longitudinal deck cracking, the developed maximum principal stresses in the deck slab shall not exceed the cracking strength of the concrete when the bridge is subjected to positive temperature gradient with traffic loads and impact allowance.
3. AASHTO LRFD (2004) recommendation for 250 psi as minimum transverse prestress required to secure the longitudinal joints in side-by-side box beam bridges seems to be impractical and unreachable especially between the diaphragms location.
4. Impact allowance of 75% recommended by AASHTO LRFD (2004) for the design of the transverse deck joints is appropriate for the design of the longitudinal joints as well.
5. Since the combination of 100% of positive temperature gradient and traffic loads usually lasts for only a few hours during the day, it was determined that using presence factor corresponding to ADTT less than 1,000 is more appropriate than using presence factor corresponding to ADTT more than 5,000.

The experimental half-scale bridge model was composed of four simply supported side-by-side box-beams of cross-section 18 in. \times 11 in. each, and a span of 20 ft. The bridge model had a 3 in. thick deck slab reinforced with one layer of reinforcement at the mid-thickness. The results of the experimental program were employed to validate the techniques of the finite element analysis -methods of applying loads and boundary conditions. In addition, the experimental results were used to evaluate the FE model input parameters such as the material properties and the element sizes to bring the numerical and experimental results into fair agreement.

Generating a FE model for the experimental half-scale bridge model provided confidence in the analysis and established the framework for the modeling approach. Yet, the experimental model analysis did not deal with numerous aspects that are essential for meeting all of the objectives of this study. For instance, the experimental model analysis did not include a simulation for AASHTO truck load; neither did it include applying environmental loads such as thermal cycles and temperature gradients. As mentioned earlier in the literature review, the formation of the longitudinal cracks between the box-beams is more likely attributed to the thermal stresses rather than to the moving live loads. Therefore, modeling a full-scale bridge was mandatory to simulate the live and thermal loads. One of the bridges that was built recently (1999) in Michigan experienced longitudinal cracks along the entire span between the box-beams. As this bridge reflects the problem of longitudinal cracks in fairly new bridges, it was selected for numerical simulation to examine the influence of each load type on the developments of the cracks. In this section, only the numerical simulation for the experimental half-scale bridge model has been presented.

3.5.1 Half-Scale Bridge Model

The experimental bridge model was constructed at Lawrence Technological University in 2006 to examine the influence of the TPT force on the development of the longitudinal cracks in the deck slab in side-by-side box-beam bridges (Labib, 2006). The bridge model was composed of four side-by-side box-beams with a cross-section and dimensions, as shown in Figure 3.5-1. The bridge model had a span of 19 ft (228 in.) and width of 75 in. The model included four transverse diaphragms: two at the ends with a width of 14 in. each and two at the mid-span (5.5 ft apart) with a width of 9 in. each. The bridge model included a 3 in. thick deck slab with one layer of reinforcement.



- 1- Slab transverse reinforcement
- 2- Slab longitudinal reinforcement
- 3- Steel stirrups #3 @ 4 in.
- 4- Shear-key
- 5- Hollow portion (10" wide and 5" deep)
- 6- Prestressing tendons ($\Phi = \frac{3}{8}$ in., $A = 0.115$ in²)
- 7- Non-prestressing tendons ($\Phi = \frac{3}{8}$ in., $A = 0.115$ in²)
- 8- Intermediate diaphragm with PVC duct for TPT strand

Figure 3.5-1 Half-scale experimental bridge model.

3.5.1.1 Bridge Model Components and Material Properties

The 28 day compressive strength of the concrete in the box-beams was 6,000 psi, while the 28 day compressive strength of the concrete in the slab was 5,700 psi. The box-beams were reinforced with:

1. Five bottom non-prestressing CFRP (DCI tendons, Diversified Composites, Inc.) tendons with a diameter of 0.375 in. and a cross-sectional area of 0.11 in².
2. Three bottom prestressing CFRP tendons with a cross-sectional area of 0.11 in². and each strand was pre-tensioned with a prestressing force of 12,000 lb.
3. Five top non-prestressing CFRP tendons with a cross-sectional area of 0.11 in².
4. Steel stirrups #3 @ 4 in.
5. Four CFRP tendons with a diameter of 0.375 in. and cross-sectional area of 0.11 in² in the transverse direction to apply transverse post-tensioning forces up to 30 kip.

The slab was reinforced with a single layer of reinforcement. This reinforcement layer was composed of longitudinal and transverse non-prestressing CFRP tendons with a diameter of 0.305 in., cross-sectional area of 0.073 in², and center-to-center spacing of 8 in. in both directions. The experimental bridge model was supported by steel roller and hinge supports.

In the finite element model, the concrete in the box-beams was modeled with an ultimate compressive strength of 6,000 psi, modulus of elasticity of 4.7×10^6 psi, and modulus of rupture of 562 psi as determined by AASHTO LRFD (2004). Likewise, the concrete in the deck slab was assumed to have a modulus of elasticity of 4.57×10^6 psi, and modulus of rupture of 550 psi. Furthermore, based on uniaxial test results, the CFRP tendons were modeled with an ultimate tensile strength of 340,000 psi, ultimate strain of 1.8%, and modulus of elasticity of 22.8×10^6 psi. The material of the tendons was assumed to behave linearly elastic until failure. The transverse tendons were modeled with the same material and provided with 6 in. \times 6 in. \times 1 in. steel bearing plate at both ends. The stirrups were not modeled in the finite element model as shear cracking was not expected. Steel bearing plates were used to simulate the supports. Each beam was provided with a 18" \times 6" \times 1" steel plate at each end. In addition, the vertical load was applied through two 15" \times 6" \times 2" steel plates with a center-to-

center spacing of 36 in. This modeling technique replicated the experimental setup Figure 3.5-2.

Several element sizes were examined in the FE model. It was found that an element size of 4 in. was the most appropriate element size to be used (Figure 3.5-3); the FE results closely matched the results of the experimental program when using this element size. All the concrete components and the steel plates were meshed using the 8-node linear brick element C3D8R; and the reinforcement was meshed using the 2-node linear 3D truss element T3D2.

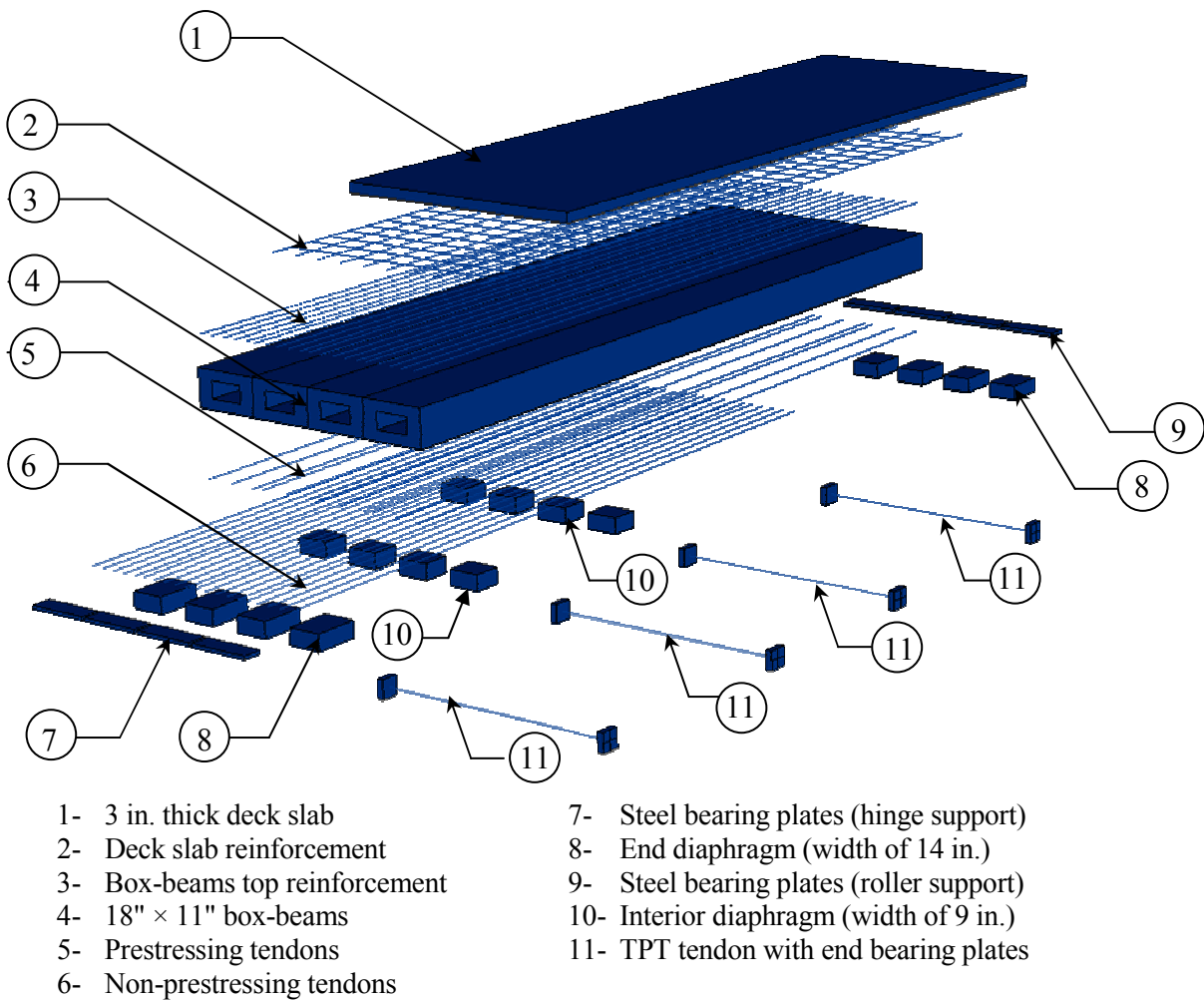


Figure 3.5-2 FE bridge model components.

No. of elements = 10,883
No. of nodes = 18,218
No. of variables = 52,346

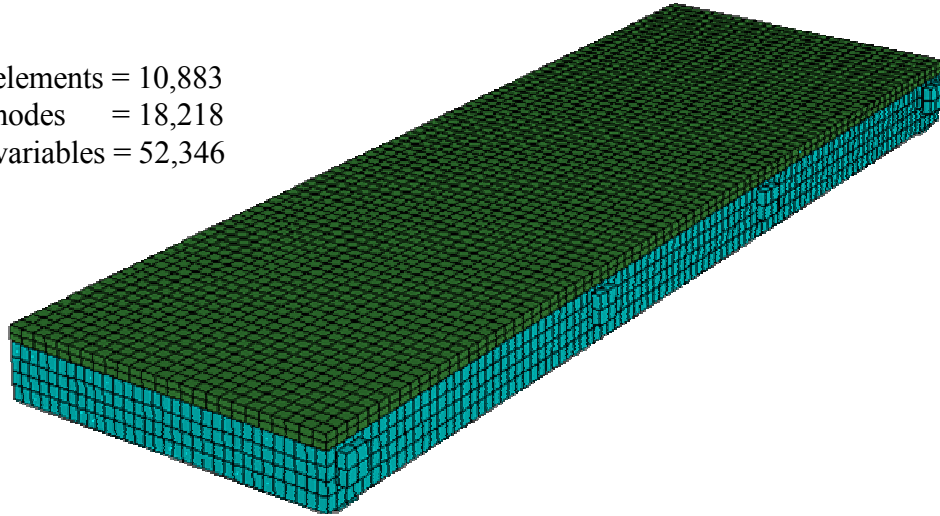


Figure 3.5-3 FE model meshing.

3.5.1.2 Loading Scheme

The loading set-up included loading beam B2, one of the interior beams (see Figure 3.5-1), with a four-point-load up to 80,000 lb with increasing increments of 10,000 lb (Figure 3.5-4 and

Figure 3.5-5). The load was then increased to failure (failure load was 130,000 lb). Loading tests up to 80,000 lb were repeated with TPT force of 0, 10, 20, and 30 kip while loading up to failure was performed with TPT force of 30 kip.

In the finite element model, loading tests without and with TPT force of 30 kip were simulated. The results presented in this section are those for loading test without TPT force. Another set of results were obtained for the case of loading with TPT force of 30 kip but was not provided to avoid repetition. The obtained results were used to evaluate the ability of the numerical models to predict the deflection and onset or locations of longitudinal cracks.



Figure 3.5-4 Load setup (experimental model).

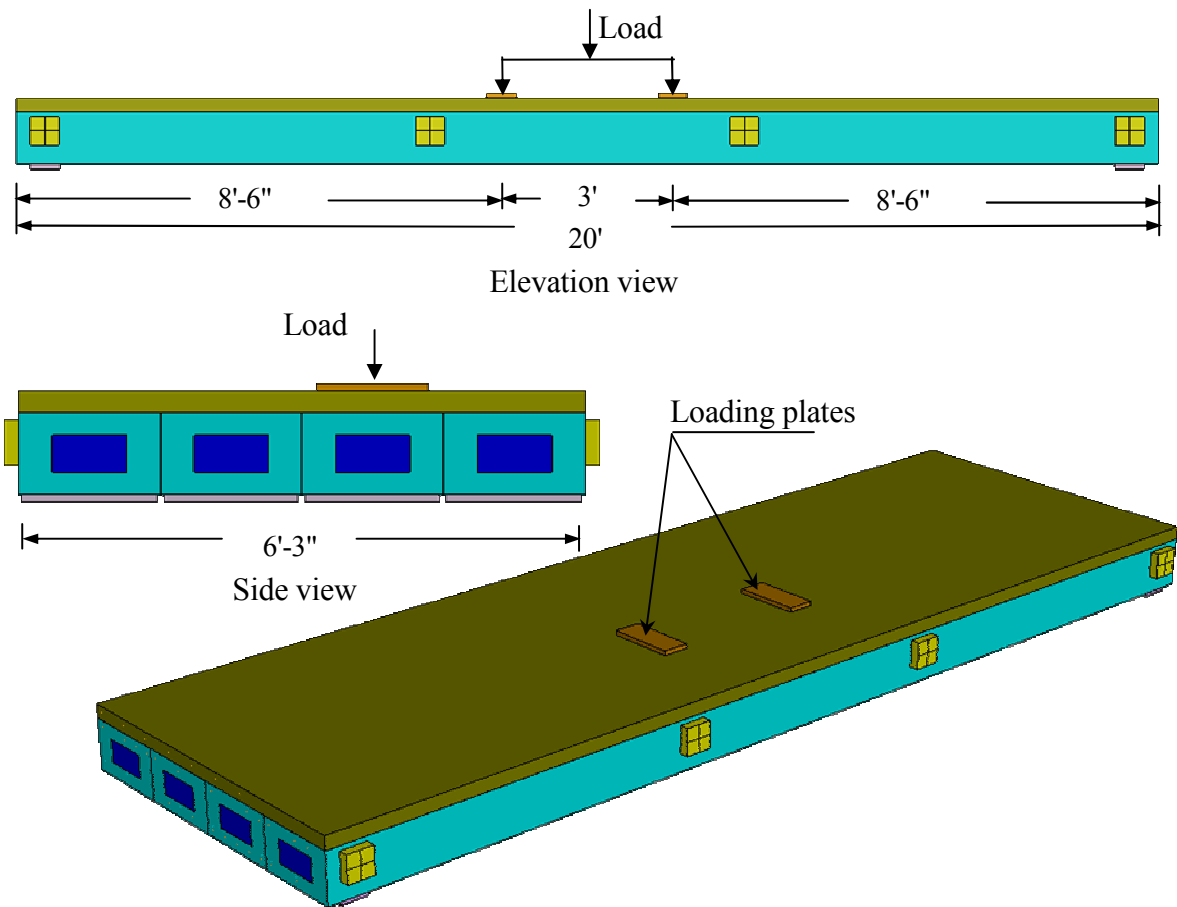


Figure 3.5-5 Load setup (numerical model).

3.5.1.3 Comparison Between Numerical and Experimental Results

The deflections of the experimental and numerical bridge models measured at the mid-span section under different vertical loads are shown in Figure 3.5-6 through Figure 3.5-11. In general, the FE results matched the experimental results. The difference between the numerical and the experimental results increased when the vertical load reached 50 kip (Figure 3.5-9). This can be attributed to the fact that after reaching a load of 50 kip, cracks started to develop in the experimental deck slab. The numerical model was able to predict the cracks location; however beyond the cracking stress, the formation of localized cracks was represented at the element level with a softening stress-strain response. Consequently, the crack size was not accurately represented in the FE model, which could be the reason for the difference between the experimental and numerical deflection results. In addition, the FE model was relatively stiffer than the experimental model. This is due to several approximation schemes used in the FE analysis, which assume ideal structures such as approximated displacement fields, integration schemes, etc.

Figure 3.5-12 through Figure 3.5-16 show the crack maps for the deck slab top and bottom surfaces under different levels of the vertical load. No cracks developed in the deck slab for vertical loads less than 50 kip. However, at a load of 50 kip, small longitudinal cracks developed at the slab bottom surface over the interior shear-key locations. The top surface, on the other hand, did not experience any cracks. The cracks propagated while increasing the vertical load to 70 kip, cracks started to appear in the slab top surface (Figure 3.5-15). The cracks continued to propagate at both the top and bottom surfaces under a load of 80 kip as shown in Figure 3.5-16. These cracks matched the reported cracks in the experimental bridge model. The cracks in the experimental model were firstly observed in the slab top surface at a load of 70 kip and then propagated under a load of 80 kip as shown in Figure 3.5-17.

In summary, the deflection and the locations of the crack development obtained from the FE model closely matched with those of the experimental results. These results validated and confirmed the adequacy of the developed numerical model and the various selected elements.

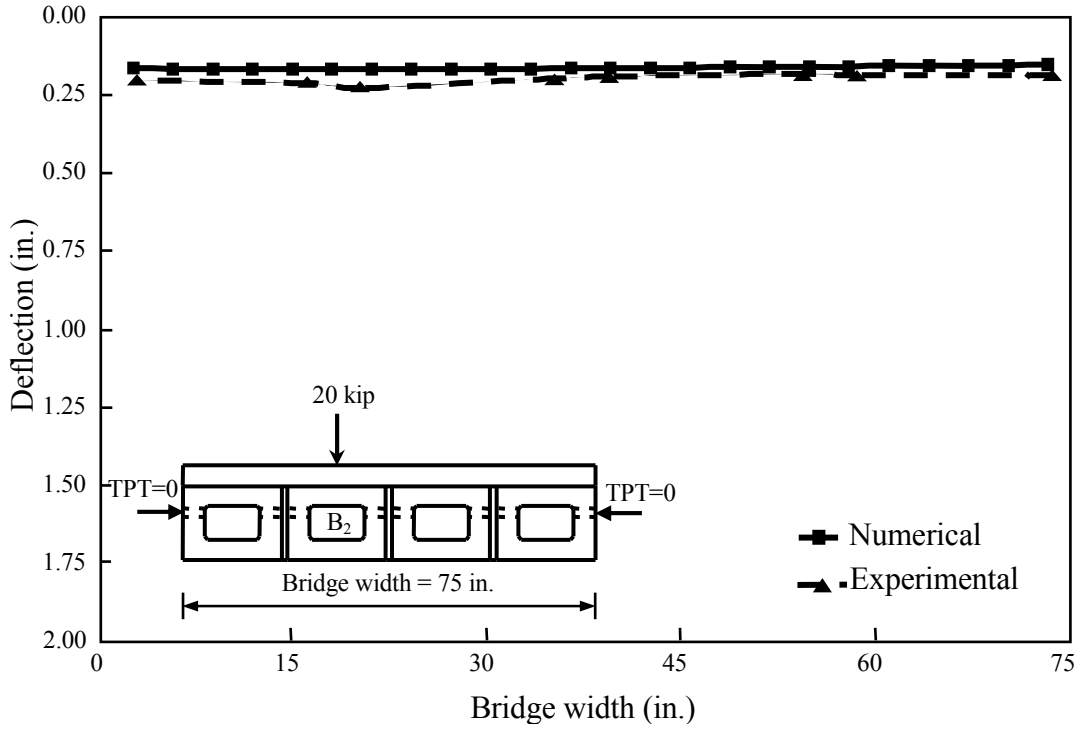


Figure 3.5-6 Deflection of the bridge model under vertical load of 20,000 lb.

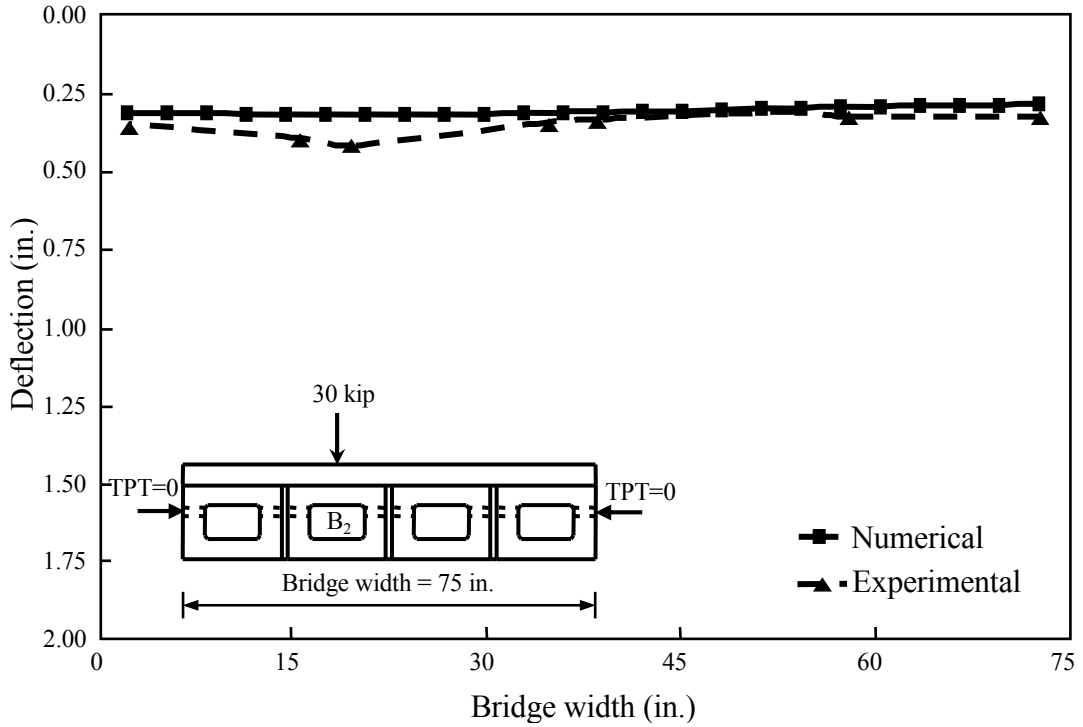


Figure 3.5-7 Deflection of the bridge model under vertical load of 30,000 lb.

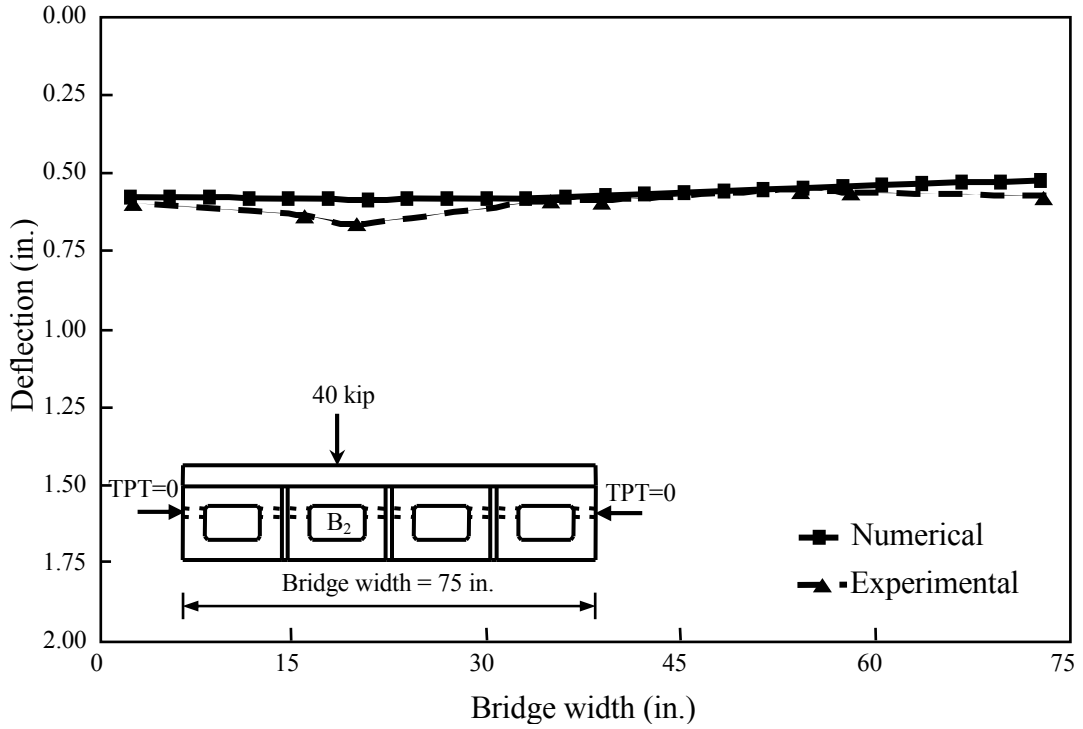


Figure 3.5-8 Deflection of the bridge model under vertical load of 40,000 lb.

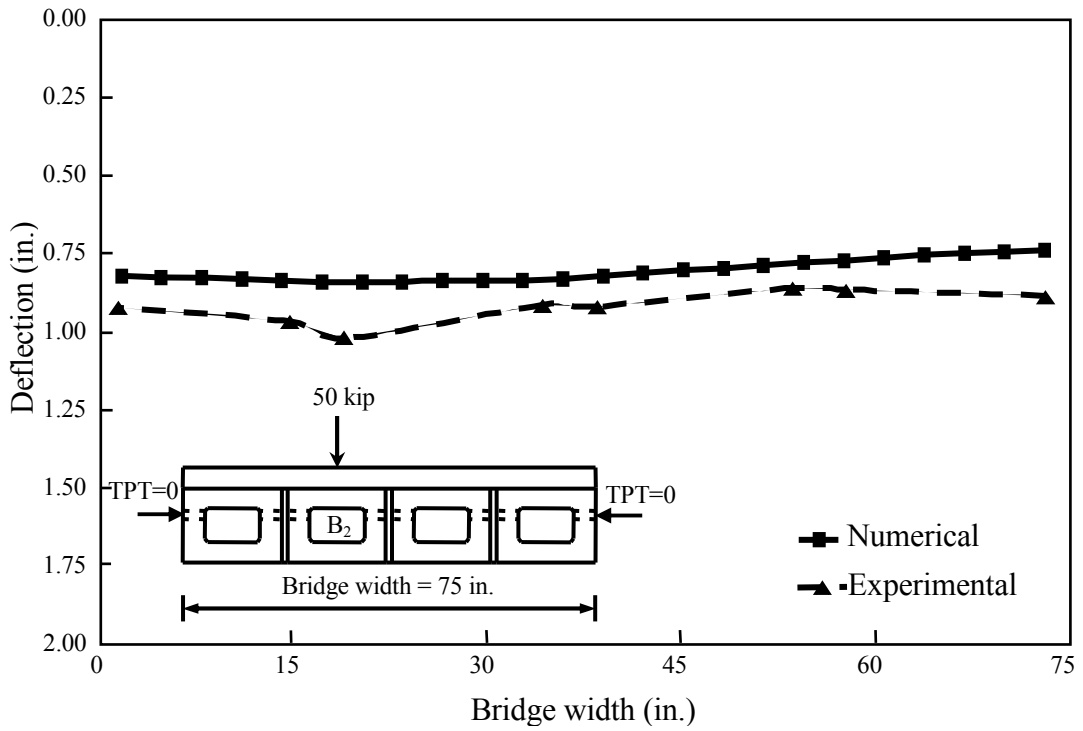


Figure 3.5-9 Deflection of the bridge model under vertical load of 50,000 lb.

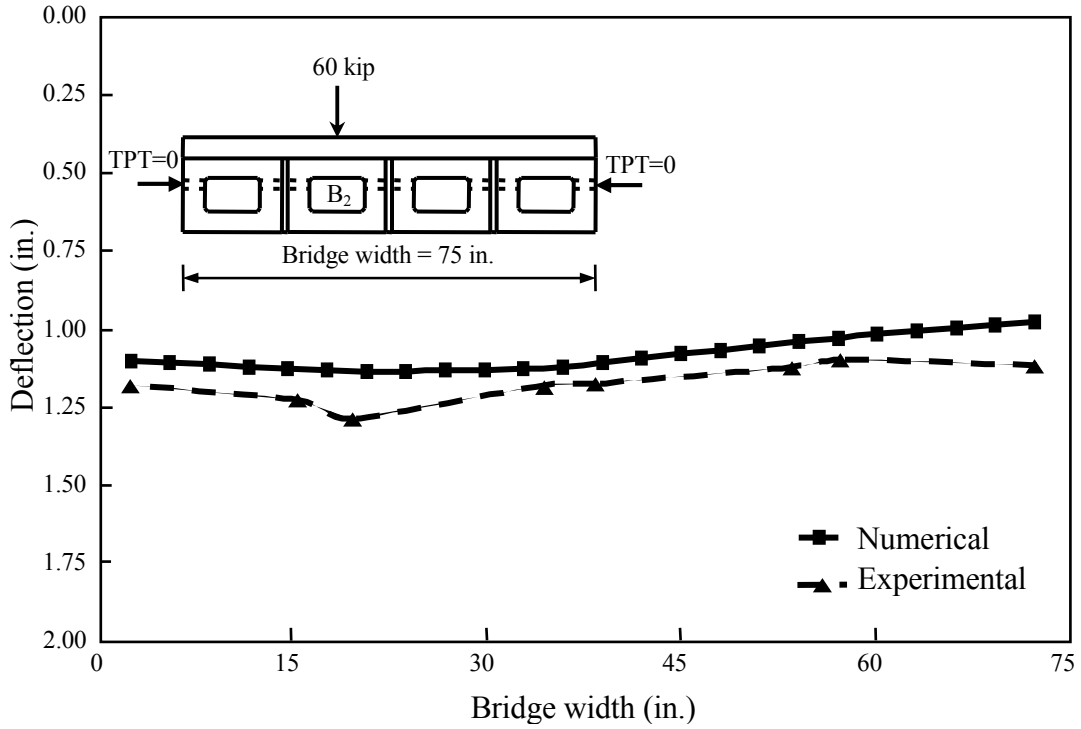


Figure 3.5-10 Deflection of the bridge model under vertical load of 60,000 lb.

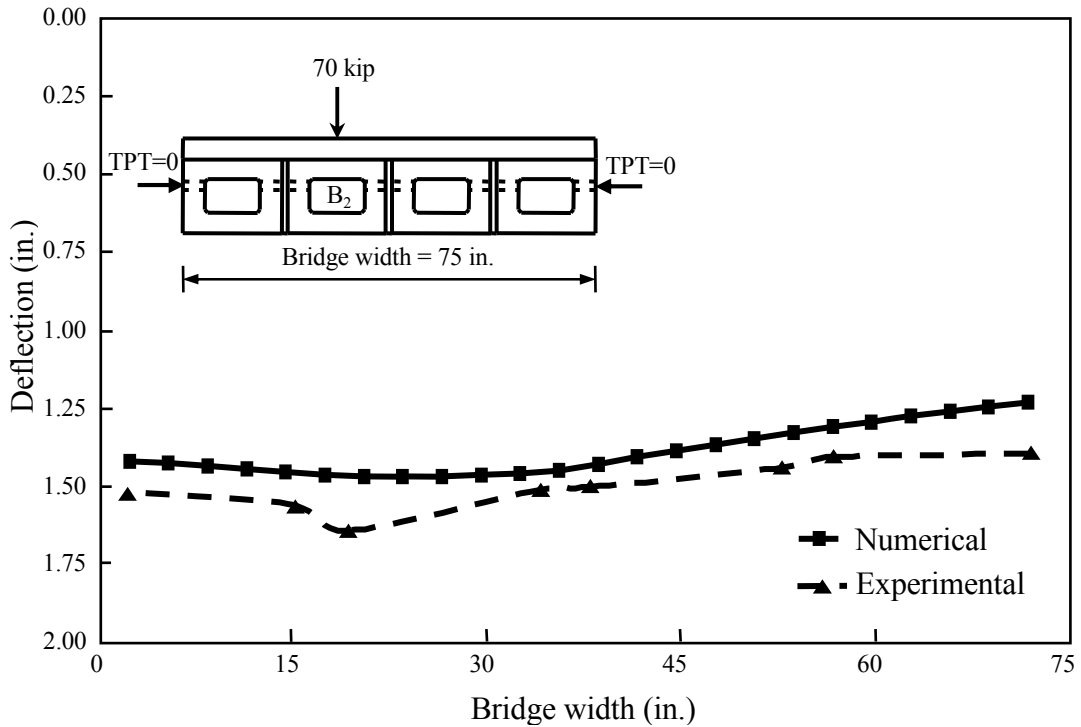


Figure 3.5-11 Deflection of the bridge model under vertical load of 70,000 lb.

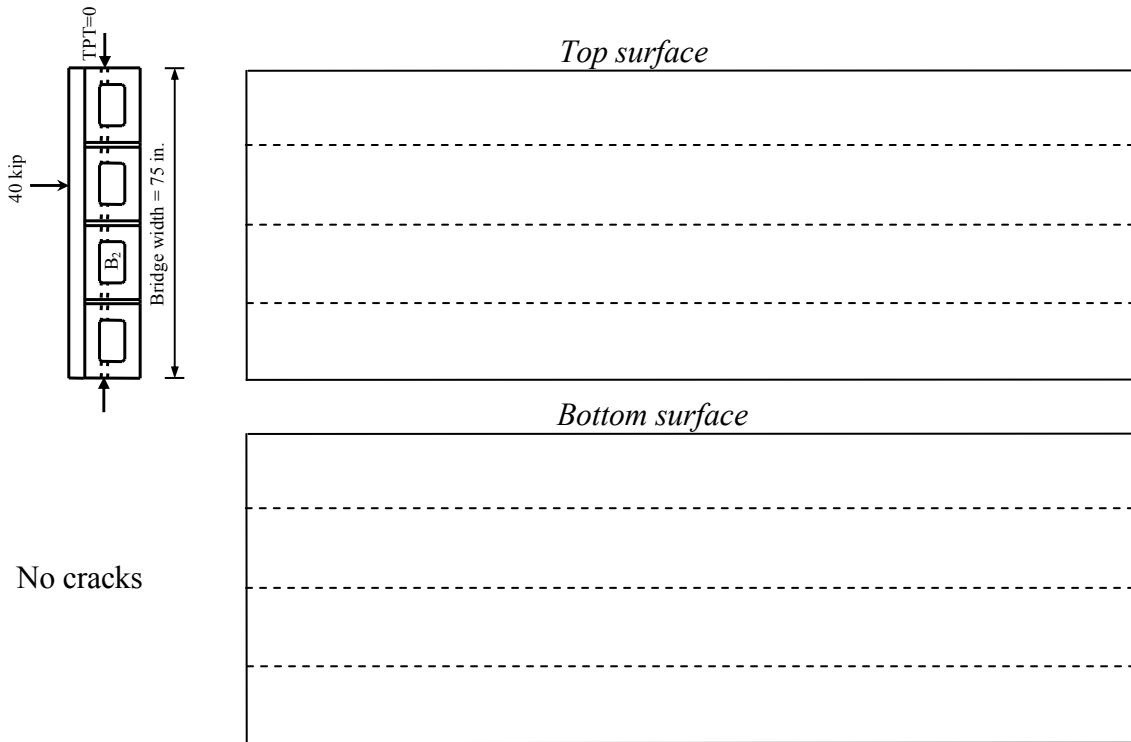


Figure 3.5-12 Crack development in the slab under vertical load up to 40,000 lb.

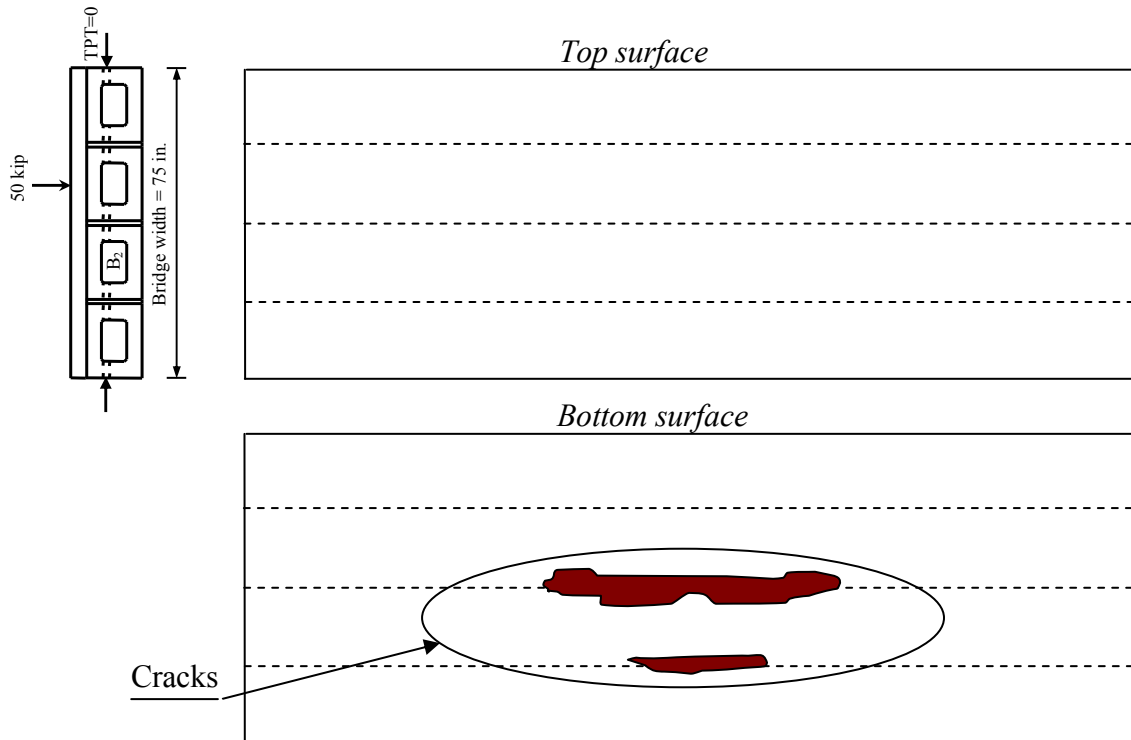


Figure 3.5-13 Crack development in the slab under vertical load of 50,000 lb.

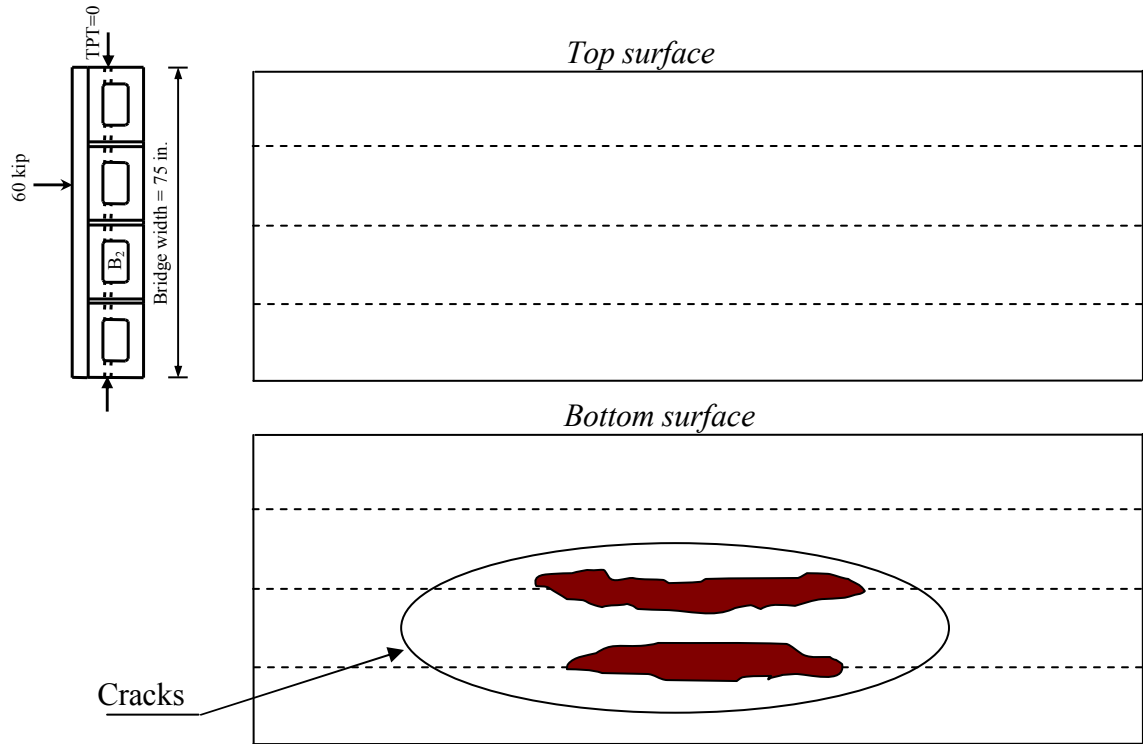


Figure 3.5-14 Crack development in the slab under vertical load of 60,000 lb.

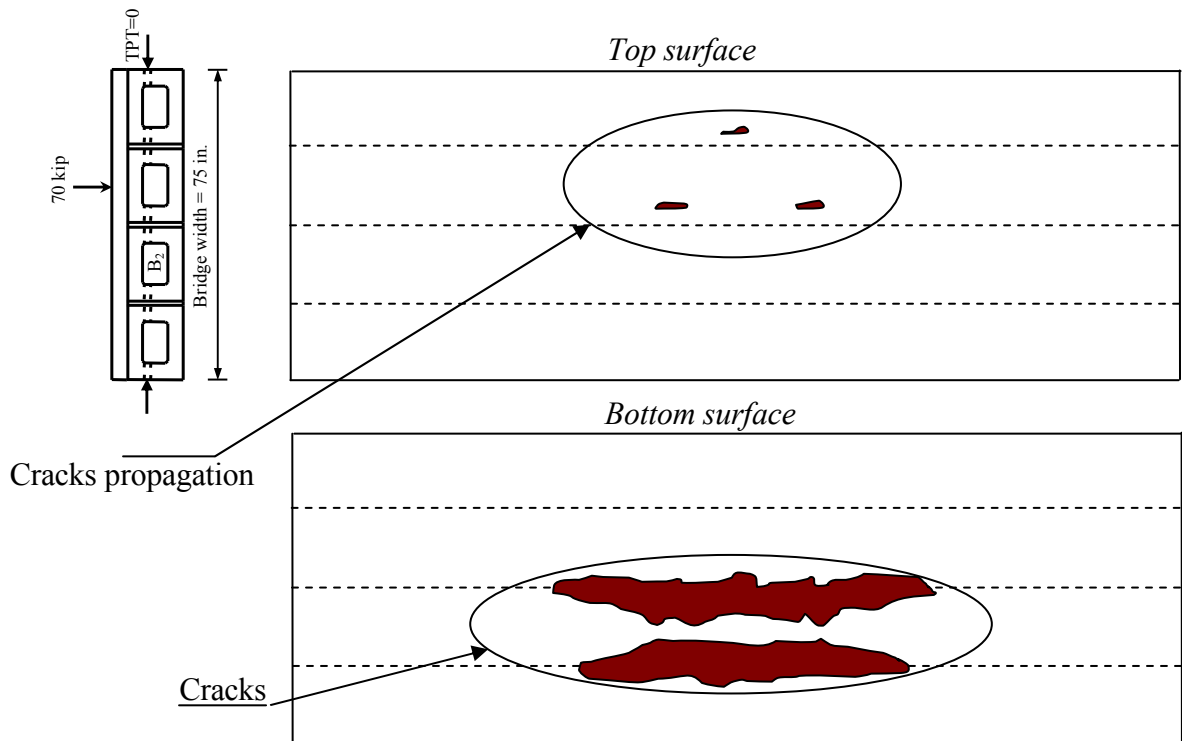


Figure 3.5-15 Crack development in the slab under vertical load of 70,000 lb.

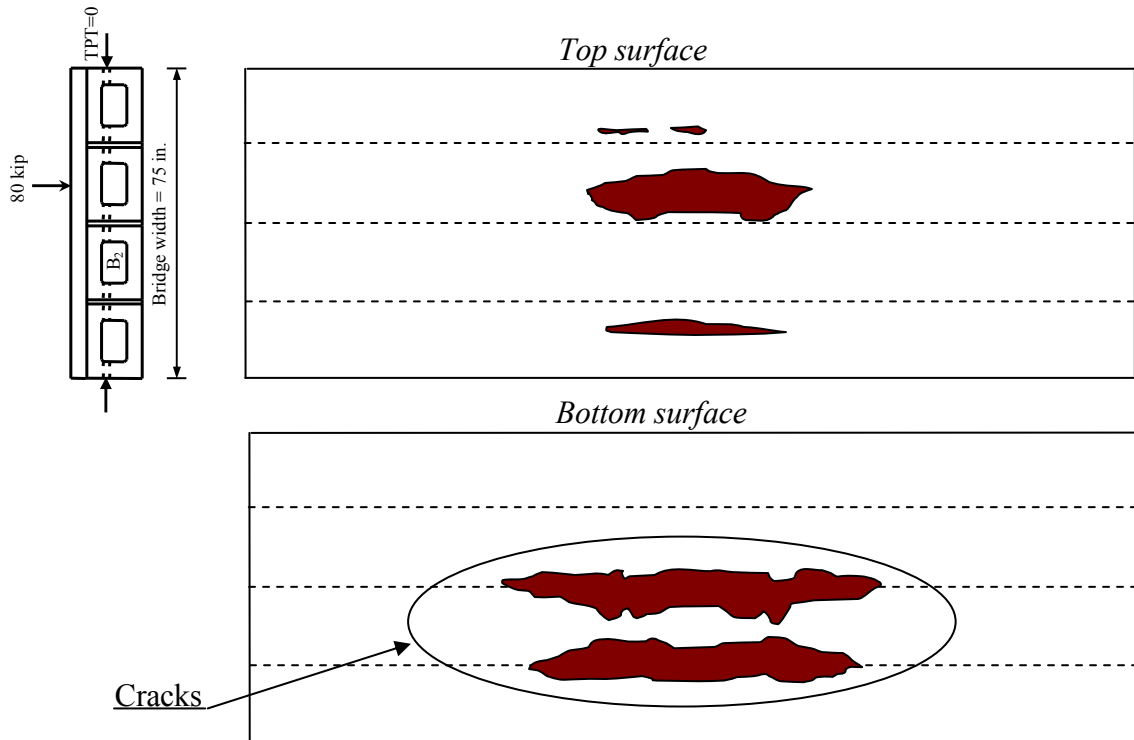


Figure 3.5-16 Crack development in the slab under vertical load of 80,000 lb.

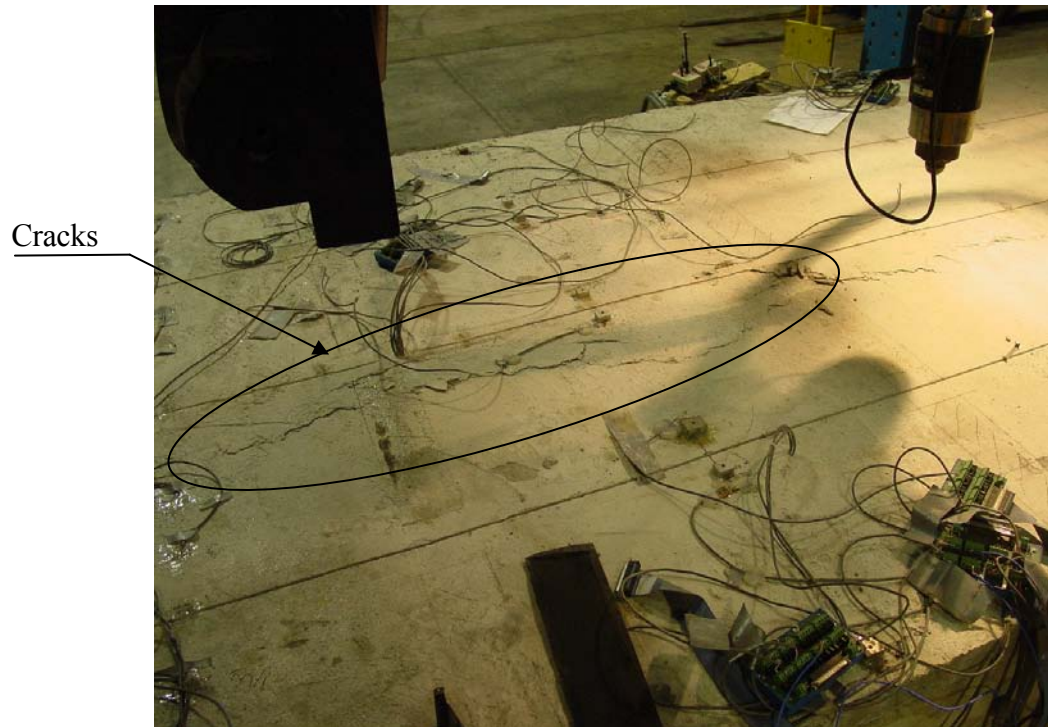


Figure 3.5-17 Crack development in the experimental bridge model under load of 80,000 lb.

CHAPTER 4: NUMERICAL INVESTIGATION OF TRANSVERSE POST-TENSIONING ARRANGEMENT

4.1 Introduction

The main objective of the finite element analysis was to eliminate the longitudinal deck cracking by establishing an adequate number of diaphragms and an appropriate TPT force level per diaphragm for wide range of bridges varying in span length and width as well. The analysis was conducted to relate the number of diaphragms to the bridge span and the TPT force level to the bridge width. Several bridge models with different spans were generated and analyzed with different numbers of diaphragms, and then wider bridge models were generated for the previous spans and analyzed with different TPT force levels. Finally, the results were summarized in charts showing the relationship between the bridge span and the number of diaphragms and the relationship between the bridge width and the TPT force level.

4.2 Adequate Number of Diaphragms

In order to establish the adequate number of diaphragms in side-by-side box-beam bridges, FE models for bridges with spans of 50, 62, 100, and 124 ft were generated. The width of the models was selected to be as small as practical in order to minimize the duration of the analysis. A width of 24 ft, which accommodates two traffic lanes without shoulders or one traffic lane with shoulders, was found to be the narrowest practical bridge width. Therefore, all the FE models in this part of the analysis were generated with a width of 24 ft. Eight side-by-side box-beams formed the bridge when 36 in. wide beams were used, and six box-beams formed the bridge when 48 in. wide beams were used.

4.2.1 Analysis Progression

The TPT arrangement is controlled by the number of diaphragms and TPT force level. An adequate transverse arrangement can be achieved by adjusting either the TPT level or the number of diaphragms. However, in some cases, increasing the TPT force level does not help in achieving an optimum TPT arrangement. Instead, the number of diaphragms has to be increased. Accordingly, the analysis to establish the adequate number of diaphragms was divided into five main steps:

1. Generating FE models following MDOT Specifications for transverse post-tensioning force and number of diaphragms.
2. Checking the development of the cracks in the deck slab under service loads.
3. Increasing the TPT level for the models that experienced cracks in the deck slab.
4. Increasing the number of diaphragms when increasing TPT level failed to eliminate crack development in the deck slab.

Repeating step 2 through 4 until eliminating the development of the cracks in the deck slab. The following sections present: first, a brief description of MDOT Specifications for TPT arrangement; second, a broad scheme for the loading and analysis steps; third, a discussion of the analysis and the results, and finally, charts showing the relationship between the number of diaphragms versus the bridge span for the 48 and 36 in. wide box-beams, respectively.

4.2.2 MDOT Specifications

Four bridge models were generated following MDOT Specifications for the TPT arrangement. The first model simulated a bridge with a span of 50 ft with four diaphragms. The second model simulated a bridge with a span of 62 ft with five diaphragms. The third model simulated a bridge with a span of 100 ft with six diaphragms; however, due to extensive details of this model, it was not feasible to model the full span. Instead, only half of the span was modeled and symmetry conditions were applied at the mid-span section. Finally, the fourth model was an example for spans over 100 ft where seven diaphragms were required. It simulated a bridge with a span of 124 ft; again, only half of the span was modeled. The following discussion offers detailed information on the behavior of each model under construction and service loads.

4.2.3 Loading Steps

Analysis and loading steps were identical throughout the entire study regardless of the model geometry or its TPT arrangement. The steps were organized as follows:

1. The pre-tensioning force was applied to the model through bottom reinforcement longitudinal steel strands. By using a force of 28,500 lb/strand, each strand was prestressed up to 70% of its ultimate strength.

2. The self-weight of the box-beams was calculated and applied as a distributed load over the top surface of the beams.
3. Virtual elements were created in between the box-beam sides in order to connect the beams together. The elements developed a friction interface between the adjacent surfaces with coefficient of friction equal to 0.7. This simulated the stage of pouring the shear-keys. As an approximation, the sides of the box-beams in the FE models were flat without the groove of the shear-key.
4. The first stage of transverse post-tensioning forces was simulated by applying a transverse force equal to 25,000 lb/location. It was assumed that the required transverse force would be applied in two stages: before and after pouring the deck slab. Subsequently, the slab could experience some compressive stresses that would contribute towards eliminating the development of the deck slab cracks. Applying the post-tensioning force in one or two stages (before and after casting the deck slab) has a little influence on the analysis as the post-tensioning force generates internal energy stored in the beams if the force is applied before casting the deck slab and in the beams and the slab if the force is applied after casting the deck slab. This level of internal energy will be used to connect the components of the superstructure and eliminate the deck cracking. In addition, the analysis were based on the assumption that un-bonded TPT strands will be used to enable future replacement for any deteriorated beam and reapplying the post-tensioning force. Subsequently, any future TPT force will be applied to the beams and the deck slab together.
5. The self-weight of the slab was applied to the model as a distributed load over the box-beams top surfaces.
6. A rigid connection was established between the deck slab bottom surface and the box-beams top surfaces. This type of connection prevented any slippage or sliding between the connected surfaces; consequently, the slab was integrated to the model.
7. The remaining TPT force was applied.
8. The weight of the wearing surface (25 lb/ft²) was applied over the slab top surface and the weight of two Type 4 barriers (475 lb/ft each) was applied along the bridge edges.

In addition, the permanent losses were deducted from the longitudinal prestressing force in the same analysis step. Losses were calculated according to AASHTO LRFD (2004) lump-sum estimate of time dependent losses as provided in Section 5.9.5.3.

9. The service loads were applied as follows:

- 100% of positive temperature gradient was applied to the FE models according to AASHTO LRFD (2004) Section 3.12.3. The positive temperature gradient is the key for developing high tensile stresses in the deck slab, which subsequently leads to deck slab longitudinal cracking once applying the traffic loads (Bebawy, 2007 and Grace et al., 2007).
- A truck load was applied over one lane of the bridge model. Two types of live loads were investigated during the analysis. MDOT Specifications for TPT arrangement were based on using standard AASHTO trucks either HS-20 or HS-25; the bridge models were checked for both trucks; the heavier truck (HS-25) was selected to represent MDOT Specifications. The analysis was also performed using the AASHTO LRFD (2004) specifications because of the detailed explanation for the load types and the load factors. In AASHTO LRFD (2004) specifications, the standard trucks are no longer considered as live load; instead, a new type of loading identified as vehicular loading HL-93 is considered. The new loading is the standard HS-20 truck along with a lane load of 640 lb/ft distributed over 10 ft wide lane. Therefore, the models were checked for both HS-25 truck and HL-93 load though the difference in the response of models under both loads was not significant. The live loads were multiplied by presence factors corresponding to (Average Daily Truck Traffic) ADTT ranging between 100 and 1,000. The presence factor was taken as 0.95 in case of two lanes loaded and 1.14 in case of one lane loaded. In addition, an impact allowance of 75% was imposed in the entire analysis.

10. The analysis was completed when the deck slab was free of any cracks under the imposed loads.

4.2.4 Bridge Models Generated Using 48 in. Wide Box-Beams

4.2.4.1 50 ft Span Bridge Model

First, the 50 ft span bridge model had a TPT arrangement that conformed to current MDOT Specifications (Figure 4.2-1). Box-beams were set to a depth of 27 in. and a width of 48 in. One CFCC per diaphragm was provided at the middle of the transverse beam. Furthermore, as an AASHTO HS-25 truck was used as a design load, a transverse post-tensioning force of 104,500 lb was provided per diaphragm.

Analysis and discussion

The discussion herein addresses only the framework of the analysis and the results. The results are presented in detail for each loading case using stress contour maps in Bebawy (2007). The response of the FE bridge model under each loading step is summarized as follows:

1. The beams experienced a camber of 1.09 in. due to the longitudinal prestressing forces. The maximum stresses in the beams were less than the allowable stresses specified for prestressed concrete (AASHTO LRFD, 2004 Section 5.9.4).
2. After adding dead load of the box-beams, the camber decreased to 0.74 in. Longitudinal and transverse stress values remained within the allowable range for the stresses.
3. After applying the first stage of the TPT force, the transverse stresses in the beams did not change significantly as the TPT force was just 25,000 lb/diaphragm.
4. Adding the slab dead load reduced the camber in the beams to 0.58 in.
5. After casting the deck slab and before applying second stage of TPT force, the stresses in the deck slab in both directions were negligible because this stage simulated the deck slab just after casting and curing.
6. After applying the second stage of TPT force, the deck slab gained some compressive stresses in the transverse direction. However, the compressive stresses were localized near the diaphragms and the ends. The maximum developed transverse stress was 155 psi, concentrated at local areas near the supports. The majority of the slab experienced compressive stresses in the range of 7 to 31 psi, which were far less than the recommended limit of 250 psi that was specified by AASHTO LRFD (2004) Section

- 4.6.2.2. The longitudinal stress distribution was not affected significantly with the applied TPT force. At the same time, applying the remaining TPT force caused the compressive pressure on the box-beam sides to reach a value of 400 psi at the end diaphragms. However, the major contact areas experienced pressure levels below 10 psi. The poor distribution of the pressure indicated that AASHTO LRFD (2004) recommendations of obtaining uniform compressive prestress through the joint are not realizable unless the diaphragms are provided every few feet.
7. The last construction stage was to deduct time dependent losses from the longitudinal prestressing forces and to apply the superimposed dead loads (SDL) over the deck slab. The transverse stresses were not affected significantly; however, some longitudinal compressive stresses developed in the slab due to the flexural action of the loads in the longitudinal direction. By the end of this stage, the beams camber decreased to 0.40 in.

Model response under service loads

1. When applying 100% of the positive temperature gradient, the slab top and bottom surfaces experienced significant increase in the longitudinal compressive stresses. In the transverse direction, a sudden increase in the compressive stresses took place in the slab top surface; with the maximum value at the span ends (626 psi) while the major area experienced stresses in the range of 300 to 384 psi. At the same time, transverse tensile stresses of a value of 261 psi developed in the slab bottom surface. Consequently, the maximum principal stress reached 267 psi at the slab bottom surface, while the top surface experienced maximum principal stresses in the average of -22 psi (compression). The deformation in the slab before and after applying the temperature gradient is shown in Figure 4.2-2.
2. Applying AASHTO HS-25 truck load with impact or presence allowances caused the longitudinal compressive stresses in the loaded lane to reach 742 psi at the slab top surface; while small tensile stresses less than 55 psi developed at the bottom surface. The transverse stresses in the slab top surface remained compressive, while the transverse tensile stresses increased to about 300 psi at the bottom surface of the slab over some shear-key locations. Moreover, the maximum principal stresses in the slab

bottom surfaces reached a value of 311 psi at the same locations. However, the deck slab was able to sustain the applied loads without developing any tensile cracks.

3. By applying AASHTO HS-25 truck load (or HL-93 load) with the impact and presence allowances, some significant cracks developed in the deck slab, as shown in Figure 4.2-3 and Figure 4.2-4. The cracks initiated from the bottom surface and developed towards the top surface. Although they did not reach the top surface, repeated loads would likely cause the cracks to propagate throughout the full depth of the deck slab.

There are two possible solutions to avoid the propagation of the cracks. The first option is to increase the TPT force in each diaphragm. The other option is to increase the number of diaphragms. As mentioned earlier in this section, the first solution to be checked was always increasing the TPT; accordingly, in the subsequent analysis, the TPT force was increased up to 200,000 lb/diaphragm while maintaining the same number of diaphragms.

1. After applying a TPT force of 175,000 lb/diaphragm (25,000 lb/diaphragm was applied before casting the deck slab), localized transverse compressive stresses in the deck slab reached 362 psi at the span ends. Yet, the majority of the deck slab experienced compressive stresses in the range between 9 and 44 psi. In the longitudinal direction, small compressive stresses were seen in the deck slab, but they did not exceed 37 psi. Some longitudinal tensile stresses of a value of 114 psi developed at local areas in the slab ends. The pressure on the box-beams sides exceeded 500 psi at the diaphragms location. However, in the areas between the diaphragms locations, the compressive pressure did not exceed 10 psi.
2. Deducting time dependent losses and applying superimposed dead loads increased the longitudinal compressive stresses in the deck slab to 147 psi but did not affect the transverse stresses.
3. After applying positive temperature gradient, the slab top surface experienced longitudinal compressive stresses up to 551 psi while the stresses were negligible in the slab bottom surface. At the same time, the transverse compressive stresses in the slab top ranged between 300 and 395 psi. The bottom surface experienced tensile stresses up

to 240 psi over some shear-key locations. The maximum principal stresses in the slab bottom surface reached a value of 256 psi (tension).

4. After applying AASHTO HS-25 truck load without impact and presence allowances, the maximum principal stresses reached 285 psi (tension) at locations of the shear-key joints in the bottom surface.
5. Although the applied TPT force was nearly twice the TPT force in the first trial, the slab experienced small cracks in the bottom surface after applying AASHTO HS-25 truck load or HL-93 load with the impact and presence allowances (Figure 4.2-5 and Figure 4.2-6). It is obvious that the model performance was improved with the large TPT force; yet, the cracking problem was not controlled entirely.

As a parametric evaluation, the TPT force was increased to 300,000 lb/diaphragm to investigate the influence of high TPT level on the model. However, the transverse stresses in the slab did not reach the limit required by AASHTO LRFD (2004); neither did the pressure on the box-beams sides in the areas between the diaphragms. Moreover, some cracks developed immediately after applying the TPT force in the slab (Figure 4.2-7) and the box-beam sides as well (Figure 4.2-8) due to the stresses localization. So, even with high TPT level, the AASHTO LRFD (2004) requirement for transverse prestress was not reachable.

The second available solution to overcome the deck cracking was to increase the number of diaphragms; the number of diaphragms was increased to five instead of four; two at the ends and three equally spaced inbetween (Figure 4.2-9). The TPT force was set to 100,000 lb/diaphragm as a first trial.

1. The transverse compressive stresses reached 148 psi in the deck slab after applying the second TPT stage with a TPT force of 75,000 lb/diaphragm. The maximum stresses were concentrated near the support locations. However, the majority of the deck slab experienced compressive stresses in the range between 5 and 33 psi. In the longitudinal direction, small compressive stresses developed in the deck slab, but they did not exceed 15 psi. Likewise, some tensile stresses were generated at local areas near the supports and reached 44 psi. The pressure on the box-beams sides exceeded 400 psi at

- the end regions. However, the regions between the diaphragms experienced pressure less than 10 psi.
2. After deducting time dependent losses and applying superimposed dead loads, the longitudinal compressive stresses reached 120 psi in the deck slab top surface at the mid-span. However, the transverse stresses were not affected by the applied loads.
 3. After applying positive temperature gradient, the slab top surface experienced compressive stresses up to 565 psi and tensile stresses up to 53 psi in the longitudinal direction. On the other hand, the transverse stresses in the slab top surface experienced additional compressive stresses averaging 314 to 394 psi. The bottom surface experienced tensile stresses up to 244 psi at the shear-key locations. The same locations experienced maximum principal stresses up to 254 psi (tension).
 4. After applying AASHTO HS-25 truck load without impact and presence allowances, the maximum principal stresses reached a value of 299 psi at the bottom surface; yet, the slab did not experience any cracks under the truck load. However, it experienced small cracks in the bottom surface after applying the truck load either HS-25 or HL-93 with the impact and presence allowances (Figure 4.2-10 and Figure 4.2-11).

Since the developed cracks were limited, some increase in the TPT level would assist in achieving an adequate TPT arrangement. A TPT force of 150,000 lb/diaphragm was applied to the modified system of diaphragms.

1. After applying TPT force of 125,000 lb/diaphragm in the second TPT stage, the deck slab experienced compressive stresses up to 227 psi. The uppermost values were concentrated at the slab ends and the rest of the slab areas experienced lower values; large areas of the slab experienced compressive stresses in the range between 11 and 54 psi. In the longitudinal direction, small longitudinal compressive stresses developed in the deck slab, but they did not exceed 22 psi. Similarly, some longitudinal tensile stresses developed at local areas near the supports and reached 83 psi. The pressure on the box-beams sides exceeded 475 psi. However, between the diaphragms, the compressive pressure was less than 10 psi.

2. After deducting time dependent losses and applying superimposed dead loads, the deck slab experienced longitudinal compressive stresses of an average of 130 psi; yet, the transverse stresses were not affected by the applied loads.
3. After applying a positive temperature gradient, the slab top surface experienced longitudinal compressive stresses of about 558 psi; yet, the average compressive stress was zero at the slab bottom surface. At the same time, the transverse stresses in the slab top surface increased to an average between 287 and 371 psi. The bottom surface experienced tensile stresses up to 219 psi. Some local areas over the shear-key joints in the slab bottom surface experienced maximum principal tensile stresses up to 229 psi.
4. After applying AASHTO HS-25 truck load without impact and presence allowances, the maximum principal stresses reached 254 psi at the bottom surface, and the slab did not experience any cracks.
5. The maximum principal stresses reached 299 psi at the slab bottom surface after applying AASHTO HS-25 truck load with the impact and presence allowances and they reached 286 psi after applying HL-93 load with the impact and presence allowances. The slab did not experience cracks in both cases (Figure 4.2-12 and Figure 4.2-13).
6. By applying post-tensioning force of 150,000 lb/diaphragm at five diaphragms, the model was capable of supporting 100% of positive temperature gradient and AASHTO HS-25 truck or HL-93 load without developing any longitudinal cracks in the deck slab. Therefore, this TPT arrangement was considered the optimum. Table 4.2-1 presents a summary for the aforementioned investigation. In addition, Figure 4.2-14 shows the contribution of each load type in the developed principal stresses in the deck slab. It is apparent that the temperature gradient was the greatest contributing factor to the tensile stresses in the deck slab.

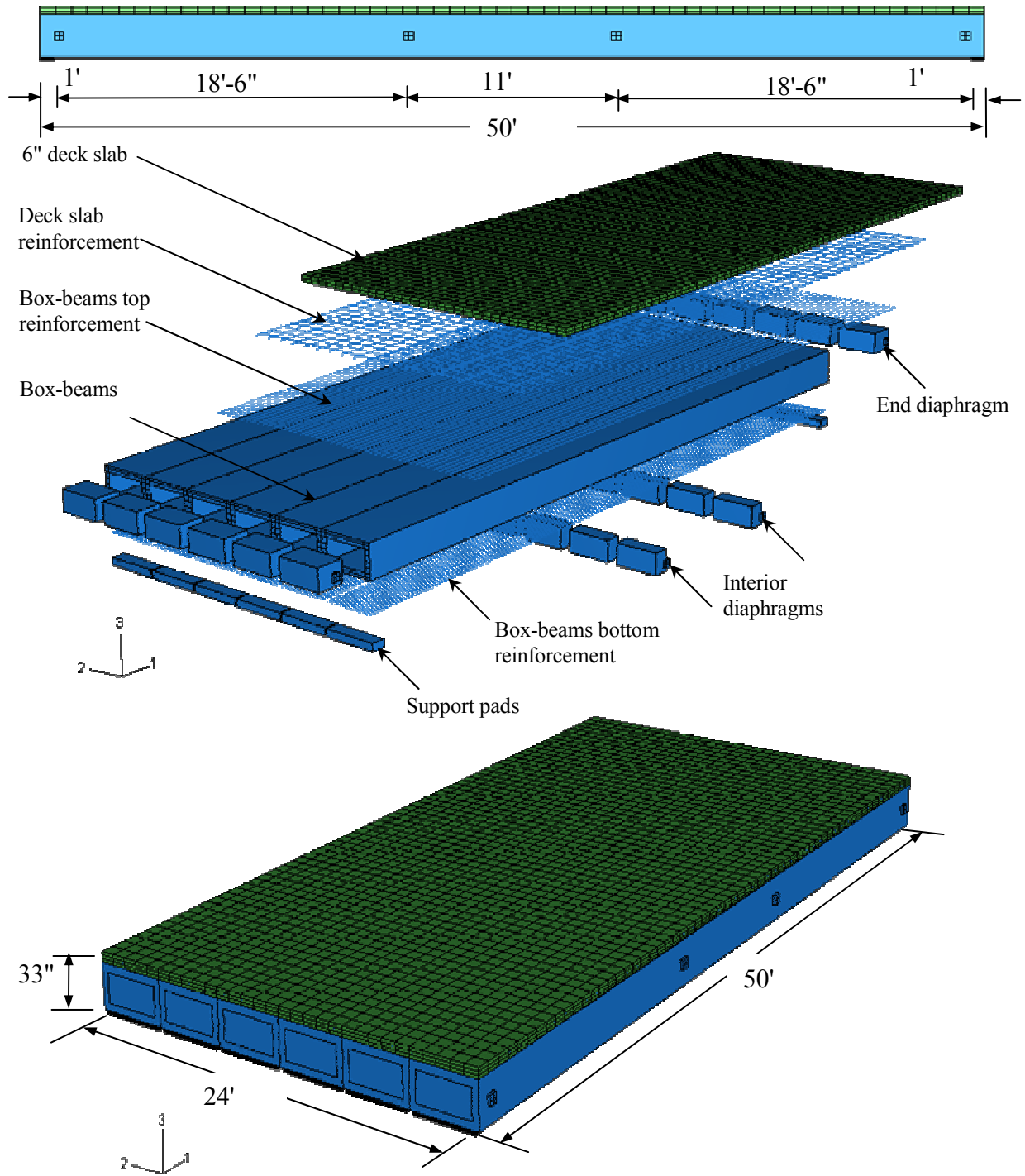


Figure 4.2-1 Assembly of 50 ft span bridge model.

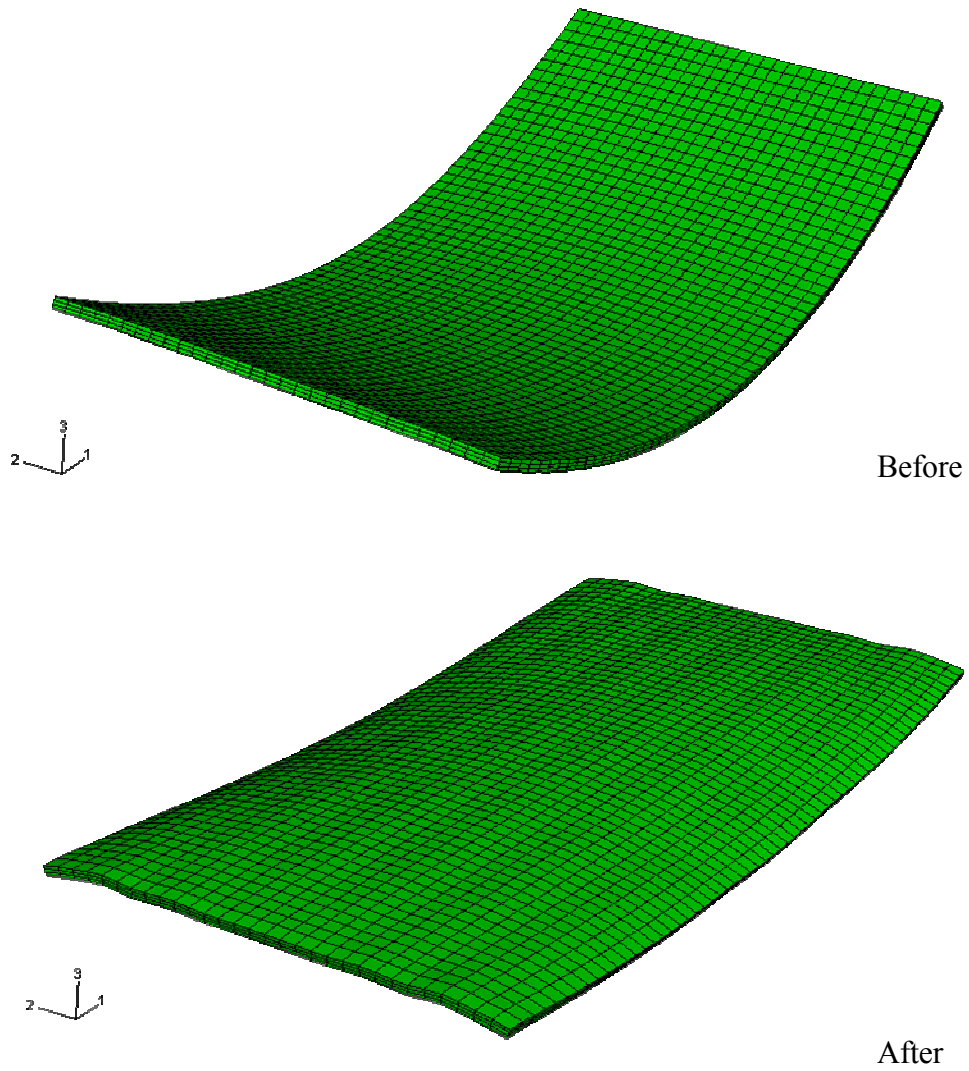


Figure 4.2-2 Exaggerated deformed shape of the slab before and after applying positive temperature gradient (Scale 1:500).

Diaphragms arrangement:

2 @ center of span (11" apart)
1 @ each end of beam

TPT= 104,500 lb/diaphragm
TPT= 104,500 lb/diaphragm

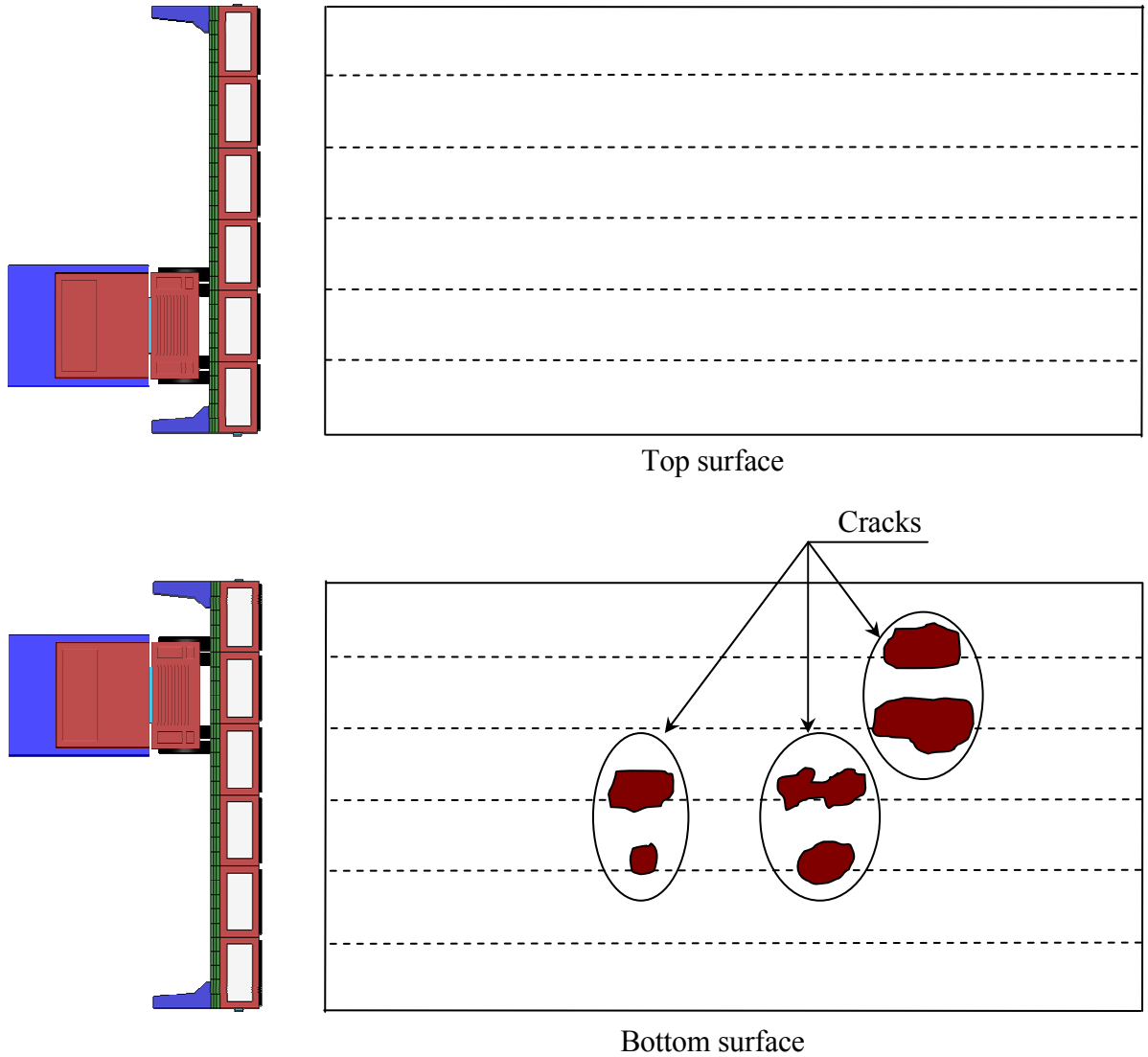


Figure 4.2-3 Crack development in the slab bottom surface after applying AASHTO HS-25 truck.

Diaphragms arrangement:

2 @ center of span (11" apart)
1 @ each end of beam

TPT= 104,500 lb/diaphragm
TPT= 104,500 lb/diaphragm

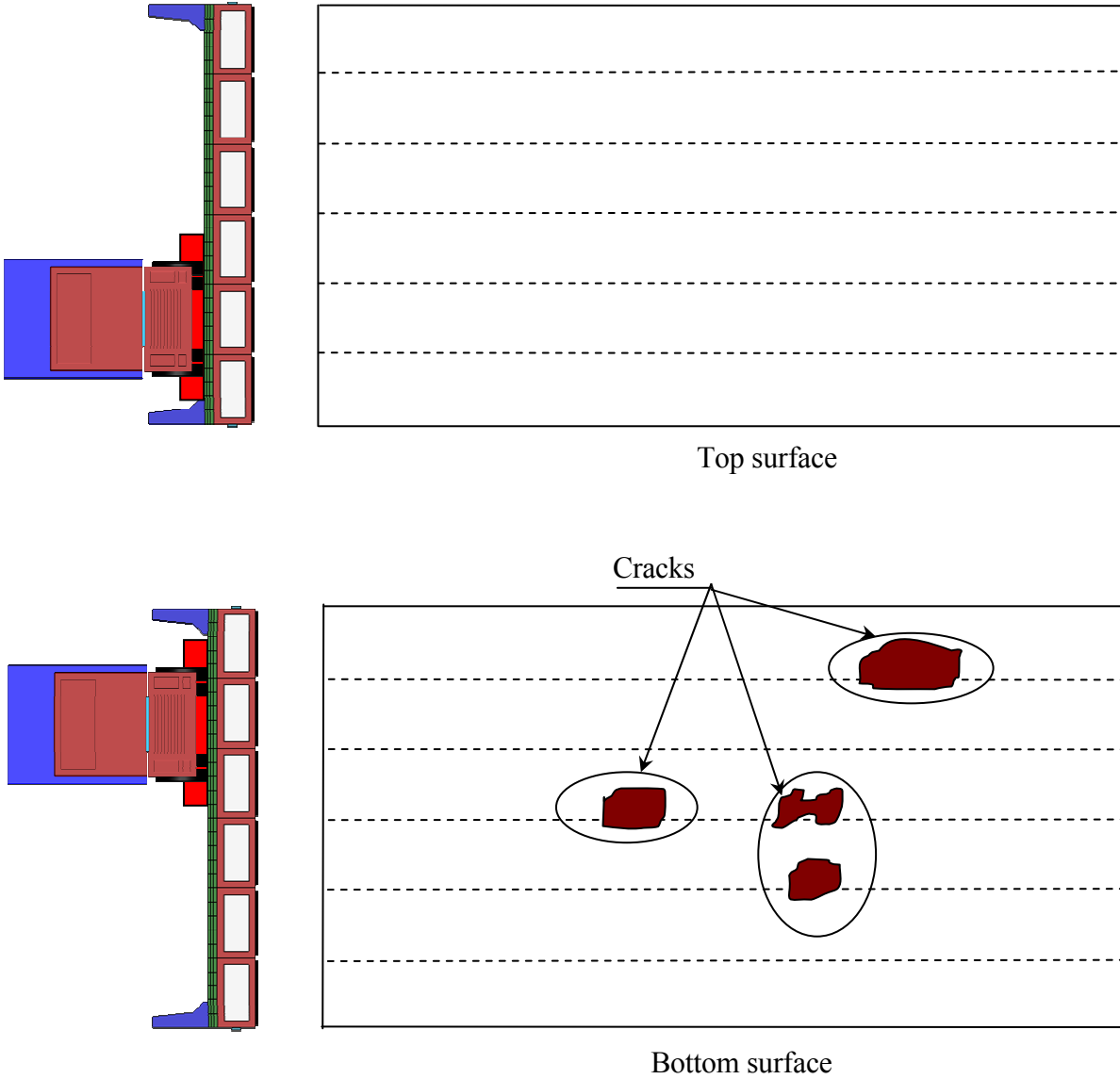
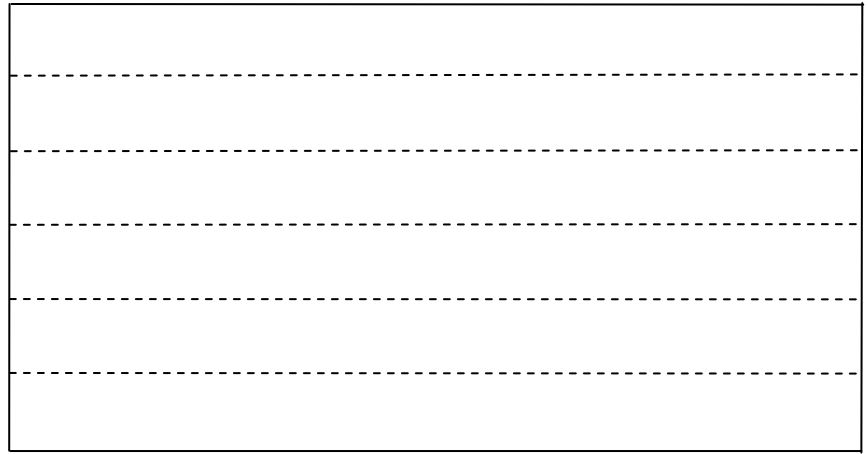
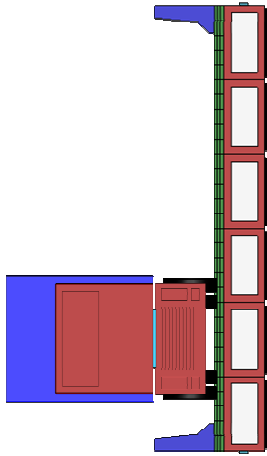


Figure 4.2-4 Crack development in the slab after applying AASHTO HL-93 load.

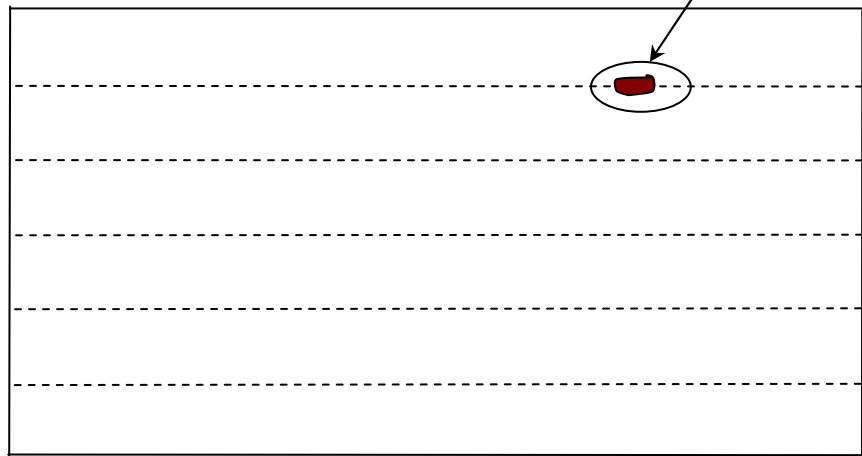
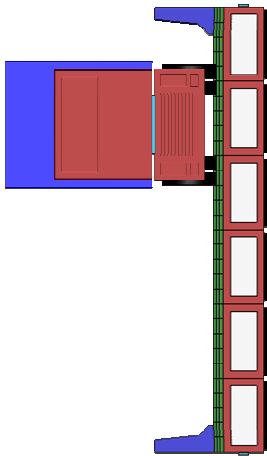
Diaphragms arrangement:

2 @ center of span (11" apart)
1 @ each end of beam

TPT= 200,000 lb/diaphragm
TPT= 200,000 lb/diaphragm



Top surface



Bottom surface

Figure 4.2-5 Crack development in the slab after applying AASHTO HS-25 truck.

Diaphragms arrangement:

2 @ center of span (11" apart)
1 @ each end of beam

TPT= 200,000 lb/diaphragm
TPT= 200,000 lb/diaphragm

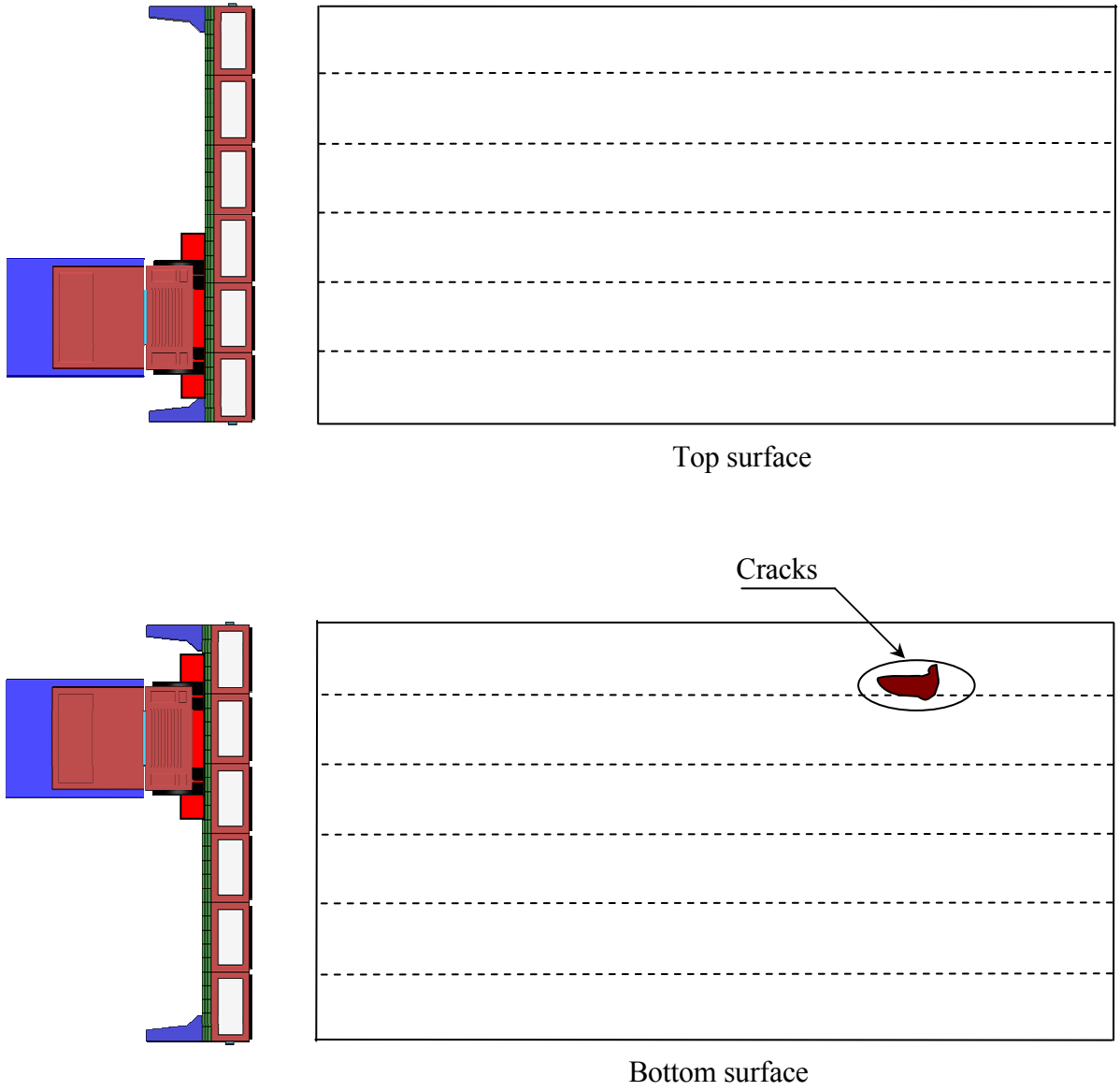


Figure 4.2-6 Crack development in the slab after applying AASHTO HS-93 truck.

Diaphragms arrangement:

2 @ center of span (11" apart)

TPT= 300,000 lb/diaphragm

1 @ each end of beam

TPT= 300,000 lb/diaphragm



Figure 4.2-7 Crack development in the slab bottom surface due to TPT force.

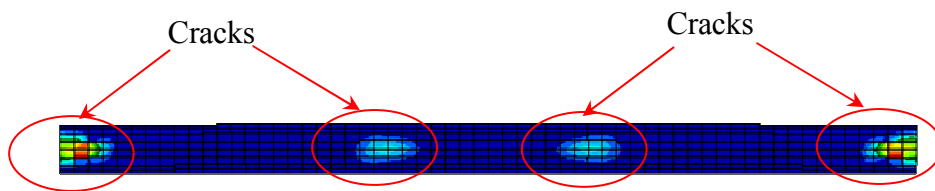


Figure 4.2-8 Crack development in box-beam sides due to TPT force.

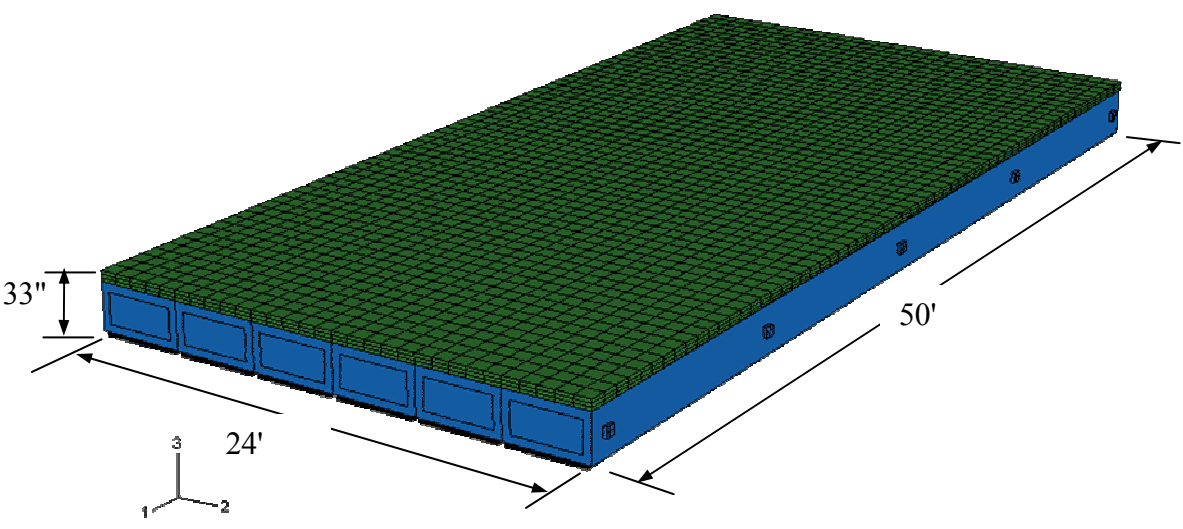
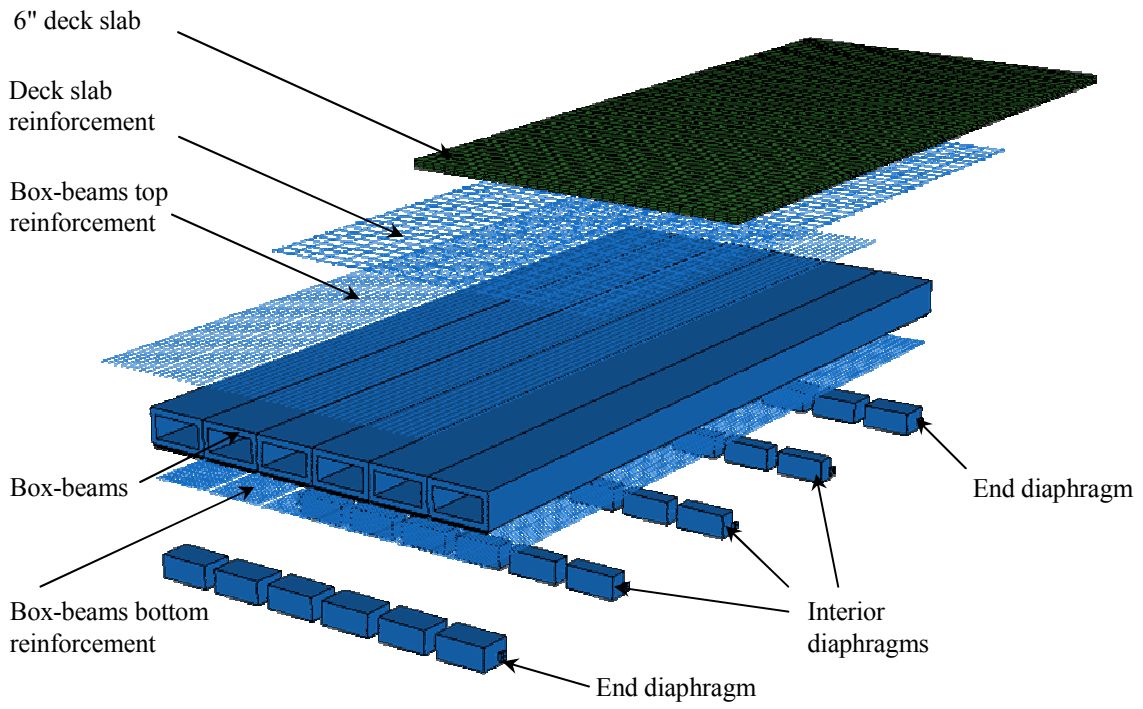
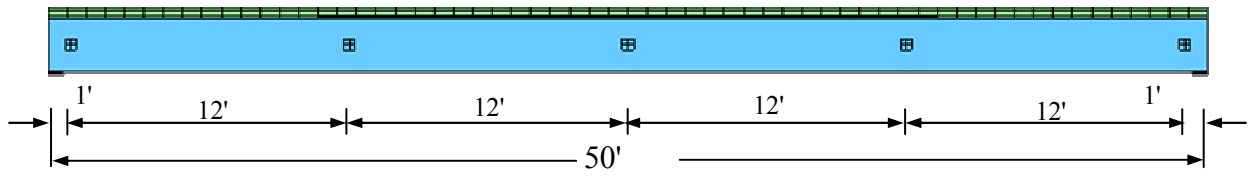


Figure 4.2-9 Modified assembly for 50 ft span bridge model.

Diaphragms arrangement:

1 @ each end of beam
3 equally spaced in-between

TPT= 100,000 lb/diaphragm
TPT= 100,000 lb/diaphragm

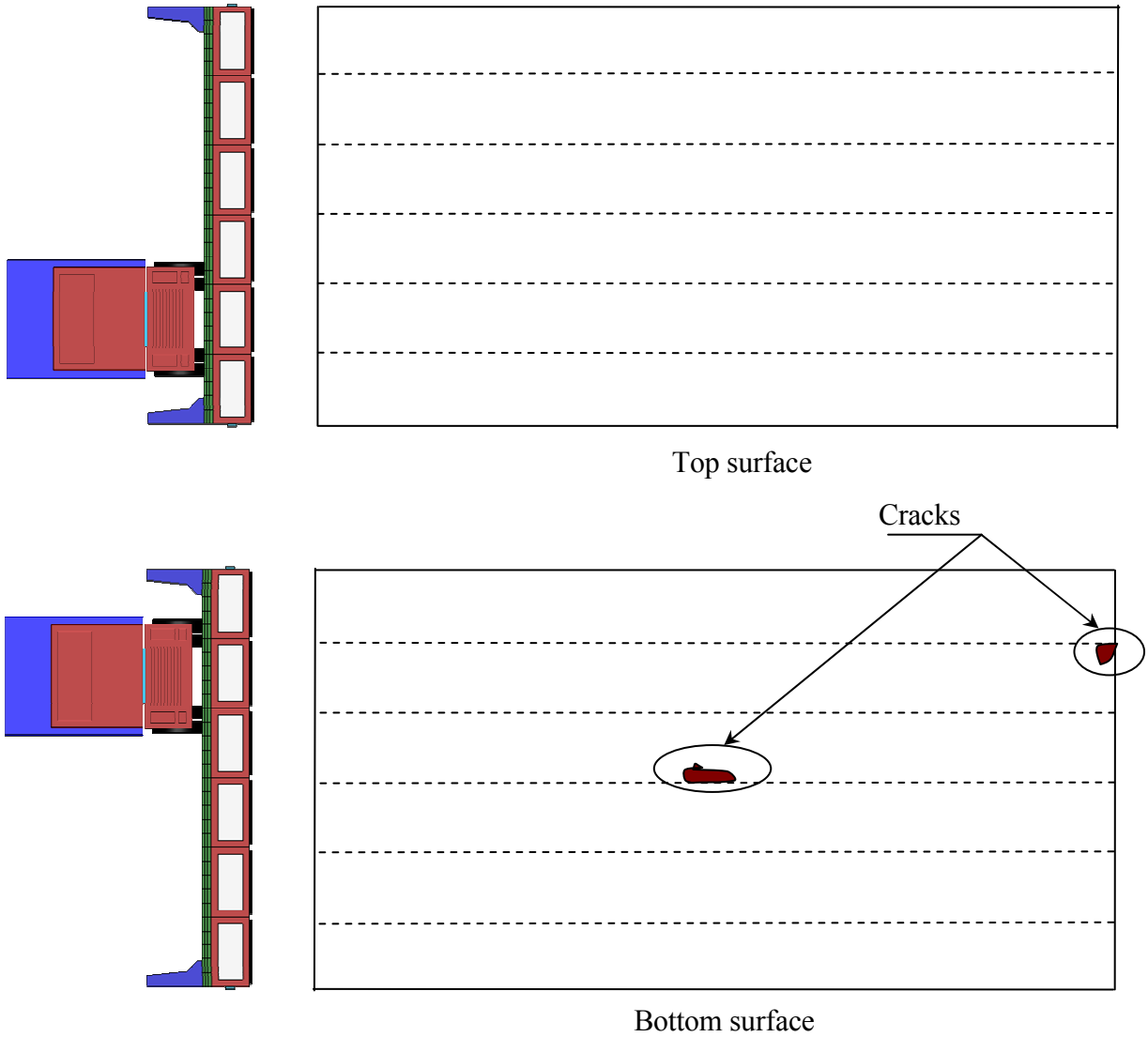


Figure 4.2-10 Crack development in the slab after applying AASHTO HS-25 truck.

Diaphragms arrangement:

1 @ each end of beam
3 equally spaced in-between

TPT= 100,000 lb/diaphragm
TPT= 100,000 lb/diaphragm

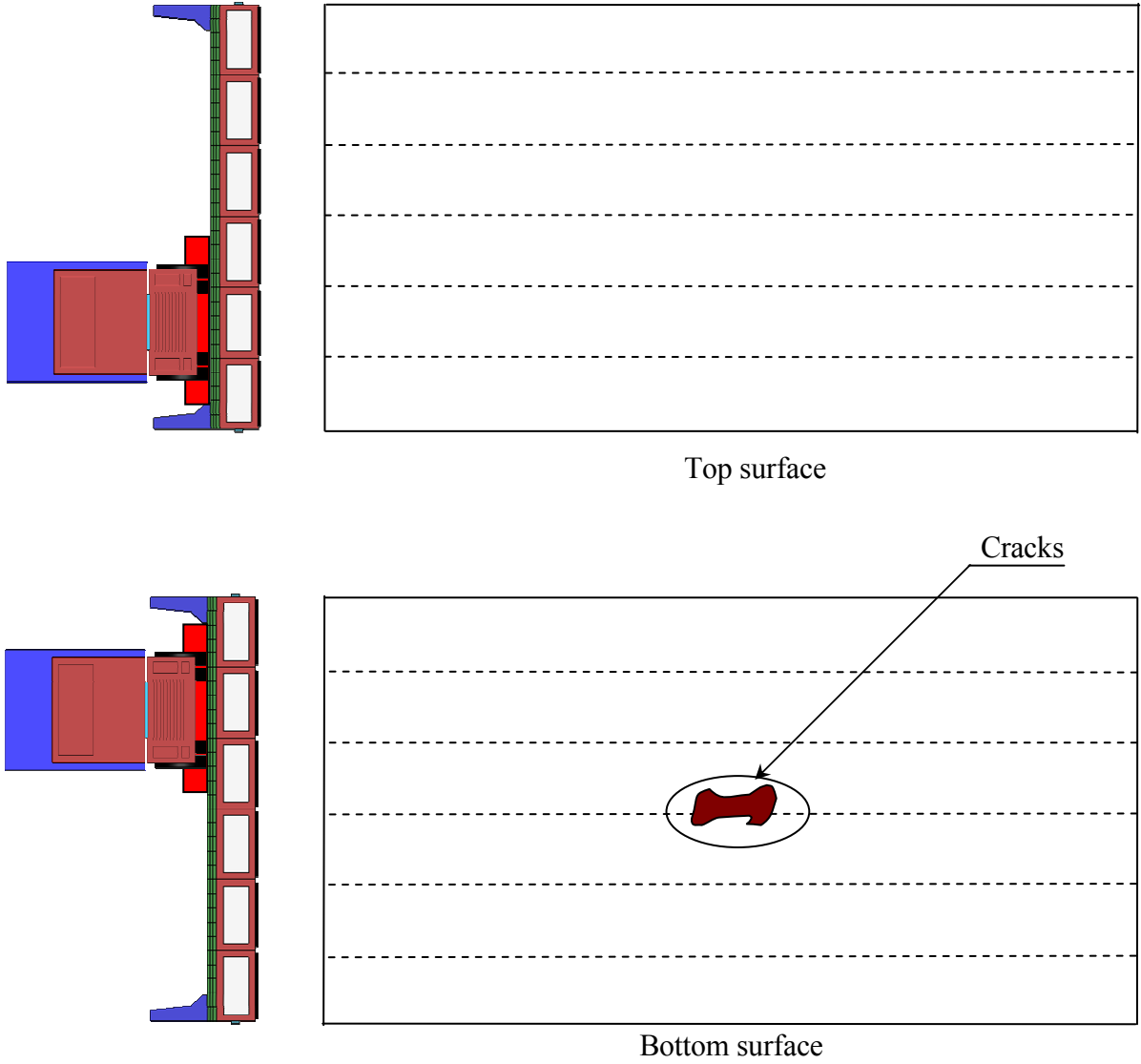


Figure 4.2-11 Crack development in the slab after applying AASHTO HL-93 load.

Diaphragms arrangement:

1 @ each end of beam
3 equally spaced in-between

TPT= 150,000 lb/diaphragm
TPT= 150,000 lb/diaphragm

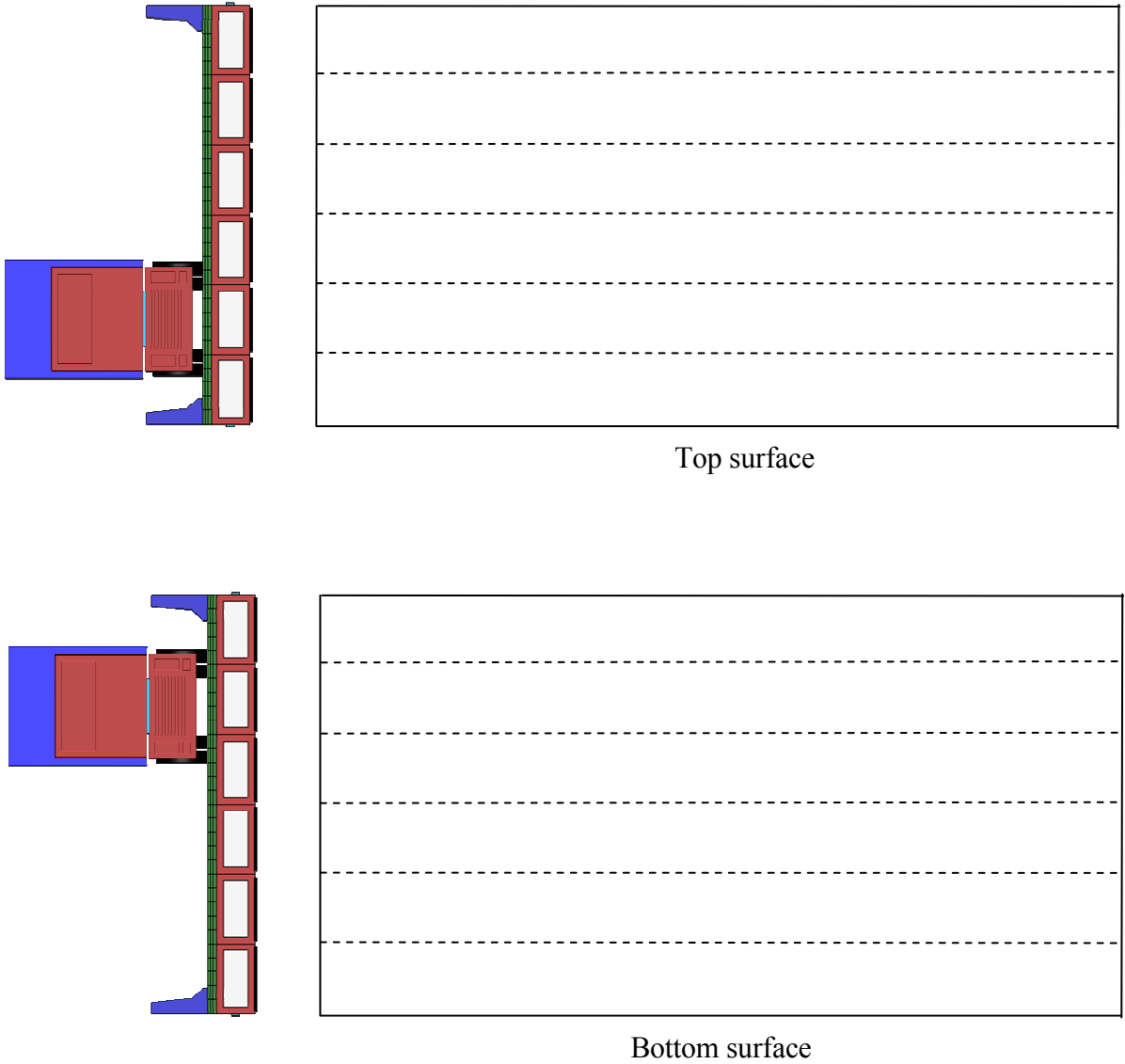


Figure 4.2-12 Crack development in slab after applying AASHTO HS-25 truck.

Diaphragms arrangement:

1 @ each end of beam
3 equally spaced in-between

TPT= 150,000 lb/diaphragm
TPT= 150,000 lb/diaphragm

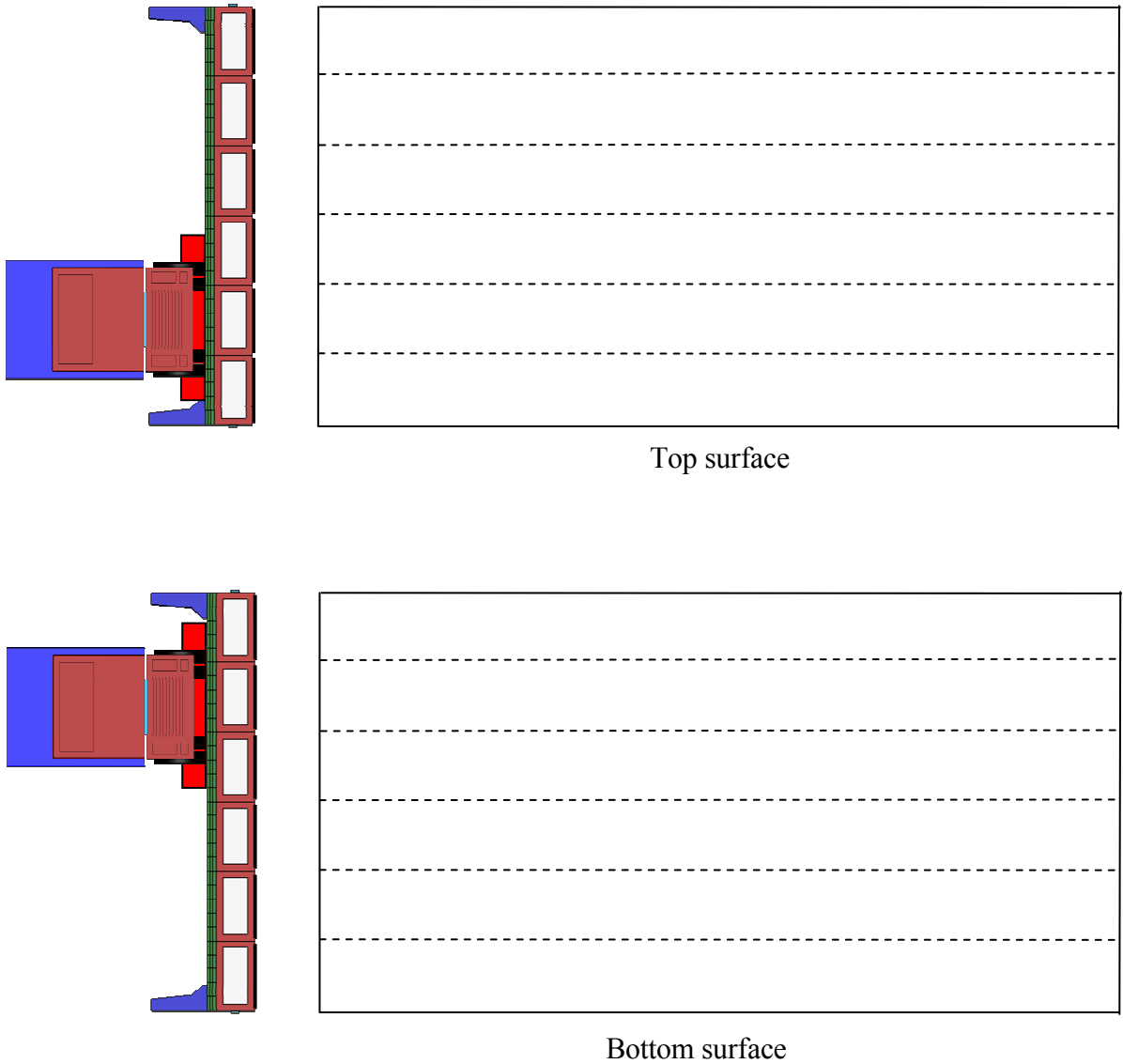


Figure 4.2-13 Crack development in slab after applying AASHTO HL-93 load.

Table 4.2-1 Maximum principal stresses in the deck slab of 50 ft span bridge model under service loads.

Model	No. of Diaphragms	TPT Force lb/diaphragm	MP Positive Gradient (psi)	MP LL+ IM (psi)	
				HS-25 truck	HL-93 load
Span = 50 ft Width = 24 ft	4	104,000	267	N/A (cracks)	N/A (cracks)
	4	200,000	256	N/A (cracks)	N/A (cracks)
	4	300,000	N/A (cracks)	N/A (cracks)	N/A (cracks)
	5	100,000	254	N/A (cracks)	N/A (cracks)
	5	150,000	229	299	286

- MP: Maximum principal stresses
- LL: Live load
- IM: Impact allowances
- N/A: Not available

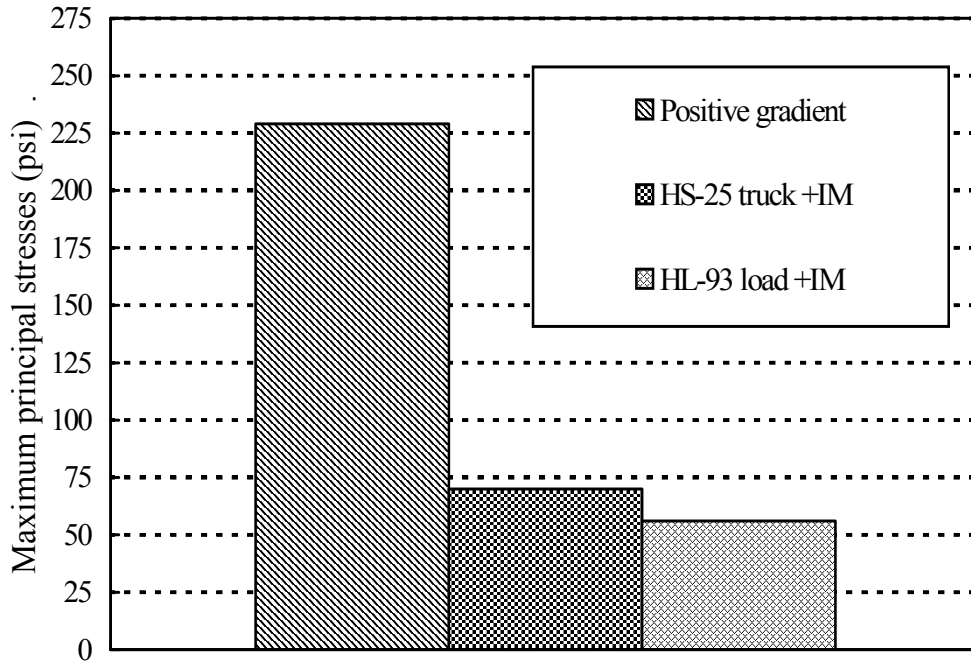


Figure 4.2-14 Service loads contribution in deck slab principal stresses (Case of five diaphragms, TPT = 150,000 lb/diaphragm).

4.2.4.2 62 ft Span Bridge Model

The second FE model was developed to simulate a 62 ft span bridge composed of six side-by-side box-beams of width 48 in. each, as shown in Figure 4.2-15. The model was provided with a TPT arrangement that conformed to current MDOT Specifications (2006), which require five diaphragms for this span; two diaphragms at the ends, two at the quarter points, and one at the mid-span. To satisfy the flexural requirements, a box-beam with a depth of 33 in. was used for this span. Two transverse strands were provided per diaphragm, with each transverse strand post-tensioned with a force equal to 52,250 lb (total of 104,500 lb/diaphragm).

Analysis and discussion

The current model was subjected to construction loads by: first, applying longitudinal prestressing forces; second, applying box-beams dead load; third, applying first stage of TPT force; fourth, adding slab dead load; fifth, applying second stage of TPT; and finally, deducting time dependent losses and applying the superimposed loads. Subsequently, service loads were applied by first applying positive temperature gradient and then applying AASHTO HS-25 truck or HL-93 load. By applying AASHTO HS-25 truck, or AASHTO HL-93 load, the deck slab developed cracks, as shown in Figure 4.2-16 and Figure 4.2-17. The cracks started developing from the bottom surface and propagated towards the top surface. Although they did not propagate to the top surface, repeated loads would likely cause the development of the full-depth cracks in the deck slab.

The first strategy used to eliminate the cracking problem was to increase the transverse post-tensioning force per diaphragm. The transverse post-tensioning force was increased to 150,000 lb/diaphragm while keeping the same number of diaphragms. The slab did not experience any cracks under the truck load without impact and presence allowances. However, it did experience small cracks in the bottom surface after adding the impact and presence allowances to the truck load. When applying AASHTO HL-93 load, the slab experienced similar cracks as well. The cracks were mainly concentrated at the mid-span over the intermediate diaphragm; so, increasing the TPT force in the intermediate diaphragm only appeared as a plausible solution; a TPT force equal to 200,000 lb/center-intermediate - diaphragm was applied while keeping the other diaphragms with TPT force equal to 150,000

lb/diaphragm. After applying AASHTO HS-25 truck load, the maximum principal stresses reached a value of 299 psi. The slab did not experience cracks.

By applying post-tensioning force 150,000 lb/diaphragm at four diaphragms and 200,000 lb/intermediate diaphragm, the model was able to support AASHTO HS-25 truck load as well as AASHTO HL-93 load with its impact and presence allowances without developing any longitudinal cracks in the deck slab. Therefore, this TPT arrangement was considered sufficient.

Instead of increasing the TPT force to 200,000 lb/intermediate-diaphragm, the cracks can be delayed by adding one more diaphragm and applying 150,000 lb in all the diaphragms. Increasing the diaphragms number has two benefits: first, high post-tensioning force can be avoided for a certain location; second, it allows better distribution for the pressure between the adjacent beams. Hence, the third trial was to examine the crack development when providing six equally-spaced diaphragms instead of five with TPT force equal to 150,000 lb/diaphragm (Figure 4.2-18).

After applying positive temperature gradient, the slab bottom surface experienced tensile stresses up to 233 psi. This value increased to 263 psi when adding AASHTO HS-25 truck load without impact and presence allowances, and then up to 306 psi when adding AASHTO HS-25 truck load with the impact and presence allowances. The slab did not experience any cracks under the AASHTO HS-25 truck or the ASHTO HL-93 load. In addition, a summary for the aforementioned investigation is presented in Table 4.2-2. Furthermore, the contribution of each load type to the principal stresses in the deck slab is shown in Figure 4.2-19.

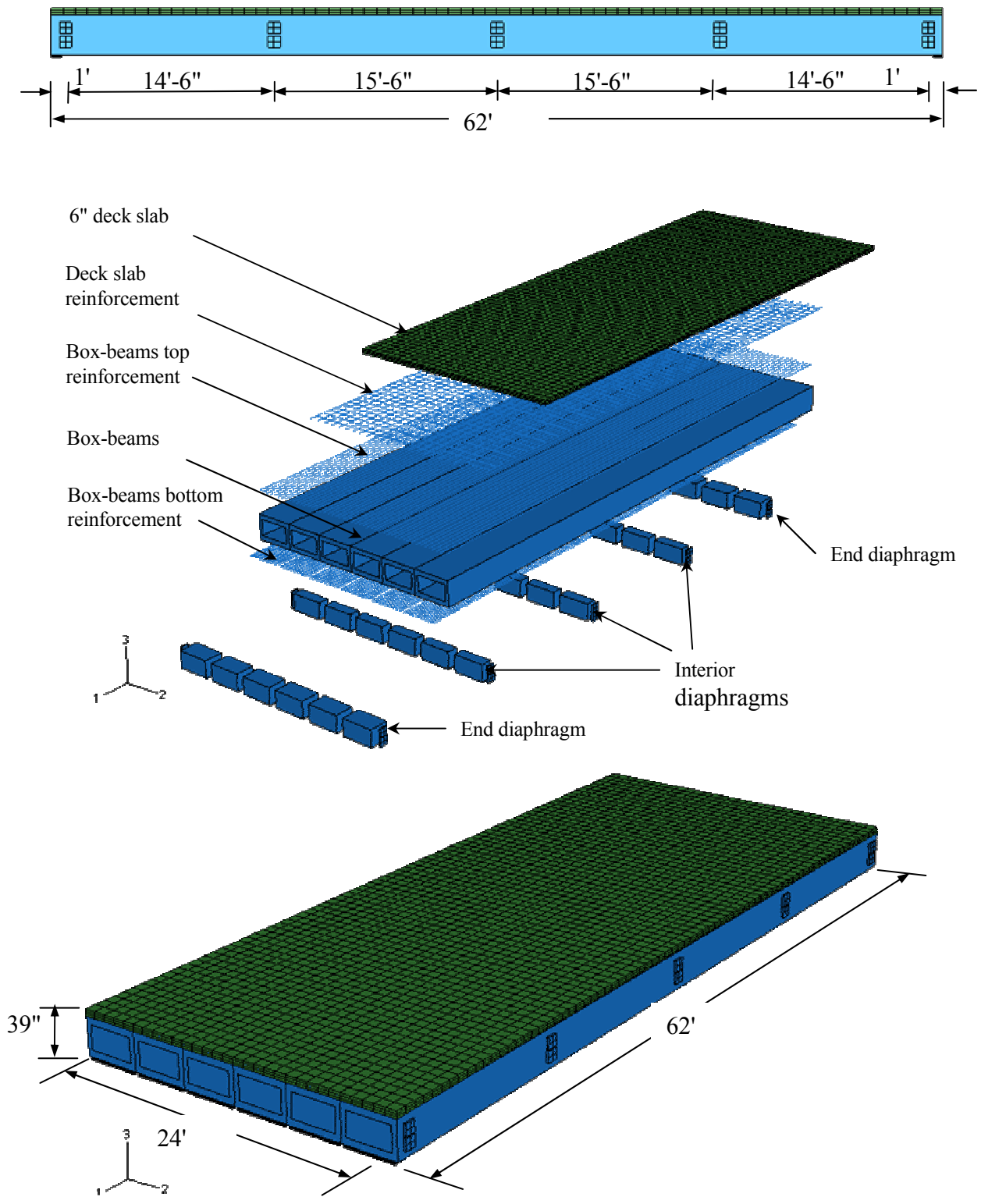


Figure 4.2-15 Assembly for 62 ft span bridge model.

Diaphragms arrangement:

1 @ each end of beam

2 @ quarter points

1 @ center of span

TPT= 104,500 lb/diaphragm

TPT= 104,500 lb/diaphragm

TPT= 104,500 lb/diaphragm

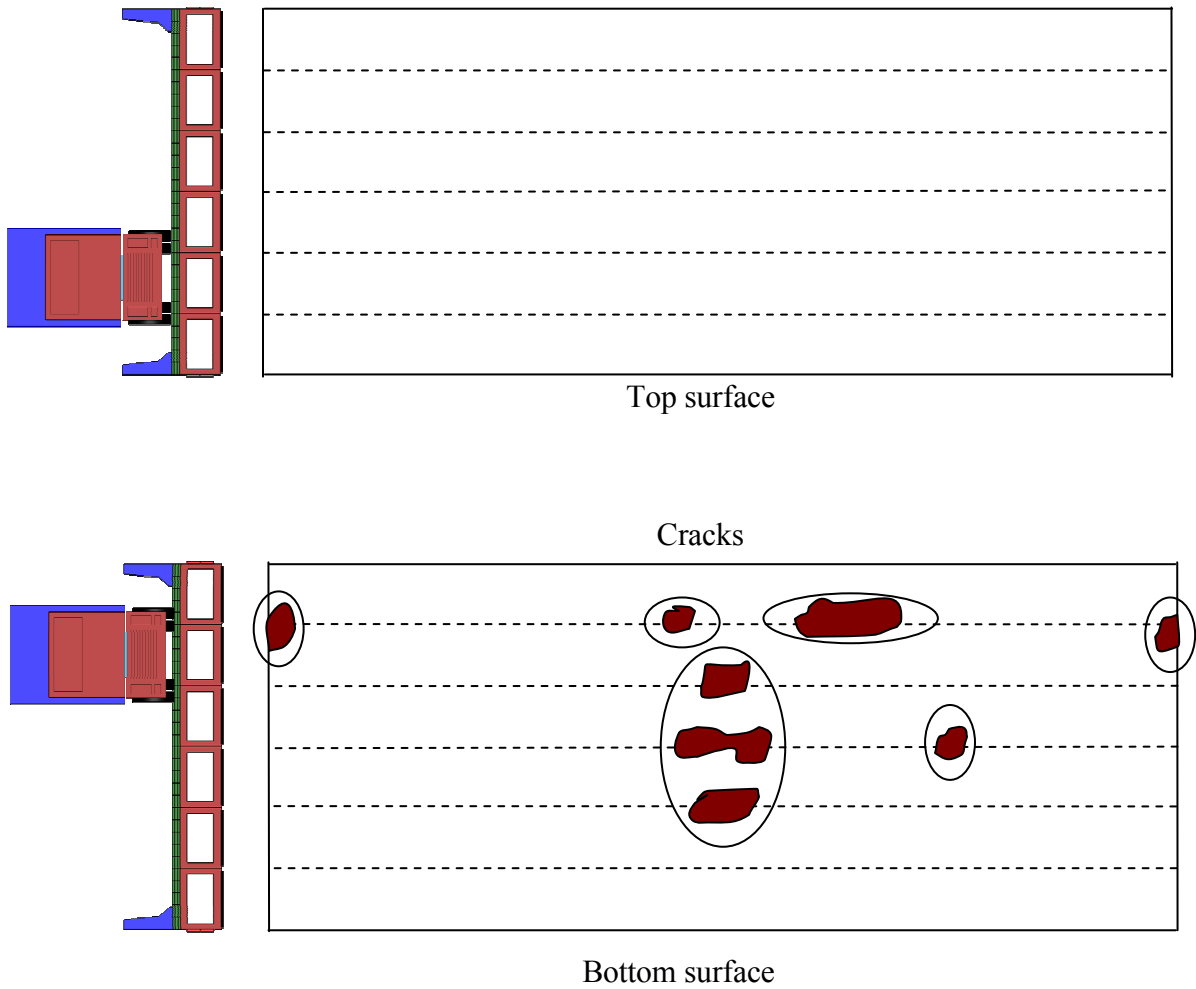


Figure 4.2-16 Crack development in slab after applying AASHTO-HS 25 truck.

Diaphragms arrangement:

1 @ each end of beam

2 @ quarter points

1 @ center of span

TPT= 104,500 lb/diaphragm

TPT= 104,500 lb/diaphragm

TPT= 104,500 lb/diaphragm

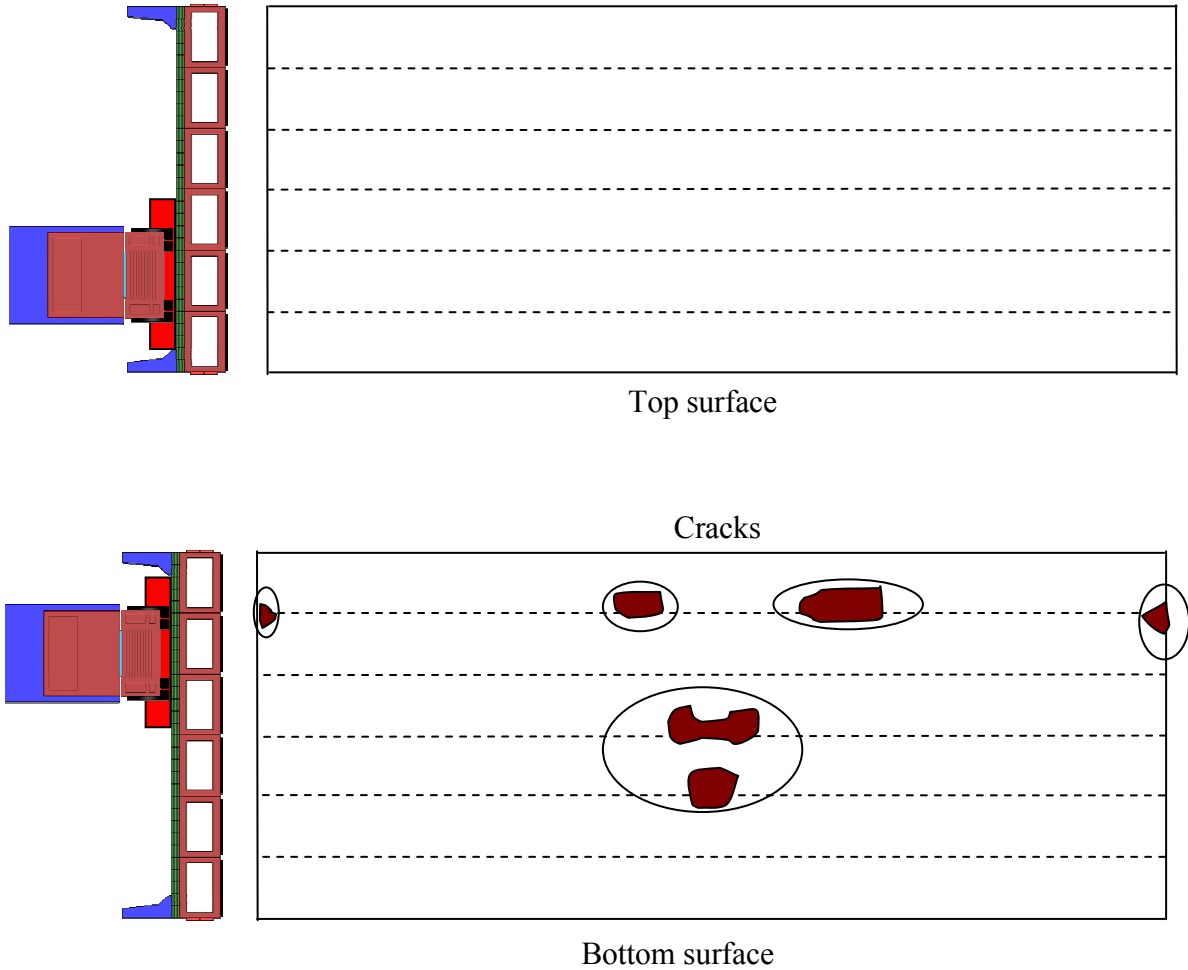


Figure 4.2-17 Crack development in slab after applying AASHTO HL-93 truck.

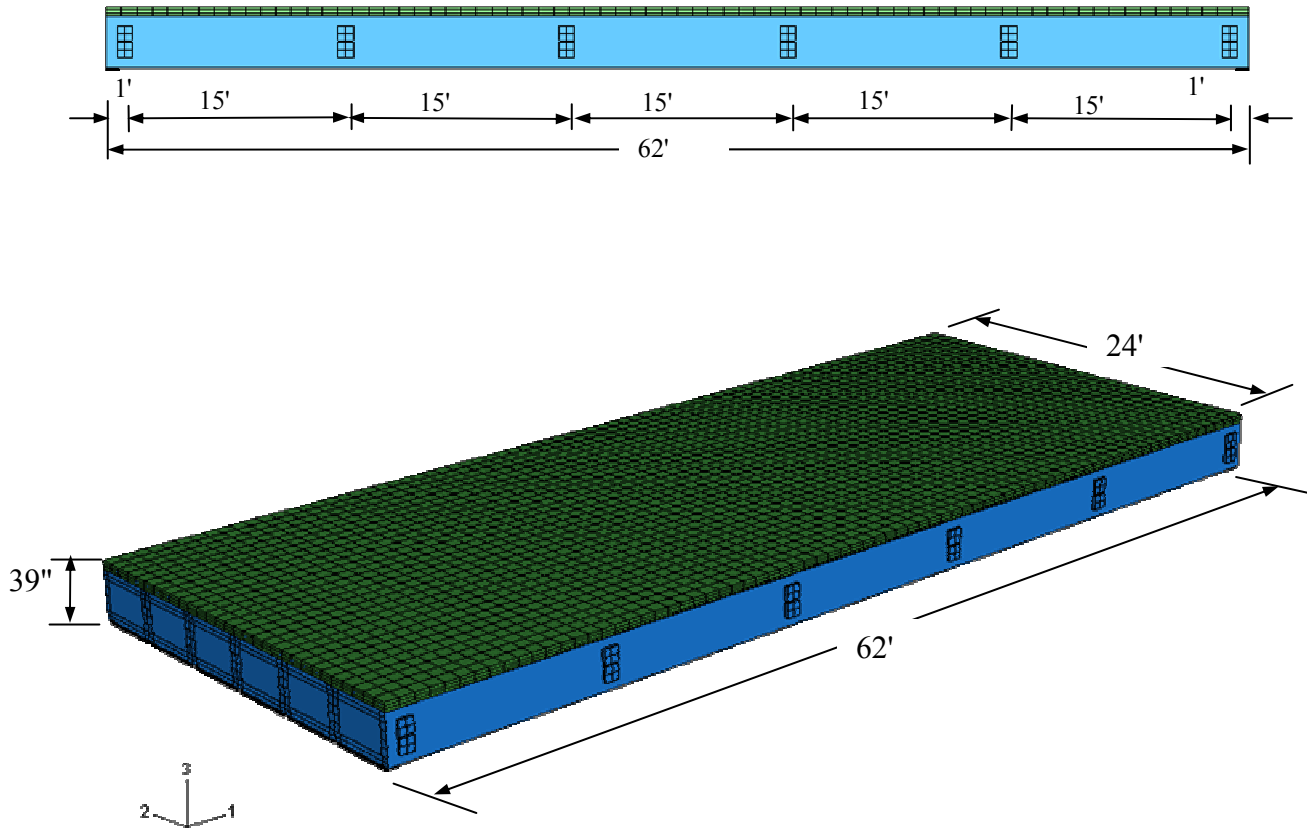


Figure 4.2-18 Assembly for modified 62 ft span bridge model.

Table 4.2-2 Maximum principal stress in the deck slab of 62 ft span bridge model under service loads.

Model	No. of Diaphragms	TPT Force lb/diaphragm	MP Positive Gradient (psi)	MP LL+ IM (psi)	
				HS-25 truck	HL-93 load
Span = 62 ft Width = 24 ft	5	104,000	265	N/A (cracks)	N/A (cracks)
	5	150,000	250	N/A (cracks)	N/A (cracks)
	5	150,000/200,000	241	299	291
	6	150,000	233	306	287

- MP: Maximum principal stresses
- LL: Live load
- IM: Impact allowances
- N/A: Not available

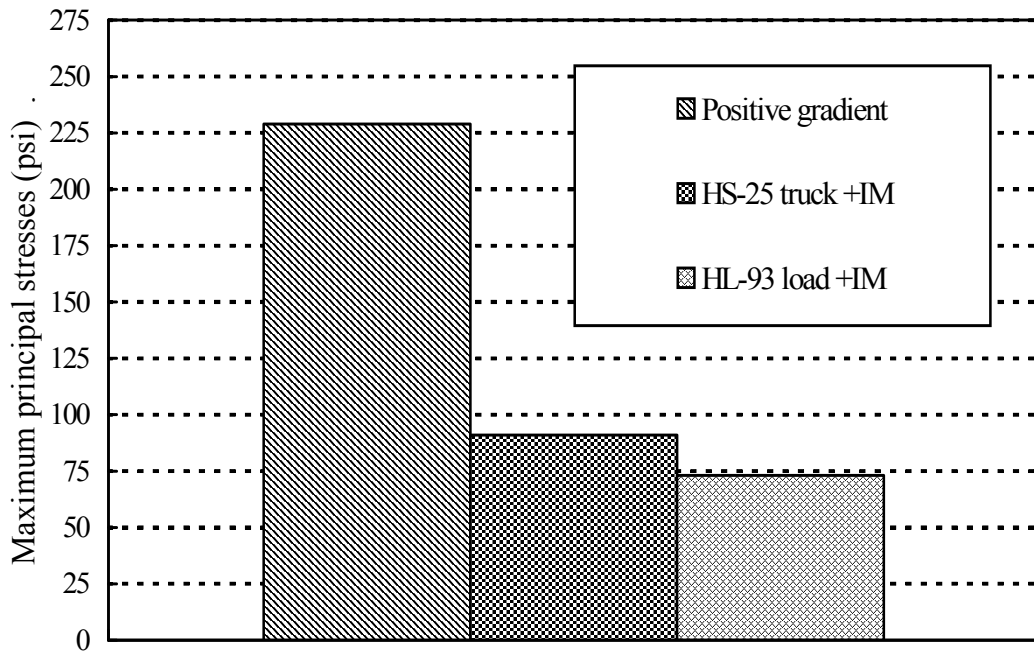


Figure 4.2-19 Service loads contribution in deck slab principal stresses (Case of six diaphragms, TPT = 150,000 lb/diaphragm).

4.2.4.3 100 ft Span Bridge Model

This FE model simulated a bridge with a span of 100 ft and width of 24 ft; yet, only half of the span was modeled and symmetry conditions were assumed across the mid-section of the span. Because of symmetry, it was not practical to apply AASHTO HS-25 truck load, non symmetric load, on a half model. Instead, an equivalent AASHTO HS-20 lane load, with concentrated load, was applied as a live load.

For 100 ft span, the truck load (not the lane load) governs the flexural design; so, a specific ratio was used to transform the lane load effect into its equivalent of the truck load. The ratio was the same as the ratio between the moment induced by AASHTO HS-25 truck load and that induced by AASHTO HS-20 lane load, which was found to be: ($M_{truck} = 1.5M_{lane}$).

For AASHTO HL-93 loading, the tandem load was used along with the lane load instead of using the truck load (because of the assumed symmetry conditions in the FE model). A transformation ratio was used to transform the tandem load effect into its equivalent of the HS-20 truck load; this ratio was found to be: ($M_{truck} = 1.27M_{tandem}$). By using these ratios, it was possible to keep the same analysis philosophy of establishing an appropriate TPT arrangement capable of connecting the box-beams to support AASHTO HS-25 truck or AASHTO HL-93 load without developing cracks in the deck slab.

The first model was provided with a TPT arrangement that conformed to MDOT Specifications (2006), which require six diaphragms for this span (Figure 4.2-20); two diaphragms at the ends, two at the quarter-spans, and two at the center (11 ft apart). To satisfy the flexural requirements, a box-beam of depth of 39 in. was used for this span; accordingly, two transverse strands were provided at each diaphragm. Each transverse strand was post-tensioned with a force of 52,250 lb (total of 104,500 lb/diaphragm).

Analysis and discussion

The analysis was performed according to the general sequence by applying: first, longitudinal prestressing forces and box-beams dead load; second, first stage of TPT force; third, slab dead load; fourth, second stage of TPT force; fifth, time dependent losses in addition to the superimposed dead loads; sixth, positive temperature gradient, and finally, equivalent AASHTO HS-25 truck load or AASHTO HL-93 load. By applying either the equivalent

AASHTO HS-25 truck load or equivalent AASHTO HL-93, the deck slab experienced longitudinal cracks between the box-beams (Figure 4.2-21 and Figure 4.2-22).

The first strategy applied to eliminate the longitudinal cracking was to increase the transverse post-tensioning force per diaphragm. The transverse post-tensioning force was first increased to 150,000 lb/diaphragm while maintaining the same number of diaphragms.

By applying equivalent AASHTO HS-25 truck load or equivalent AASHTO HL-93 load, the slab experienced small cracks in the bottom surface. The cracks were mainly concentrated at the mid-span over the intermediate diaphragm. Therefore, there were two options to eliminate the cracks, either increasing the TPT force per diaphragm or increasing the number of diaphragms. Generally, increasing number of diaphragms had more influence on crack control than increasing the TPT force. Therefore, the final trial was to increase the number of diaphragms from six to seven. The seven diaphragms were equally spaced, as shown in Figure 4.2-23.

After applying a positive temperature gradient, the slab experienced tensile stresses of 234 psi at the bottom surface. These tensile stresses increased to 353 psi when adding equivalent AASHTO HS-25 truck load, and to 351 psi when adding equivalent AASHTO HL-93. The slab finally did not exhibit any cracks under service loads. Table 4.2-3 presents a summary for the aforementioned investigation and Figure 4.2-24 shows the contribution of each load type to the principal stresses in the deck slab.

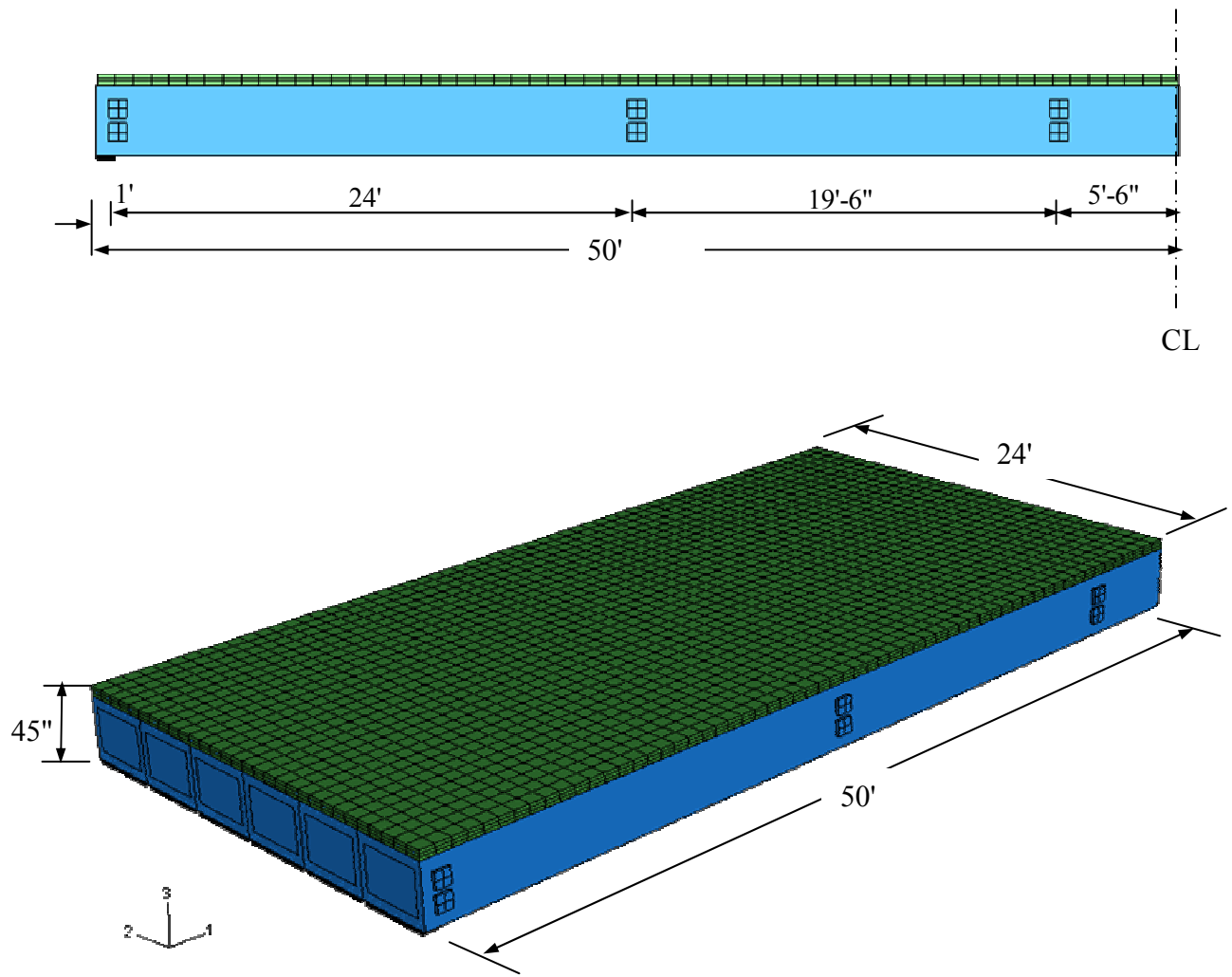


Figure 4.2-20 Assembly for 100 ft span bridge model.